WL-TR-95-4010

NDE X-RAY COMPUTED TOMOGRAPHY APPLICATIONS RESEARCH

S. Trent Neel
Robert N. Yancey
Dennis S. Eliasen
David H. Phillips

Advanced Research and Applications Corp.
425 Lakeside Drive
Sunnyvale, CA 94086

November 1994

Final Report for Period August 1989 - September 1994

MATERIALS DIRECTORATE
WRIGHT LABORATORY
AIR FORCE MATERIEL COMMAND
WRIGHT-PATTERSON AFB OH 45433-7734

NOTICE

WHEN GOVERNMENT DRAWINGS, SPECIFICATIONS, OR OTHER DATA ARE USED FOR ANY PURPOSE OTHER THAN IN CONNECTION WITH A DEFINITELY GOVERNMENT-RELATED PROCUREMENT, THE UNITED STATES GOVERNMENT INCURS NO RESPONSIBILITY OR ANY OBLIGATION WHATSOEVER. THE FACT THAT THE GOVERNMENT MAY HAVE FORMULATED OR IN ANY WAY SUPPLIED THE SAID DRAWINGS, SPECIFICATIONS, OR OTHER DATA, IS NOT TO BE REGARDED BY IMPLICATION OR OTHERWISE IN ANY MANNER CONSTRUED, AS LICENSING THE HOLDER OR ANY OTHER PERSON OR CORPORATION, OR AS CONVEYING ANY RIGHTS OR PERMISSION TO MANUFACTURE, USE, OR SELL ANY PATENTED INVENTION THAT MAY IN ANY WAY BE RELATED THERETO.

THIS REPORT IS RELEASABLE TO THE NATIONAL TECHNICAL INFORMATION SERVICE (NTIS). AT NTIS, IT WILL BE AVAILABLE TO THE GENERAL PUBLIC, INCLUDING FOREIGN NATIONS.

THIS TECHNICAL REPORT HAS BEEN REVIEWED AND IS APPROVED FOR PUBLICATION.

THOMAS J. MORAN
Nondestructive Evaluation Branch
Metals and Ceramics Division

TOBEY M. CORDELL, Chief
Nondestructive Evaluation Branch
Metals and Ceramics Division

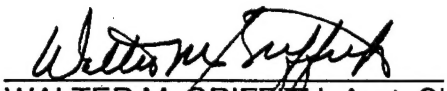

WALTER M. GRIFFITH, Asst. Chief
Metals and Ceramics Division
Materials Directorate

IF YOUR ADDRESS HAS CHANGED, IF YOU WISH TO BE REMOVED FROM OUR MAILING LIST, OR IF THE ADDRESSEE IS NO LONGER EMPLOYED BY YOUR ORGANIZATION, PLEASE NOTIFY, WL/MLLP, WRIGHT-PATTERSON AFB OH 45433-7817 TO HELP US MAINTAIN A CURRENT MAILING LIST.

COPIES OF THIS REPORT SHOUL.D NOT BE RETURNED UNLESS RETURN IS REQUIRED BY SECURITY CONSIDERATIONS, CONTRACTUAL OBLIGATIONS, OR NOTICE ON A SPECIFIC DOCUMENT.

DISCLAIMER NOTICE

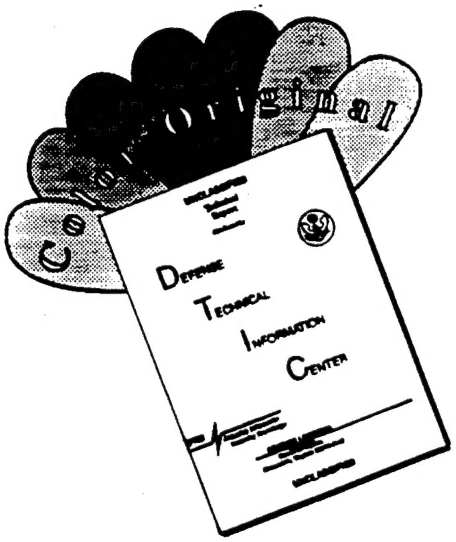

THIS DOCUMENT IS BEST QUALITY AVAILABLE. THE COPY FURNISHED TO DTIC CONTAINED A SIGNIFICANT NUMBER OF COLOR PAGES WHICH DO NOT REPRODUCE LEGIBLY ON BLACK AND WHITE MICROFICHE.

REPORT DOCUMENTATION PAGE

FORM APPROVED
OMB NO. 0704-0188

1. AGENCY USE ONLY (Leave blank)	2. REPORT DATE	3. REPORT TYPE AND DATES COVERED
	November 1994	Final Report - August 1989 - September 1994

4. TITLE AND SUBTITLE
NDE X-Ray Computed Tomography Applications Research

5. FUNDING NUMBERS
C - F33615-89-C-5618
PE - 62102F
PR - 2418
TA - 02
WU - 48

6. AUTHOR(S)
S. Trent Neel, Robert N. Yancey, Dennis S. Eliasen, and David H. Phillips

7. PERFORMING ORGANIZATION NAMES(S) AND ADDRESS(ES)
Advanced Research and Applications Corp
425 Lakeside Drive
Sunnyvale, CA 94086

8. PERFORMING ORGANIZATION REPORT NUMBER

9. SPONSORING/MONITORING AGENCY NAMES(ES) AND ADDRESS(ES)
Materials Directorate
Wright Laboratory
Air Force Material Command
Wright-Patterson AFB OH 45433-7734

10. SPONSORING/MONITORING AGENCY REPORT NUMBER
WL-TR-95-4010

11. SUPPLEMENTARY NOTES
N/A

Accesion For
NTIS CRA&I
DTIC TAB
Unannounced
Justification
By
Distribution /
Availability Codes
Dist | Avail and / or Special
A-1

12a. DISTRIBUTION/AVAILABILITY STATEMENT
Approved for public release; distribution is unlimited.

12b. DISTRIBUTION CODE

13. ABSTRACT (Maximum 200 words)

This report summarizes research efforts in X-ray computed tomography at Wright Laboratory. Attention is focused on applications development efforts that have been successful in coupling CT with engineering functions to provide new insight to materials and processing issues in a cost effective manner. A sampling of the myriad of applications to be covered in this report includes: tracking of densification during the processing of composite materials and ceramics, measuring the thickness of internal walls in castings, failure analysis of an aircraft landing gear actuator, and verification of modeling damage zones in slug impacted fiberglass armor. Extrapolation of specific studies to broader horizons are offered.

14. SUBJECT TERMS
NDE, Ultrasonics, metal matrix composites, ceramic matrix composites, nondestructive characterization of advanced composite fiber matrix interface, characterization, matrix consolidation characterization, image expansion, digital processing of ultrasonic signals

15. NUMBER OF PAGES
68

16. PRICE CODE

17. SECURITY CLASSIFICATION OF REPORT	18. SECURITY CLASSIFICATION OF THIS PAGE	19. SECURITY CLASSIFICATION OF ABSTRACT	20. LIMITATION OF ABSTRACT
Unclassified	Unclassified	Unclassified	Unlimited

Table of Contents

Table of Contents
(Continued)

List of Figures

List of Figures
(Continued)

Foreword

This final report was prepared by Advanced Research and Applications Corporation (ARACOR), Sunnyvale, California, for the Wright Laboratory/Materials Directorate. It documents the work performed under Air Force Contract F33615-89-C-5618, "NDE X-Ray Computed Tomography Applications Research," for the period 18 September 1989 to 18 September 1994. The focus of the program was to: a) identify NDE requirements which may be met both technically and economically using X-ray CT, b) develop X-ray CT methodology to meet those requirements, and c) generate a data base to verify the methodology.

The Project Manager is Dr. Thomas Moran of the Wright Laboratory/Materials Directorate, WL/MLLP, Wright-Patterson AFB, OH, 45433. The Principal Investigator for ARACOR for the first 3 years of the program was Mr. Robert N. Yancey. The Principal Investigator for ARACOR for the last 2 years of the program was Mr. Trent Neel.

Executive Summary

Computed tomography (CT) has been called one of the 10 most significant scientific achievements of the past 25 years. Indeed, CT has been one of the most important diagnostic tools in the medical profession since the first clinical CAT scanner was patented in 1972.[1] CT has also proven very successful as a nondestructive inspection technique for quality assurance testing of solid rocket motors, nozzles and aircraft components. However, the full potential of CT is just now beginning to be realized through its application to arenas such as process development, product design, failure analysis and model verification. The unique capabilities of the Wright Laboratory CT Facility provide an ideal environment for such efforts.

This report summarizes research efforts in X-ray computed tomography at Wright Laboratory. Attention is focused on applications development efforts that have been successful in coupling CT with engineering functions to provide new insight to materials and processing issues in a cost-effective manner. A sampling of the myriad of applications to be covered in this report include: tracking of densification during the processing of composite materials and ceramics, measuring the thickness of internal walls in castings, performing the failure analysis of an aircraft landing gear actuator, and measuring damage zones in slug impacted fiberglass armor. Extrapolation of specific studies to broader horizons are offered.

Some key themes regarding the effective use of CT emerged from the present research. It was determined that CT can be a powerful tool for process development; it can be used to substitute for destructive analysis, to perform effect of defect studies, and to follow parts through successive stages of processing. CT is also effective as a tool for design verification, model verification, failure analysis, and quality assurance. Application areas studied include advanced (metal-, ceramic-, and polymer-matrix) composites, aeropropulsion structures, flight vehicle structures, metal castings, electronic components, rocket propellant, and space vehicle components. Many of these application studies resulted in a better understanding of how CT can be best utilized. The studies also resulted in new tools or capabilities that make CT inspection more efficient and useful. Some of these tools include the development of methodologies for the accurate dimensional measurement of internal passages in metal castings, reverse engineering capabilities to turn CT image data into CAD representations of components, customized image analysis tools for extraction of key information from the images (e.g., fiber positions in metal-matrix composites), and 3-D image rendering from a series of contiguous CT slices.

The key conclusion from the research is that CT provides a useful inspection technique for a broad range of applications. CT can be much more than a quality assurance tool to inspect materials or components at the end of the manufacturing line. In many cases, CT is most effective when used up-front during the development of new material systems, new material processes, or new manufacturing procedures. Additionally, CT has proven effective in monitoring material or dimensional integrity throughout the operational life of a system and CT successfully contributes as a tool for failure investigations and post-mortem analyses. Thus, CT can be applied in a variety of ways from cradle to grave to provide expedient and accurate information on the internal features of materials and components.

1.0 Introduction

1.1 Report Orgainization

This report summarizes research conducted at the Wright Laboratory/Materials Directorate X-ray Computed Tomography (CT) Research Facility. The report is divided into four main sections plus an appendix. Section 1.0 introduces the CT research facility and the capabilities of the two CT systems, LAM/DE and Tomoscope. Section 2.0 focusses on several important areas significantly enriched by the application of CT. Section 3.0 broadens the range of CT application examples through short 1-2 page summaries of a variety of material and component application studies performed at the CT facility. Section 4.0 provides an overview of system enhancements and advanced analysis tools planned and in progress. The Appendix provides an overview of the X-ray imaging modalities, computed tomography, digital radiography, dual-energy, and laminography for the interested reader. Performance measures for the two CT systems derived from their configuration at the time of the report are also presented in the Appendix.

1.2 Wright Laboratory CT Research Facility

The Wright Laboratory/Materials Directorate is a leader in the development and application of CT technology. The X-ray CT Research Facility was instituted as a center for developing improved CT equipment and analysis procedures and to identify successful applications for this evolving technology. As the contributions of CT have become better understood and defined, specific improvements in CT equipment and the related software have been conceived. The Air Force has diligently sought such improvements, both for Air Force applications and as tools for industry.

The Wright Laboratory/Materials Directorate maintains two industrial X-ray CT systems in the research facility. Both CT systems were designed and built by the Advanced Research and Applications Corporation (ARACOR) headquartered in Sunnyvale, California. ARACOR is a leading U.S. manufacturer of high-energy, radiation-based imaging systems and has built, to date, 13 high-energy CT systems and 2 high-energy real-time radiography systems. ARACOR provides on-site support personnel to perform research activities, operate and maintain the equipment, and interface with industry as an agent for transferring defense technology to serve commercial needs.

1.2.1 LAM/DE

The first CT system at Wright Laboratory was installed in October of 1989. The LAM/DE high-energy CT system was developed as a test bed for investigating laminography (LAM) and dual energy (DE) radiographic techniques.[2-3] LAM/DE also serves as a research instrument for computed tomography and digital radiography applications.

In July of 1991, LAM/DE was upgraded to its current configuration (at the time of this report) with the addition of a 420-keV peak-energy X-ray source at 5.0 mA with a 1.5-mm (0.06 in.) focal spot. LAM/DE has a resolution aperture which is variable from 0.63 mm (0.025 in.) to 4.5 mm (0.177 in.) and a slice thickness aperture which is variable from 1.2 mm (0.047 in.) to 15 mm (0.591 in.). LAM/DE has the capacity to handle objects up to 625 mm (25 in.) in diameter, 400-mm (16 inches) high and 100 kg (220 lbs.). LAM/DE has moderate CT resolution of approximately 1 mm (0.040 in.) and typical scan times of about 15 to 25 minutes per slice. The combination of a large handling system and high-energy source lends itself to a wide variety of applications from small materials research samples to large, fully

fabricated components and makes LAM/DE an ideal tool for applications research. Figure 1 shows a LAM/DE CT image of an ordinary flashlight.

1.2.2 Tomoscope

The Tomoscope is a micro-focus CT system designed primarily for the characterization of advanced materials.[4] The Tomoscope first became operational in August of 1991. The system incorporates a CCD-based detector package and a 200-keV microfocus X-ray source for high-resolution applications. Resolutions of 40 μm (0.0015 in.) have been achieved to date. The handling system on Tomoscope was designed for small samples and is capable of handling objects up to 100 mm (4 in.) in diameter, 180-mm (7 in.) high and 5.5 kg (12.5 lbs.). The Tomoscope has an effective resolution aperture of 25 μm and a thickness aperture which is variable from 50 μm (0.002 in.) to 1 mm (0.039 in.). The current radiation source provides a 200-keV (195 nominal) polychromatic X-ray beam at 0.45 mA with a 50-μm (0.002 in.) spot size. An upgrade of the Tomoscope source to a 360-keV peak-energy micro-focus X-ray source at 1.0 mA with a spot size of 60 μm (0.0024 in.) is nearing completion. Typical CT scan times for the Tomoscope (with the current 200-keV source) range from 30 to 120 minutes per slice. Figure 2 shows a Tomoscope CT image of a No. 2 wooden pencil.

1.2.3 Image Analysis

Image analysis is fundamental to the successful application of X-ray imagery. The CT Research Facility offers a broad range of image analysis tools to complement the extensive imaging capabilities. The digital X-ray imaging modalities presented in this report lend themselves to statistical analysis. The application of statistical image analysis tools (e.g., histogram analysis, density graph along a line, etc.) to enhance the presentation of the imagery is used throughout this document. Advanced image analysis tools, such as morphological filtering and automated dimensioning, are also presented.

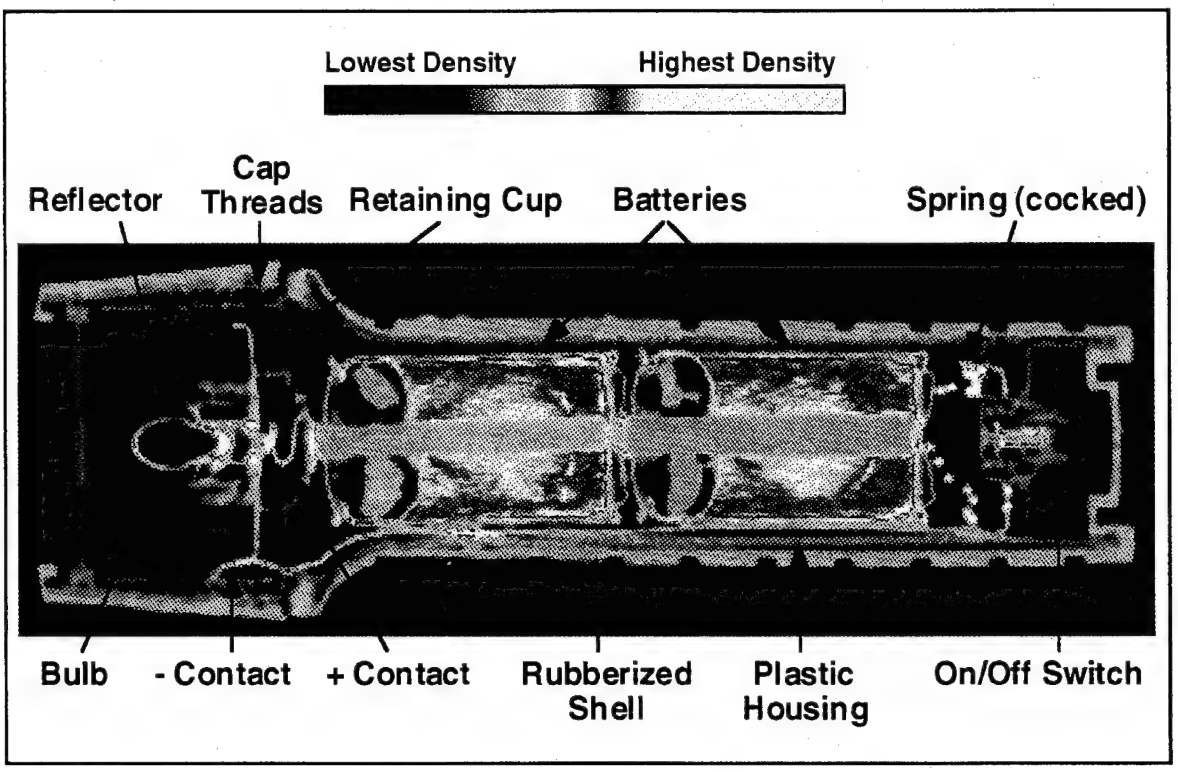

Figure 1. LAM/DE CT image of a flashlight

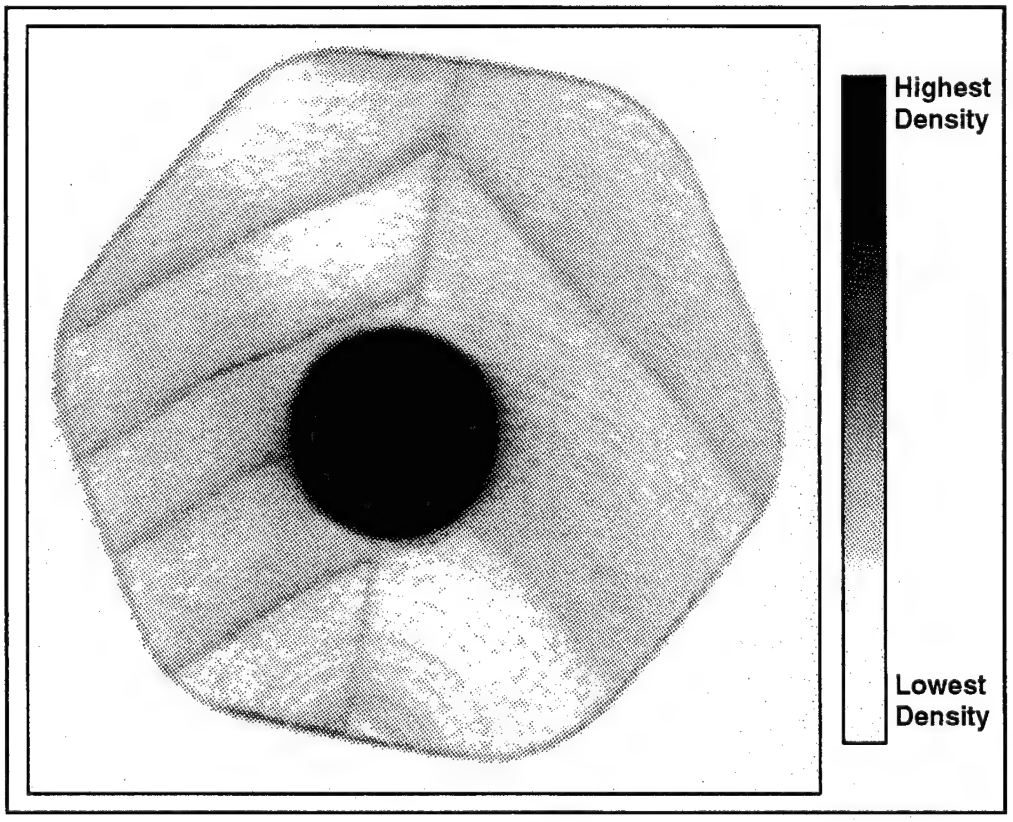

Figure 2. Tomoscope CT image of a wooden pencil

2.0 Applications Scope

Research was conducted on a wide variety of applications for many different defense and industrial customers.[5-7] Through the course of the research, several prominent areas were enriched by the application of CT. For example, CT was shown to be an important tool for process development. Some key applications of CT in the area of process development are presented in the following sections. Additionally, contributions of CT in the areas of design verification, model verification, failure analysis, and quality assurance will be presented.

2.1 Process Development

Process development has long been an arduous trial-and-error task of altering one or two process parameters and testing the part to evaluate the effects of the process changes. This procedure is costly in both time and money, particularly for modern materials that have complex processing cycles. There are three notable areas where CT can provide useful process development information and be cost-effective. These areas are: 1) substitution for costly destructive analysis, 2) supply data for effects of defects studies, and 3) pedigree evaluation. These three uses of CT can speed up process development cycles as well as provide more confidence in the final processed part.[8]

2.1.1 Destructive Analysis

Process development groups often expend substantial resources performing destructive evaluation of materials and components to understand and characterize the internal makeup of parts. For example, foundries will often cut up several castings to inspect for material and dimensional anomalies. Destructive evaluation efforts entail several disadvantages which primarily include the extensive cost associated with losing many components to cut ups, the time involved in labor intensive characterization of the cut up sections, and the inability to gather comprehensive data critical for expedient assessment of casting process parameters. CT can act as a substitute for a number of destructive analysis techniques currently used and provide added capabilities thus far unattainable by traditional methods. This approach can significantly enhance and accelerate process development efforts.

2.1.2 Effects of Defects Studies

The term "defect" is often a very difficult one to define. For example, a crack termed as a defect may not actually be detrimental to the part. This concept is very important in composite materials. Traditionally defined damage such as cracks may actually enhance the performance of some composites by relieving stress concentrations, thus improving the performance of the part. As materials become increasingly complex, the term "defect" needs to be used very carefully. CT can assist in determining the impact of a particular defect on part performance. Features identified prior to material testing can be correlated with test results. This allows process development efforts to focus on those defects that actually degrade part performance.

2.1.3 Pedigree Evaluation

Many modern materials undergo a number of complex processing steps. Some composite materials undergo repeated lay-up, consolidation, curing, and post-curing cycles before the process is complete. Collecting CT data at key stages of process development can

help locate the onset of problems. If parts are only inspected at the end of all processing or at limited stages, then underlying causes leading to defects cannot be easily ascertained. Pedigree evaluation provides a method of tracking the evolution of a defect while optimizing a process. Incipient flaws can be detected in the early stages of process development. When detected early these precursors to material degradation can be corrected or, at worst, unnecessary processing of flawed material can be avoided. CT data used in this manner can significantly expedite new development efforts.

As an example, CT was used for pedigree evaluation of CMC components being developed for use in high-performance turbine engines.[9] Chemical vapor deposition (CVD) is a technique being investigated for fabrication of CMC components. CVD takes a ceramic fiber preform and forces a hot gas into the structure which deposits ceramic material on the fibers. Several processing runs are required for each component. A goal of CVD processing is to produce a component free of excessive porosity while minimizing the number of required CVD runs. A potential problem with CVD processing is that the chemical vapors preferentially deposit ceramic material on the outer layer and near surface areas of the preform. The external surfaces can densify to the point that interior areas of the part are no longer subjected to the vapors. This can result in significant porosity (or lower mean density) at the center of the part

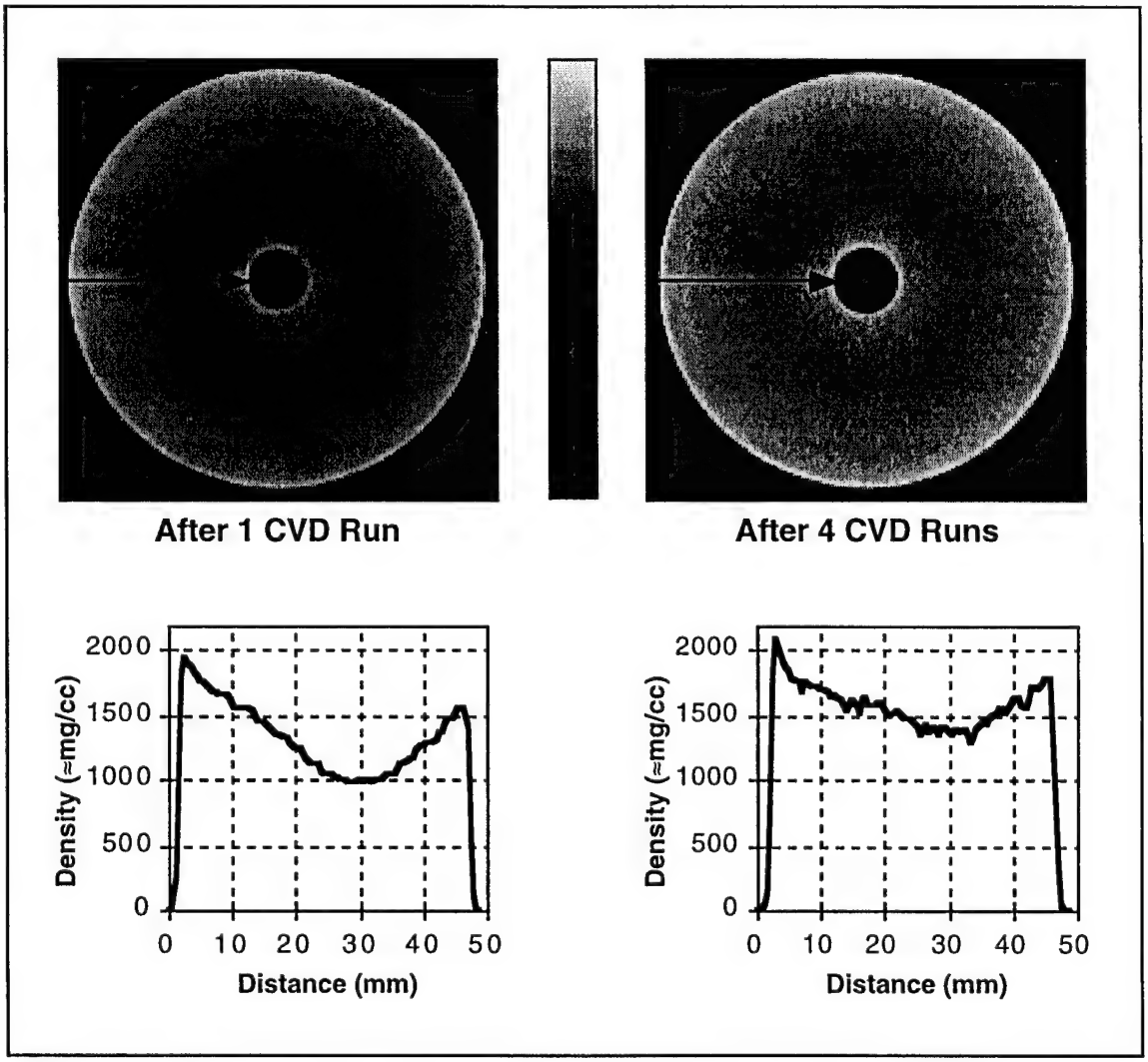

Figure 3. Pedigree evaluation of the CVD process

as well as wasted processing time. CT can track internal density gradients and surface densification after each processing run. This characterizes the process in such a way that the optimum number of CVD runs is identified. Eliminating CVD runs or reducing the time of each run can translate into significant cost savings.

Figure 3 shows CT imagery from a 200-mm-diameter CMC disk at two stages of CVD processing. The image on the left shows the disk after one CVD run and covers a density range of approximately 1.0 g/cc to 1.9 g/cc. The image on the right shows the disk after four CVD runs and covers the density range of approximately 1.4 g/cc to 2.0 g/cc. Density values along a line through the disk are graphed below each image. In both disks, the density is lowest midway between the outside surface and the inner hole. However, after four CVD runs, the variation is less dramatic and the disk is becoming more uniformly dense.

2.2 Design Verification

In addition to material characterization and flaw detection, CT provides faithful geometric representations through cross-sectional planes. A nondestructive geometric acquisition tool enables dimensional measurement of internal features without destructive sectioning and can also provide a cost effective path for reverse engineering. These valuable capabilities applied to the area of design verification are discussed in the following sections.

2.2.1 Dimensional Measurement

A study was conducted at the Computed Tomography Research Facility to determine the feasibility of using CT for dimensional inspections.[10-11] Dimensional characterization of intricate components with detailed internal features is both costly and time consuming by traditional methods. Customary metrology tools include coordinate measuring machines (CMM) and laser scanning systems. CMM records surface profiles of a part through the intimate contact of a probe moving along the surface. Laser scanning provides a topographical map of the surface of an object by using a noncontact laser beam. To acquire information on internal features, CMM and laser scanning require destructive sectioning to expose internal details. A measurement technique based on CT technology would allow geometric interrogation and characterization of inaccessible features without destroying the part.

The CT-based measurement methodology described below was applied to an intricate aluminum sand casting. The casting has a height of 255 mm (10 in.), a maximum diameter of 320 mm (12.6 in.), a weight of 14 kg (30 lbs.), and it contains numerous internal passages. Two of these passages are separated by a thin wall whose minimum thickness is the feature of interest to be measured. Figure 4 shows a typical CT image through the thin-wall region. Note that the CT image provides a density map through a region that would be exposed through destructive sectioning by conventional methods.

For the study, sets of independent measurements were acquired from two different castings to determine not only the wall measurements but the confidence of those measurements. Following the CT measurement of the two castings, the manufacturer measured the thin wall regions using conventional methods. The castings were sectioned open and the thin wall region was incrementally milled and measured. The CT measurements and the measurements obtained through destructive evaluation are shown in Figure 5.

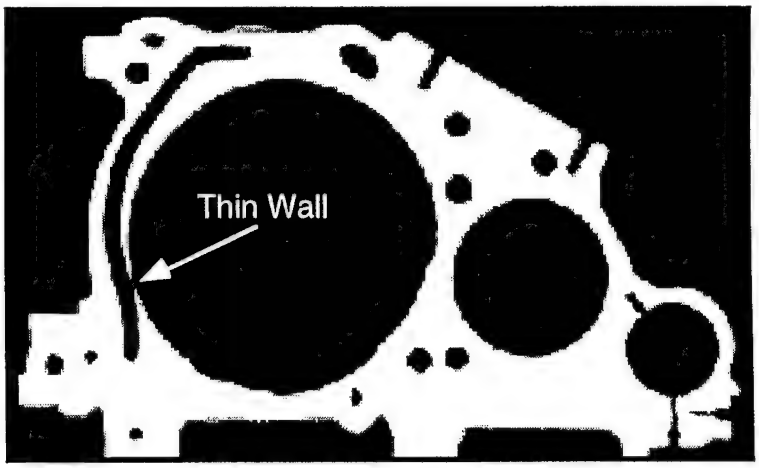

Figure 4. LAM/DE CT image showing thin wall region

	CASTING A	CASTING B
CT Measurement	1.45 ± 0.09 mm (0.057 ± 0.003 in.)	0.56 ± 0.09 mm (0.022 ± 0.003 in.)
Cut-up Evaluation	1.45 mm (0.057 in.)	0.51 mm (0.020 in.)

Figure 5. Table of CT thickness measurements vs. destructive evaluation

The standard deviation for each set of CT measurements was about 0.025 mm (0.001 in.). Thus, wall measurements from CT data can be determined with a three-sigma confidence of about ± 0.076 mm (0.003 in.). Note that the cut up evaluation measurements were within the three-sigma confidence interval. The standard deviation of the measurements depends on the resolution of the system and the pixel size. For this study, dimensional measurements with a standard deviation of about 0.025 mm (0.001 in.) were obtained from CT imagery with 0.332 mm (0.013 in.) pixels. Any improvement in the resolution and pixel size should result in a comparable improvement in the standard deviation of the measurements. Also, typical CT scan times for this study were just under 20 minutes each. The scan times could be significantly reduced if such high confidence in the measurements is not required.

Using CT for dimensional measurement has several advantages over traditional methods of dimensional characterization. CT is nondestructive; internal features can be measured without losing the asset. CT dimensional characterization can be performed without part-dependent programming as is common with coordinate measuring machine methods. The measurement procedure can easily be applied to a wide variety of objects with various geometries and material compositions. CT imagery can be collected in times ranging from a few minutes to a few hours. A tremendous cost savings over traditional methods is realized with CT analysis; parts are preserved, programming time is not required, and CT analysis of a complex part can be done in a matter of several hours.

2.2.2 Reverse Engineering

Another area of CT application related to dimensional measurement is reverse engineering. Reverse engineering is an important technology to the Department of Defense and

in the manufacturing industry. Often in the manufacturing of spare or replacement parts, CAD descriptions or even original hard copy drawings do not exist. In other cases, drawings may be inaccurate due to manufacturing process changes that were never updated on the drawing or CAD file. With rapid prototyping applications, a CAD file is required and must be generated from hard copy drawings if the CAD description does not yet exist.

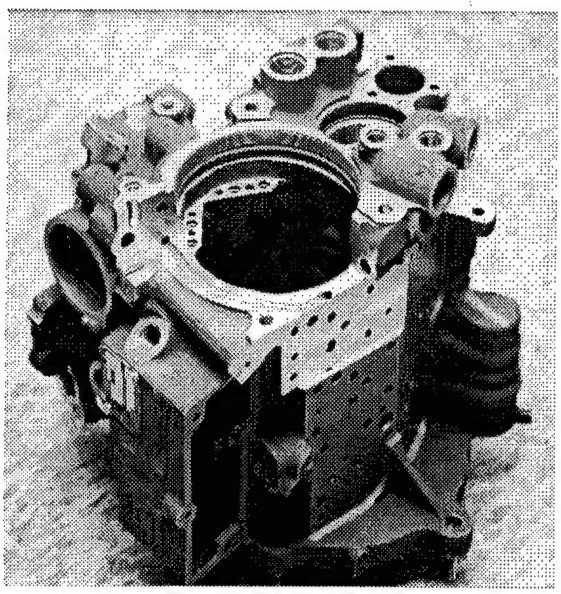

Figure 6. Photograph of aluminum casting

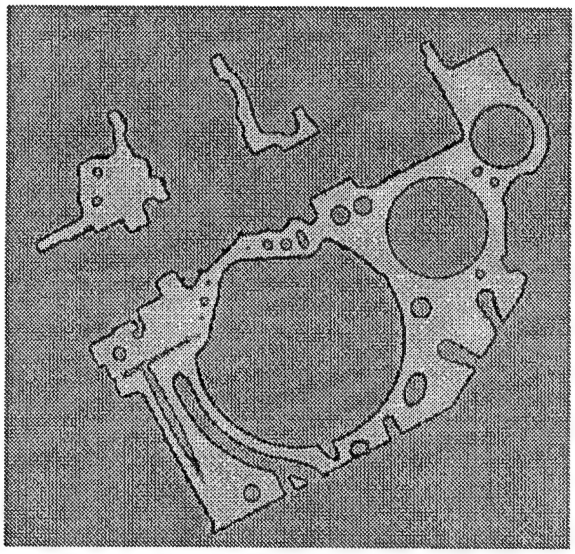

Figure 7. CT image through cut-out region

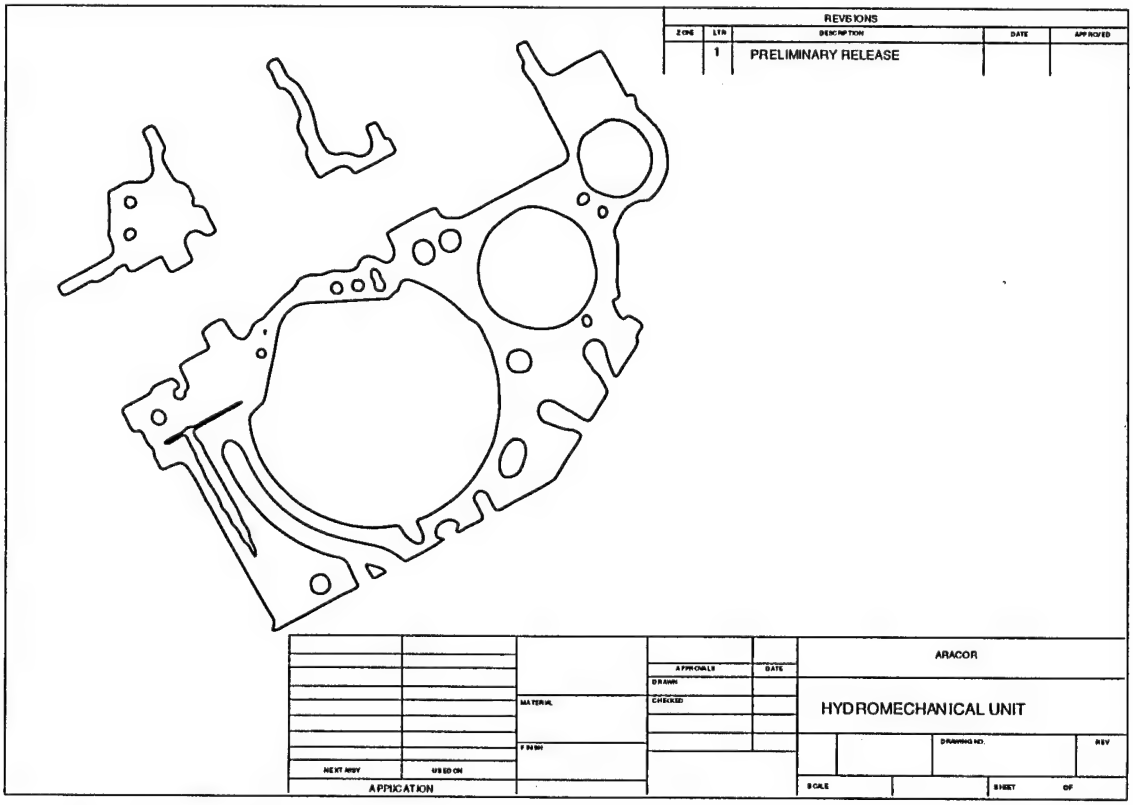

Figure 8. CAD representation of Al casting acquired from CT data

Given the fact that thin walls can be accurately measured through CT analysis, it is a simple extrapolation to acquire precision contours through the entire image. CAD representations of original parts can then be generated from the contours.[12] Figure 6 shows a photograph of the aluminum casting. Figure 7 shows a CT image of the casting. A contour was generated from the CT image of Figure 7 and processed into the CAD representation of Figure 8. The CAD drawing was generated from CT data. CT can provide a quick, cost effective method of creating CAD representations of existing parts or of comparing an existing component with its engineering documentation.

2.3 Model Verification

Another area of process development where CT can make an impact is in the verification of processing and structural models.[13] Models generally require information regarding the internal structure of the object to be analyzed. For example, a simple mechanical analysis of a composite material would require as input the volume fraction of the fibers relative to the matrix. A more complex model may require data on the spatial distribution of the fibers while an even more complex model may need the location of porosity or defects and other variations in density within the matrix. A typical approach to obtaining these data would be to make assumptions for a given part based on destructive analysis of similar components. CT can provide a significant advantage over this approach in that the internal makeup of the actual test object can be determined and used as input to the model. Predictions from the model can then be compared with test results and destructive analysis.

Figure 9 shows the CT image of a metal-matrix composite (MMC) coupon inspected with the high resolution Tomoscope CT system. The sample contains a random distribution of fibers and some cracks running between fibers. Image processing tools were applied to the CT imagery to produce the idealized representation of the composite shown in Figure 9. The idealized image is created by defining the fiber diameter, sample dimensions, center location of each fiber, and crack starting and ending points. Thus, CT data can provide volume fractions of fibers and matrix, a detailed map of precise fiber positions, and statistical parameters detailing fiber and crack distributions. Providing accurate parameters to a model allows the model to better represent structural and microstructural reality. Small deviations from the true parameters can result in inaccurate predictions or unwarranted confidence in an invalid model. CT provides an excellent nondestructive means of supplying accurate information on geometry and density variations as well as defects and flaws that can enhance the accuracy of modeling predictions.

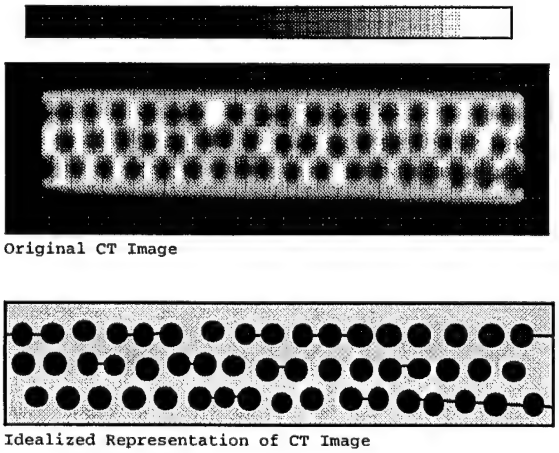

Figure 9. Tomoscope study of MMC coupon

Another contribution of CT to modeling is that input data can be generated at various stages of processing or testing. While destructive analysis means the end of testing for a given part, CT can be used to verify intermediate results from a model. An example of this can be seen in the soil mechanics field. Models have been developed to predict the compaction of soil under varying loads. Figure 10 shows a CT image of two cylinders. The cylinder on the left is filled with spherical marbles of various sizes. The cylinder on the right is filled with rocks. The marbles are used as a control since their geometry can be determined accurately from the CT data given the *a priori* information about their shape (i.e., spherical). This information aids in the determination of the number of "touching points" on each rock (i.e., the number of points touching another rock). The procedure can then be used to determine the behavior of the rocks under various forms of compaction. CT provides the model with the initial distribution of the rocks and is later used to verify model predictions by compacting the rocks and generating the new distribution. The actual rock distribution is used in the model rather than approximating the distribution with an idealized representation of the rocks.

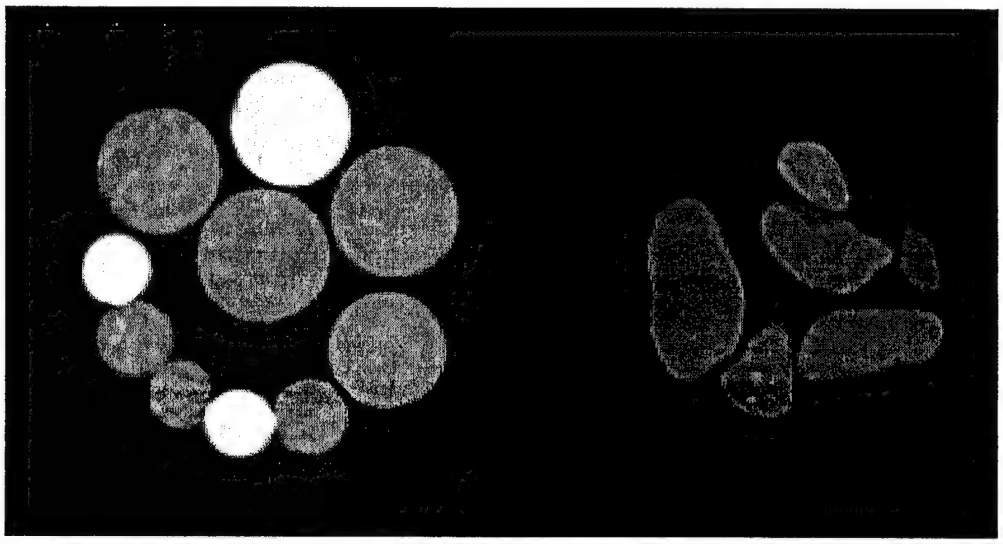

Figure 10. LAM/DE CT image of rock packing

2.4 Failure Analysis

A common problem encountered in component level failure analysis occurs when disassembly alters the conditions of failure. For example, an assembly which is spring loaded could have a kink in the spring which would not be easily detected if the spring is unloaded during disassembly. Computed tomography is well suited to the analysis of failed components. To illustrate this we will consider the case of a failed proximity switch for an aircraft landing gear actuator. The switch failed in operation and could not properly indicate that the landing gear was down and locked into position. Figure 11 shows a digital radiograph and CT image of the actuator. The region of interest in this component is the actuator pin which is located vertically through the center of the component and glides inside of a support shaft. The pin cannot be distinguished from the shaft in the radiograph and in some areas the shaft is completely blocked by the superposition of other features in the object.

The CT image of the failed actuator shown in Figure 11 was acquired at the location indicated on the digital radiograph. The CT image clearly shows that the actuator pin is not centered within the support shaft. The pin had become cocked during operation and jammed

inside the support shaft. This analysis supported the suspicions of the aircraft's maintenance crew.

Additionally, the actuator is a spring loaded device and the actuator pin was under an applied load in its failed condition. Destructive analysis or inspection by disassembly of this component would have resulted in an unloading of the spring mechanism and release of the pressure which caused the actuator pin to jam. This disruption in the actual failure condition would have allowed the pin to dislodge and would have eliminated all evidence of the source of failure.

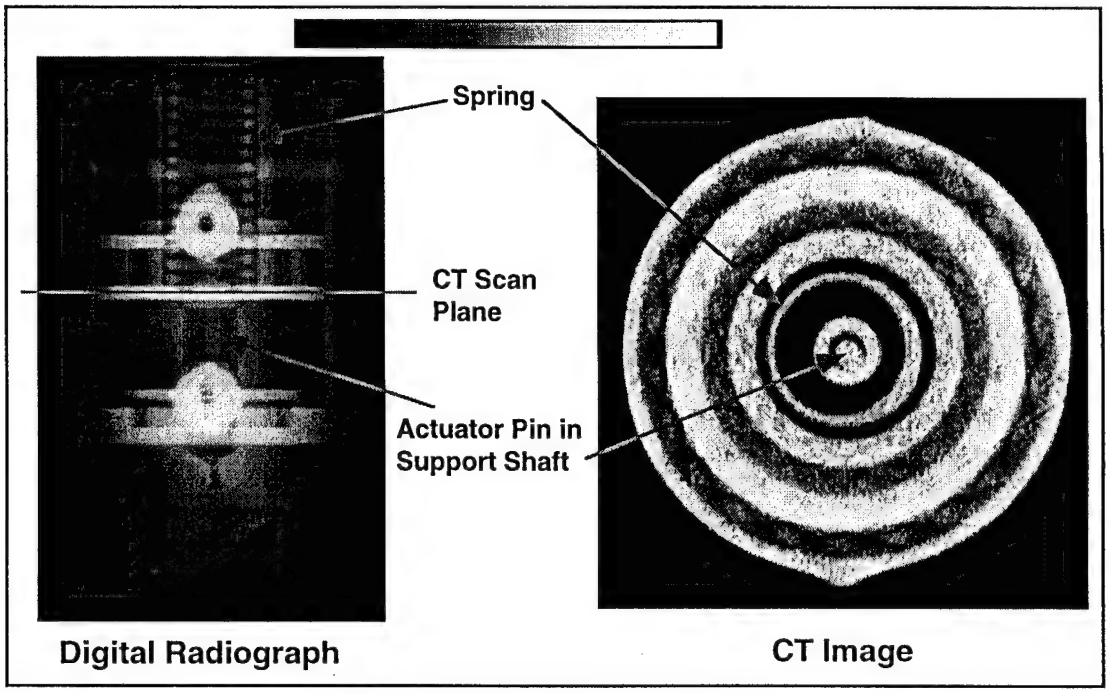

Figure 11. Landing gear actuator

2.5 Quality Assurance

CT has the potential for tremendous cost savings in the area of quality assurance. As an example CT analysis was conducted on fiberglass leaf springs used on large trucks. The springs had been rejected; ultrasonic inspection indicated interior damage. The manufacturer conducted destructive analysis of similar leaf springs that had failed ultrasonic inspection. The cut up analysis showed the springs were incorrectly diagnosed by ultrasonic testing. Figure 12 shows the CT imagery for other springs rejected by ultrasonic testing. Various stages of porosity or cracks were observed. Some of the damage states were acceptable and some were not. The two springs at top right and bottom left show obvious cracks which are cause for rejection of the part. The spring on the top left shows porosity which is connected. This is also cause for part rejection. The spring on the bottom right shows small pockets of porosity. Since the porosity is not connected, this part is still acceptable. The conclusion of the study was that CT could detect the difference between three states of damage: 1) cracks, 2) connected porosity, and 3) unconnected porosity. Ultrasound could detect the presence of porosity but could not distinguish between the different states.

In some cases, as with the fiberglass leaf springs, CT can differentiate critical and noncritical defects where ultrasound or other NDT modalities cannot. However, in other

applications, CT can be used to strengthen the diagnostic ability of another NDT modality. Damage state indications detected by ultrasound, for example, could be correlated with CT inspection results to develop improved ultrasonic accept/reject criteria. Improved quality assurance tests can result in recapturing improperly failed components and in appropriately pulling units that should not have passed a quality assurance screen. Cost savings are realized in both areas.

Some quality assurance testing is traditionally done by destructive analysis only. For example, if an inaccessible dimensional measurement is required, a number of samples are taken from each lot for destructive sectioning. If an unacceptable failure rate occurs, the entire lot is scrapped. CT can acquire the dimensional characterization of an inaccessible feature without destructive analysis (see Section 2.2 Design Verification), thus retaining the sample parts. Also, if the failure criteria for the lot is reached, the entire lot need not be scrapped. CT can sort the acceptable units from the lot through the application of CT-based accept/reject criteria.

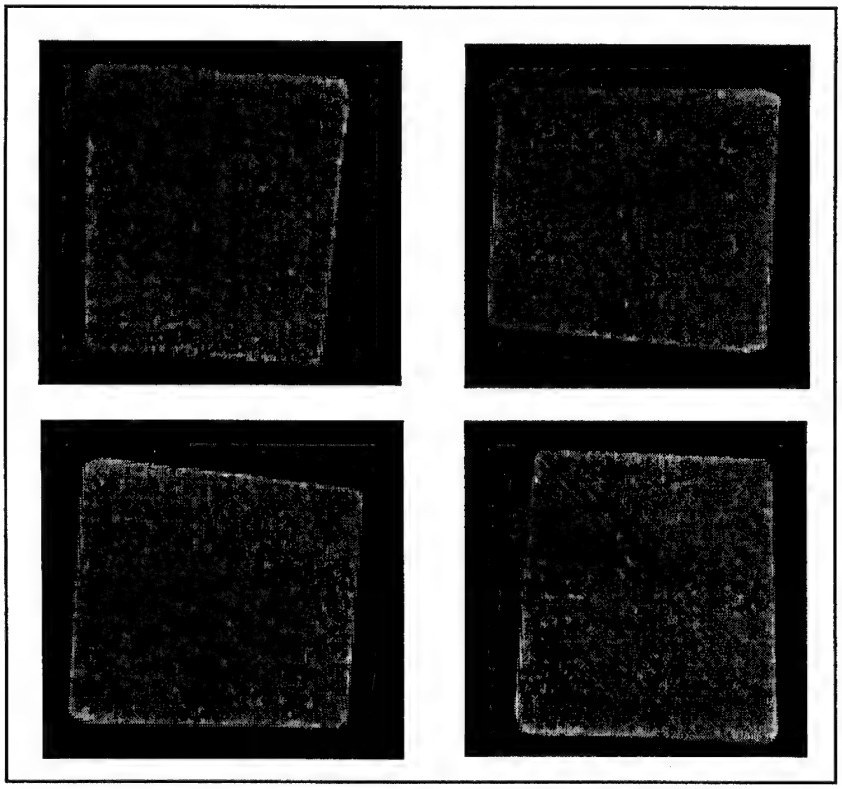

Figure 12. LAM/DE CT image of fiberglass leaf spring

3.0 Material and Component Evaluations

Computed tomography research of the Wright Laboratory/Materials Directorate over the last 5 years demonstrated the success of X-ray imaging techniques for a wide variety of applications. This section of the document presents a small sampling of notable applications covering a broad range of material and component types. Each application is presented as a brief 1 to 2 page summary. The following table identifies application areas for the studies covered in this section.

	Page Number	Process Development	Design Verification	Model Verification	Pedigree Evaluation	Quality Assurance	Failure Analysis	Other Application
Composites								
MMC Core Analysis		x	x				x	
MMC Coupon Analysis		x		x			x	
CMC Coupon Analysis		x		x			x	
CMC Hoops		x						
Ceramic Processing		x		x	x			
Composite Nozzle		x	x		x			
Composite Phone Pole		x				x		
Composite Airfoil		x	x	x				
C-C Brake Rotors		x		x				
Fiberglass Panels				x			x	
Castings								
Hinge Casting		x				x	x	
Fuel Pump							x	
Tenth Century Statue								Art Authentication
Other Materials								
Carbon Samples						x		
Carbon Foams		x						
Fatigue Test Specimen				x				
Solid Rocket Propellant				x		x		Chemical Migration
Other Components		x		x	x			
Thermal Storage Units								
Air Conditioner Unit		x	x	x				
Airbag Initiators		x						
Crystal Oscillator						x	x	
Electric Insulator						x	x	

Figure 13. Table of evaluation summaries

MMC Core Analysis

- Process Development
- Design Verification
- Model Verification

Metal-matrix composite (MMC) ring structures are being developed for aeropropulsion applications such as jet engine rotors. Figure 19 shows two LAM/DE CT cross sections of an MMC ring 200 mm in outer diameter by 25 mm thick with a square cross section 25 mm on edge.[14-15] The core of the ring (which is dark in the images) is a titanium matrix, SiC fiber MMC. The core is wrapped in a thick titanium cladding (the bright outer edges). Ideally, the MMC core should be centered in the ring and its cross section should have a uniform shape. Deviation from ideal may result in loss of strength and an unbalanced center of rotation. The data can be useful during process development to determine the effect of processing changes on the internal structure of the ring. The data can also be used to check the as-manufactured configuration versus the as-designed configuration and then model directly the as-manufactured configuration to see if it meets the design goals.

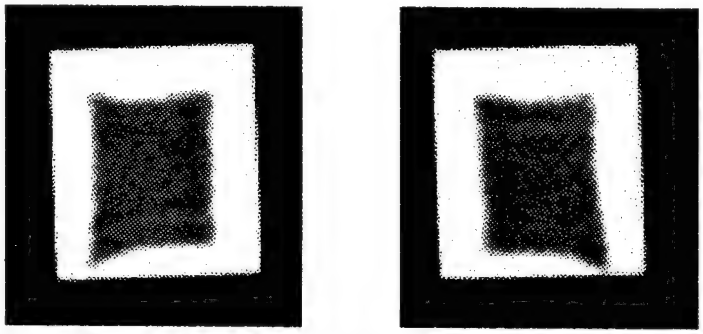

Figure 14. CT images of an MMC ring with an off-center core

MMC rod structures are manufactured for use as tensile test samples. Figure 15 shows LAM/DE CT cross sections of three machined rods. Originally the rods were being manufactured and machined prior to any CT analysis. As Figure 15 clearly shows, because the MMC core was not centrally located in the titanium cladding, the machining operation actually cut into the MMC core in some cases. CT scans were taken of the rods before machining in an effort to provide guidance to the machining operation. The actual location of the rod was noted and machining was performed such that the core would be left in the center of the sample.

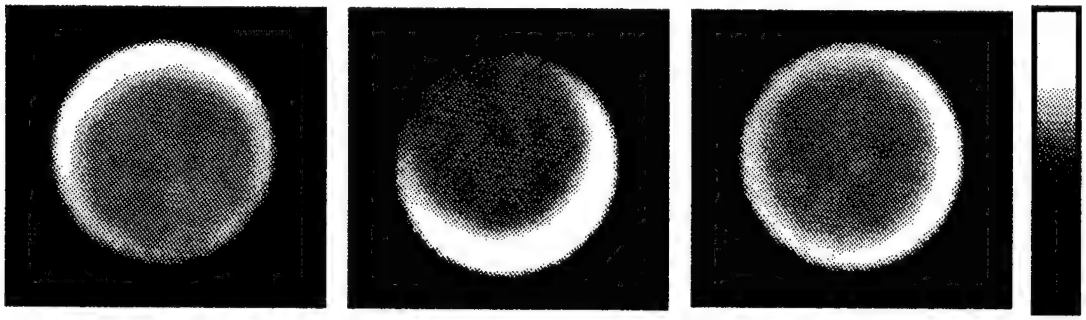

Figure 15. CT images of machined MMC tensile test rods

MMC Coupon Analysis

- Process Development
- Model Verification
- Failure Analysis

Figure 21 illustrates the results of a Tomoscope study of a metal-matrix composite sample which was wrinkled during manufacture. The sample is a $[0/90]_{2s}$ symmetric lay-up; that is, the SiC fiber layers are oriented at zero and then 90 degrees with the central two layers in the same orientation. The wrinkle is illustrated in the figure. Two orthogonal CT slices are shown. Section A-A cuts across the wrinkle and the indentations on each side identify the wrinkle in the image. A large spacing between fibers in the second ply from the left can be seen in this image. Section B-B cuts parallel to the wrinkle and the long indentations in the middle identify the wrinkle. In this image, several of the fibers running perpendicular to the CT slice plane appear to be missing. These images coupled with radiographic images indicate the wrinkle was caused by wide spacing between two fibers over a given region. The spacing caused the composite to "cave-in" during processing and subsequently break many of the fibers running perpendicular to the wrinkle. Finding the cause of wrinkles during production has been a major concern. CT was instrumental in identifying the effect of the wrinkles. These data could be useful during process development to assist in determining the cause of the wrinkles.

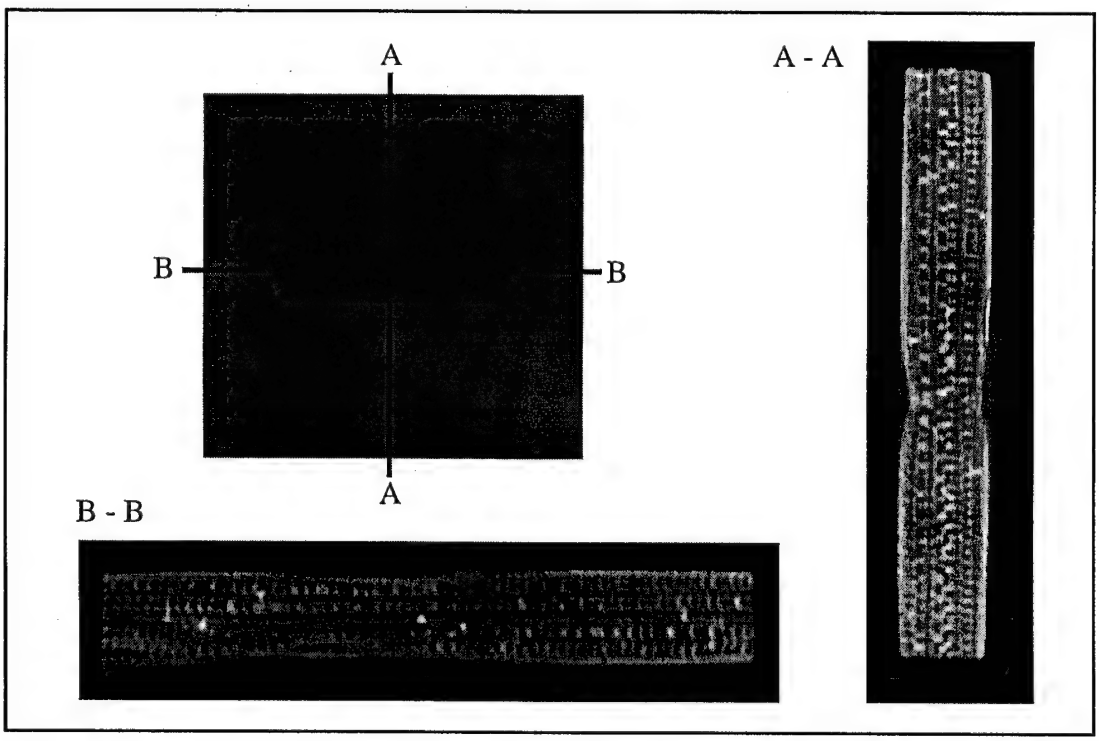

Figure 16. Wrinkled MMC specimen

CMC Coupon Analysis

- Process Development
- Model Verification
- Failure Analysis

Figure 17 illustrates the results of a Tomoscope study of CMC coupons tested to failure.[16-18] The CMC specimens consisted of unidirectional plies of SiC fibers (142 μm diameter) in a Si_3N_4 matrix. During tensile testing, some of the SiC fibers break. Due to tensile strains in the fibers and a weak fiber-matrix bond, the broken fibers "pull-back" and leave a void in the material which is referred to as fiber pull-out. The top image is a digital radiograph (DR) of a CMC coupon showing the presence of fiber pull-outs which show up as dark vertical lines. The CT image at the bottom is taken at the line location indicated on the digital radiograph. Here, the fiber pull-outs show up as dark "holes" in the composite. These images illustrate the difference between radiography and CT. DR can detect the presence of features and CT can detect the presence and location of features. The data were used to better understand the failure mechanisms in these composites as well as verify models of the failure process. Future work will couple these data with processing models to determine how to best process this material to meet the performance requirements.

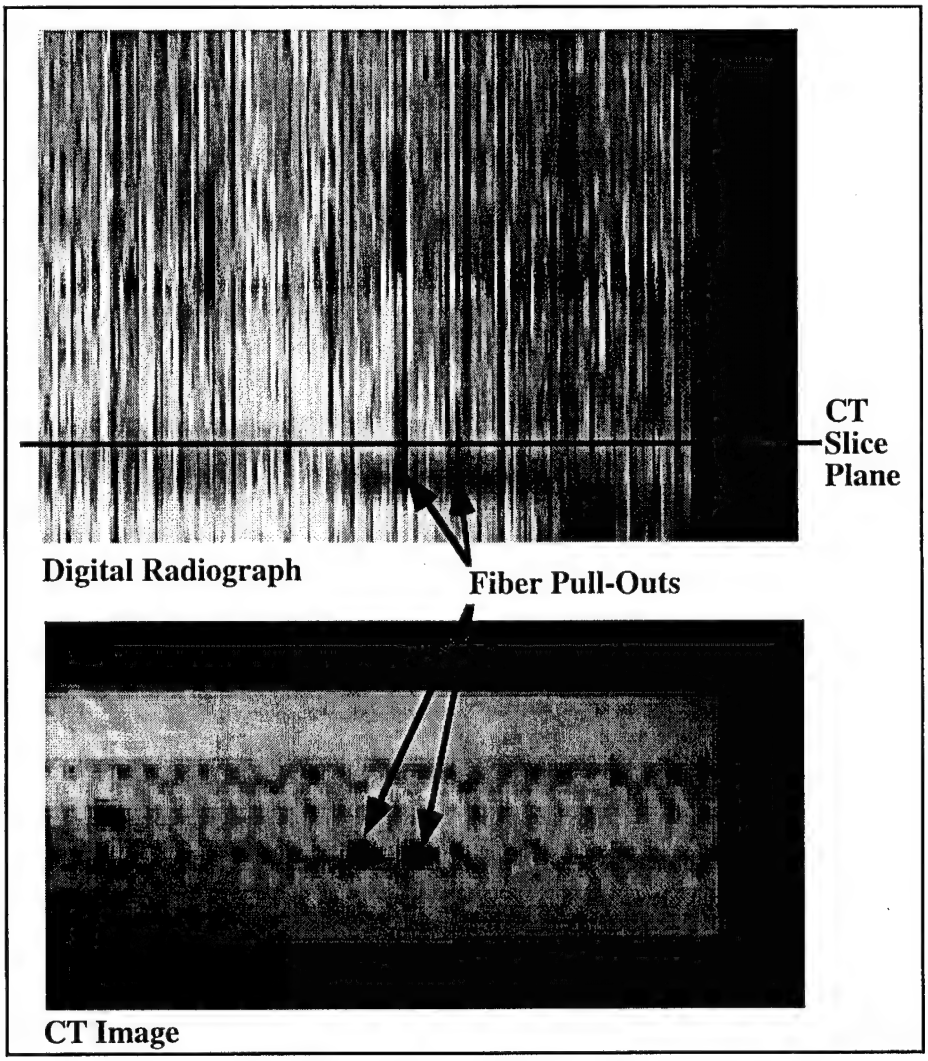

Figure 17. CMC with fiber pull-out

CMC Hoops

- **Process Development**

Figure 20 presents an example of LAM/DE imagery obtained in the inspection of a group of ceramic-matrix composite hoops. A comparative analysis among the hoops was requested. The hoops were processed using different methods and the CT data provided an efficient method of highlighting the material variations resulting from the different processing methods. Measures of the variability of hoop density was provided through a histogram analysis of the imagery. The histogram peaks indicate the average density of each set and the width of the bottom of the peaks indicate the variability. Note how clearly the histograms of the two hoops shown in Figure 20 contrast the densification of the hoops. Additionally, voids and delaminations were detected. Density variations of greater than 30% across the wall were seen in several hoops. The graph of Figure 20 showing density along a line through Hoop #1 depicts an example.

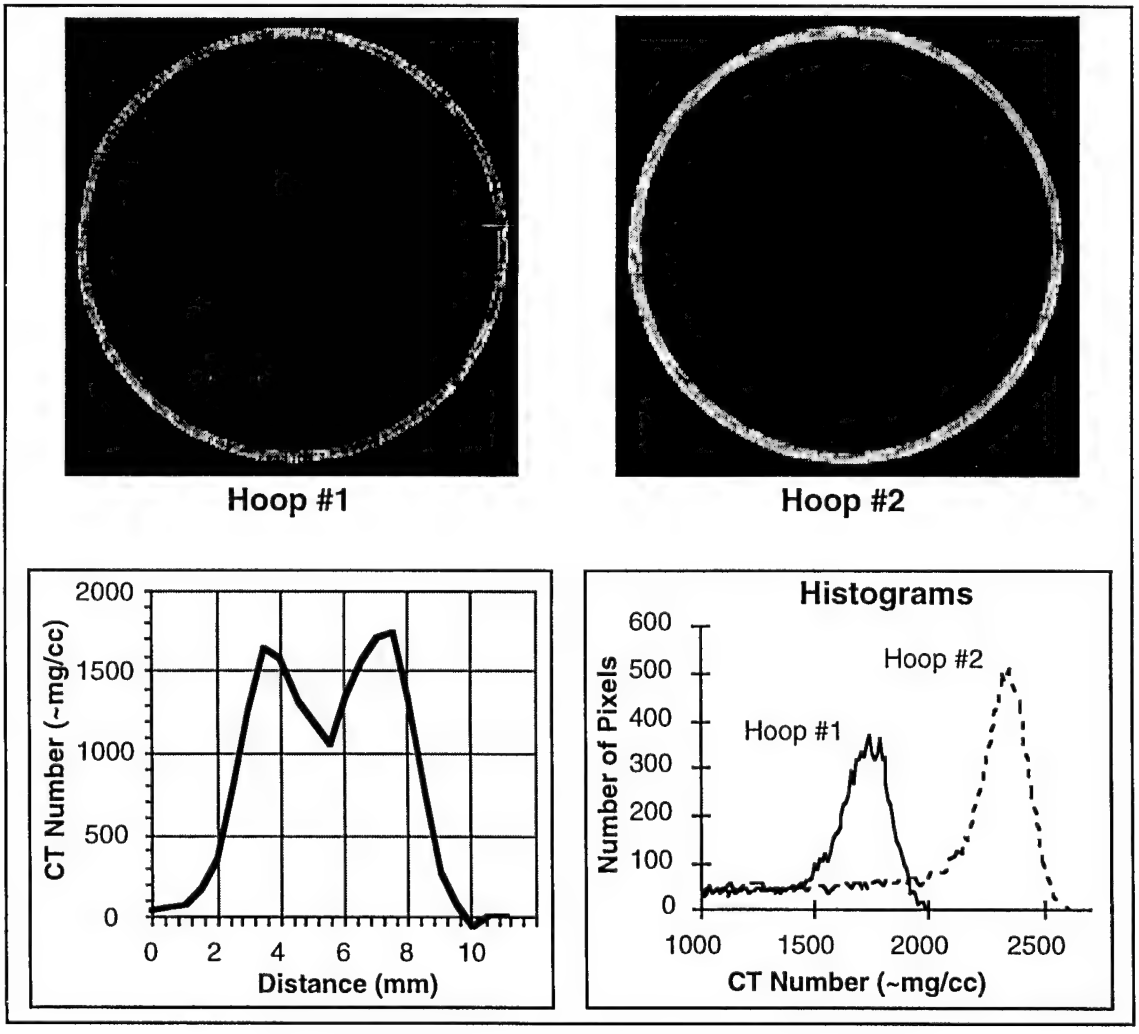

Figure 18. Ceramic matrix composite (CMC) hoops

Ceramic Processing

- Process Development
- Pedigree Evaluation
- Model Verification

Researchers at The Ohio State University are using CT to study the evolution of density gradients during dry pressing and firing of ceramic powders. One of the many advantages CT offers to this research is the ability to monitor changes in density during the actual pressing and firing operations. Additionally, while most research in this field has focused on increasing overall compact density, CT provides the unique capability to evaluate compact uniformity and how it is affected by variations in processing. Compact uniformity is a property of ceramic powder processing which significantly influences part quality because a nonuniform compact may result in warping or cracking due to differential shrinkage during firing. This work has lead to the first quantitative measure for compact quality.

Figure 19 shows histograms of three dry pressed ceramic compacts. The compacts are of the same shape and size but were made with different material compositions. Conventional analysis of these compacts would involve measuring the overall density and visually evaluating the quality of the part. In Figure 19, the high clay batch presses most easily and is visually of the highest quality, followed by the intermediate batch and then the high frit batch. There is little visual difference in quality between the high clay and intermediate batches. The quality of a compact is a function of the distribution of its density. Compact quality can therefore be defined by the width of the histogram generated from CT data. With this approach, the difference in quality of all three compacts is readily apparent and easily quantified.

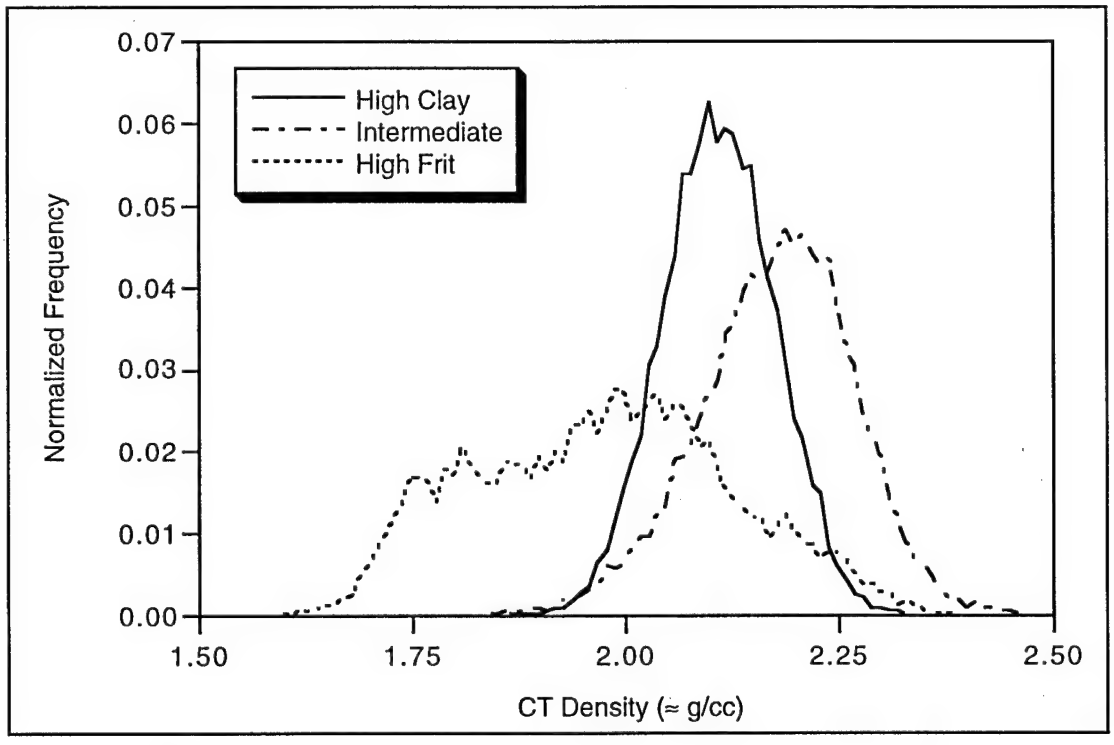

Figure 19. Histograms of three dry pressed ceramic compacts

Figure 20 shows three LAM/DE CT images of a ZnO compact at different stages of dry pressing. A specially designed electro-mechanical press was used to collect the CT data *in situ*. The images show a significant change in the density gradients in the early stages of pressing. This is the first time low pressure density gradients have been visualized and has led to new understanding of the dry pressing process. The results are being employed to verify dry pressing models and as input for sintering models.

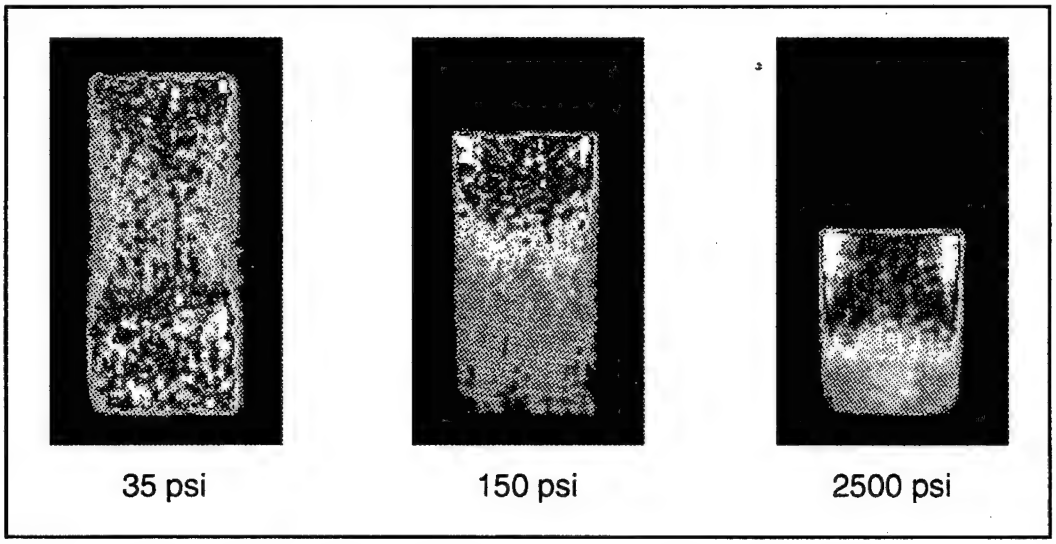

Figure 20. Ceramic powders at various stages of dry pressing

Figure 21 shows three LAM/DE CT images of a ZnO compact prior to and during firing. The image on the left shows the compact in the as-pressed state. Note the small low density zone located in the center of the compact. This low density zone is approximately 3.5% less dense than the immediately surrounding regions. After 5 minutes of sintering at 1100 °C, this seemingly insignificant gradient has evolved into a defect which is 17.5% less dense than the surrounding regions. After 20 minutes of sintering the defect is 18% less dense. This is an example of how CT can both track defects across processing stages and aid in the evaluation of the effect of defects.

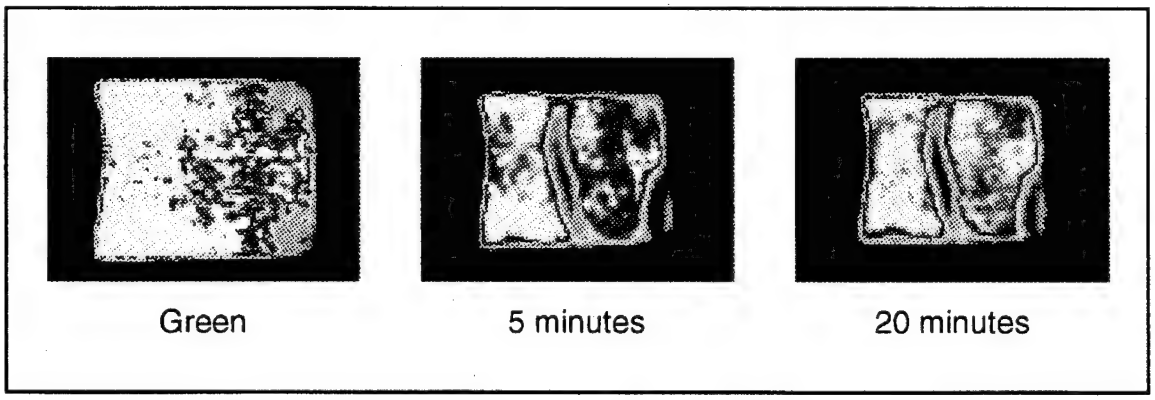

Figure 21. Ceramic compacts at various stages of sintering

Composite Nozzle

- Process Development
- Pedigree Evaluation
- Design Verification

CT inspection of a 3-D woven-composite thrust vectoring nozzle was performed to identify internal defects and provide a method of comparing the part dimensions before and after operational testing. CT inspection revealed separation of the layers throughout the part (Figure 22). This separation appears as a low density semicircular region and is consistent with the density of the resin. This indicates the separation of the layers is a resin rich region and not a delamination. Effect of defect studies had shown a delamination to be a serious concern, but a narrow resin rich region has no effect on part performance. The CT images also illustrate the effects of operational testing. Hot gasses passing through the nozzle resulted in an erosion of the interior wall. This erosion is manifested as a loss of material and significant decrease in density at the interior surfaces. To illustrate the decrease in density, histograms of the density distribution through the CT images before and after operational testing are included. The effects of the hot gasses can be seen by the broadening of the histogram and the emergence of a secondary peak which indicates a significant increase in the fraction of the low density regions. A key feature of this testing is that the CT images were acquired from the same nozzle before and after testing. CT imagery acquired in this way helped in determining the effects of operational testing and qualify the design for the hot gas environment.

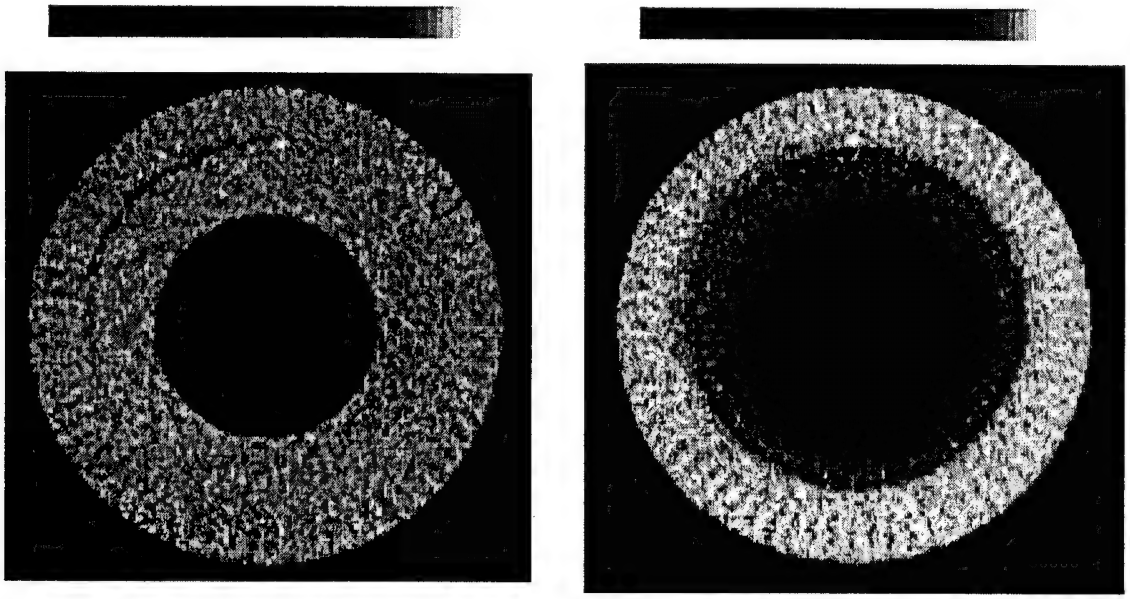

Before Operational Testing

After Operational Testing

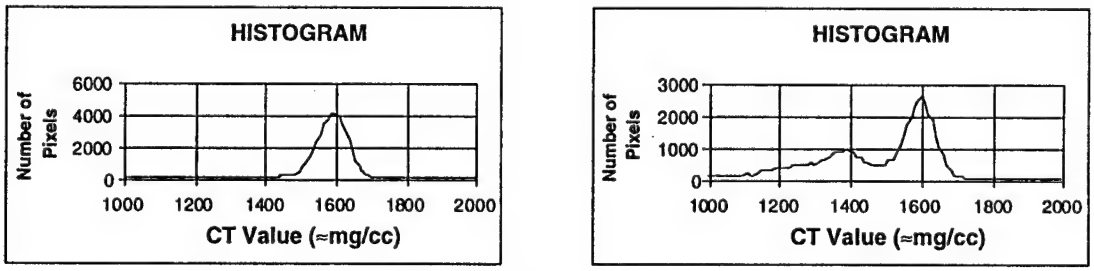

Figure 22. LAM/DE CT images of a composite thrust nozzle

Composite Phone Pole

- **Process Development**
- **Quality Assurance**

A 2-foot section of a prototype, fiberglass composite power pole exhibited a longitudinal crack through visual inspection. The section is a hexagon approximately 1 foot in diameter with longitudinal "T-slot" like tracks for scaling the pole. Anomalies were detected throughout the object (Figure 23). Thinning of the material and voids were observed in the region of the visually detected crack. A similar thinning condition was noted in the next track to the right (counter-clockwise). Additionally, radial cracking was detected in each of the track flanges. Typically, the crack patterns exhibited little change over several inches. Data of this type can be used to determine processing changes that could help eliminate cracks and voids in the composite structure, especially in the high stress regions.

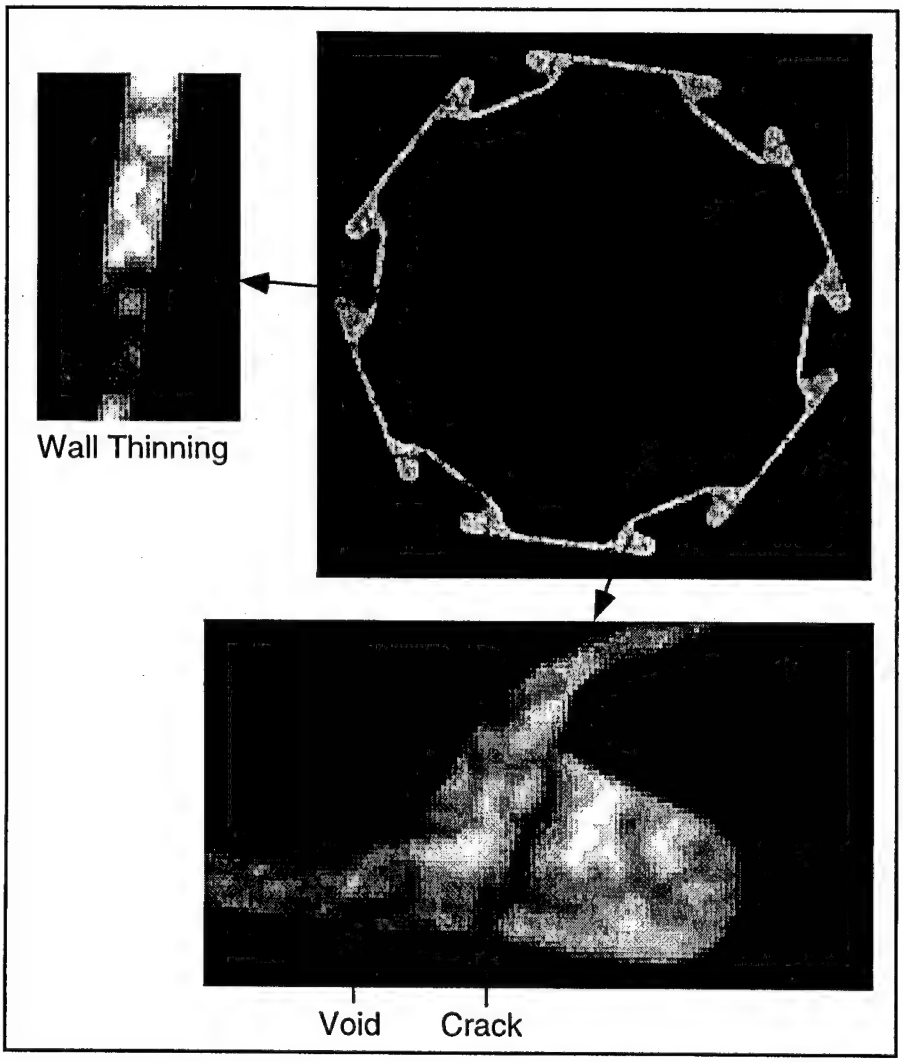

Figure 23. Prototype power pole

Composite Airfoil

- Process Development
- Design Verification
- Model Verification

Figure 24 shows a CT image of the airfoil section of an aircraft propeller blade. The blade consists of a foam core (shown in blue) surrounded with a chopped Kevlar fiber composite material (shown in red). An aluminum piece (shown in white) is fastened to the leading edge of the airfoil. In this particular case, a seal had broken near the root of the blade allowing oil to penetrate the foam core. CT was originally used to inspect the foam core to determine the extent of oil leakage along the length of the blade. The oil appears as light blue near the center and right-center of the foam core. In addition to identifying the extent of oil in the foam core, the CT images also revealed cracks in the Kevlar composite at both the leading and trailing ends of the air foil. Although this blade has flown several hundred hours in service, CT could have been used during process development and during service inspections to determine if the cracks were caused from processing conditions or service conditions. The data could be coupled directly with a finite element model to determine the effect of the cracks on the structural performance of the blade. The CT data could also be used to determine the proper position of the foam core within the Kevlar composite structure.

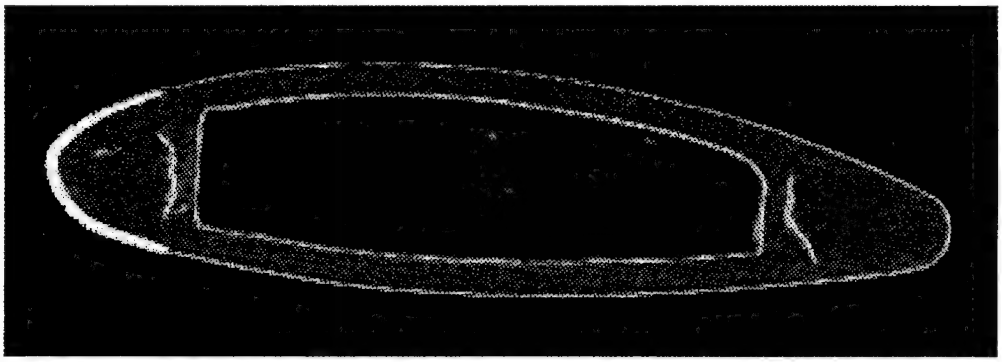

Figure 24. CT image of composite airfoil

C-C Brake Rotors

- **Process Development**
- **Model Verification**

Carbon-carbon materials have traditionally been produced through chemical vapor infiltration. A new process referred to as rapid densification (RD) has reduced the time needed to produce carbon-carbon brake disks for aircraft and high-performance race cars by a factor of 100.[19] Chemical vapor deposition (CVD) requires hundreds of hours for a gas such as methane to permeate a carbon preform and deposit carbon on the fibers. CVD works from the outside in; the outside surfaces tend to densify first and block the flow of vapors to the interior surfaces. The RD process immerses the preform in boiling liquid hydrocarbon. The hydrocarbon penetrates easily to the center of the preform where densification begins. A "deposition front" is created that works its way from the center out.

The CT image of Figure 25 shows a disc used for developing predictive models for the RD process. A modeling approach was employed for the RD process to enhance the understanding of the chemistry and physics of the process. The model allows developers to quickly adjust processing without the requirement for numerous empirical trials. CT was instrumental in determining the extent of densification following particular process cycles. From the CT-derived modeling data, process parameters can be changed to achieve densification goals.

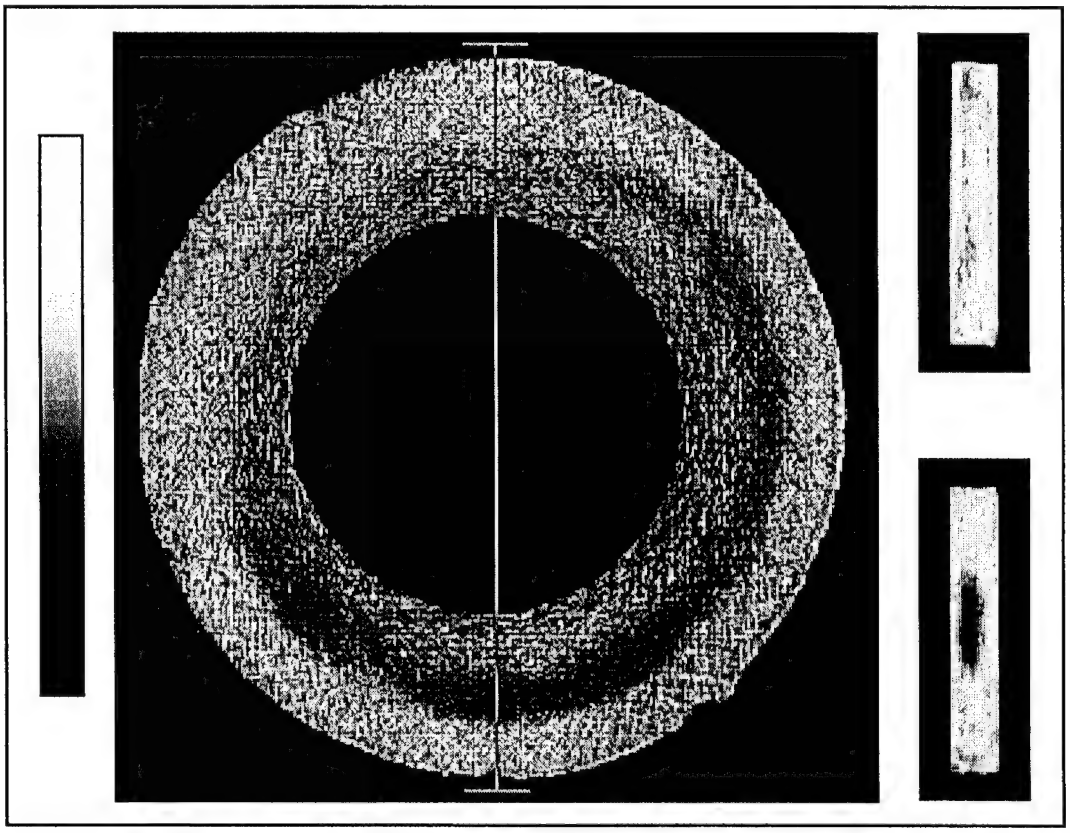

Figure 25. CT images of C-C disk for brake rotors

Fiberglass Panels

- Failure Analysis
- Model Verification

CT was successfully used to determine the state of damage in thick fiberglass panels subjected to ballistic impact.[20] This material is being considered for armor applications. The LAM/DE system was used for small panels (~ 100 mm x 100 mm) and the Hill AFB 9 MeV system was used for larger panels (~500 mm x 500 mm). Figure 26 shows orthogonal CT slices through an impacted panel. The top image shows the penetration of the slug and the damage that occurs in front of and behind the slug position. The damage zone appears as an hourglass shape with the widest section at the top and the smallest region about 1/4 the way into the plate from the bottom. This shape damage zone is typical for all the panels studied. The bottom three images show CT slices at various slice positions through the panel. Slice 1 shows a large circular damage zone around the slug which can be seen in the center of the panel. Slice 2 shows a smaller and less severe damage zone and Slice 3 shows the largest damage zone.

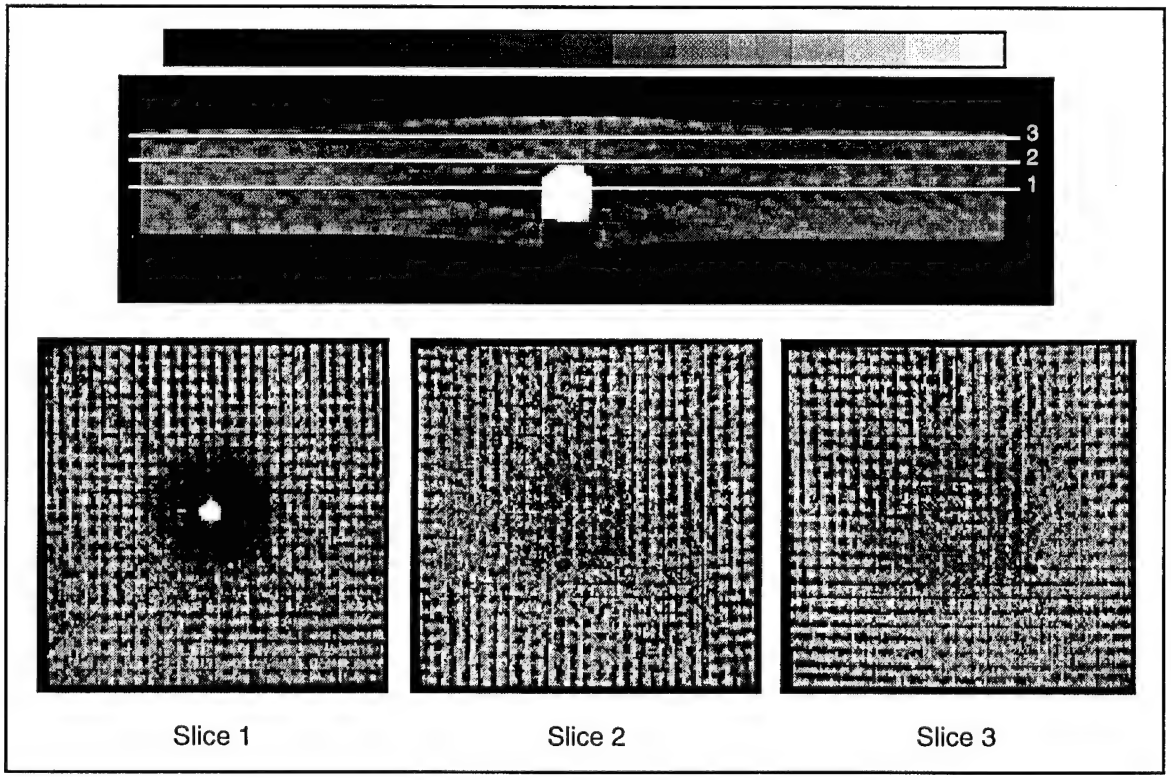

Figure 26. CT imagery of fiberglass impact panels

Image analysis techniques were developed to accurately determine the size of the damage zone. Visually, the shape and size of the damage zone is apparent. Quantitatively determining the shape and size of the damage zone is more difficult. As shown in all the images, the cross-weave nature of the fiberglass laminate creates several small pockets of resin rich regions. These show up in the images as small dark regions in a hatch pattern. The CT density of these regions is similar to the CT density of the damage zone. A simple thresholding technique, therefore, will usually produce a damage zone which will include the resin rich regions as well as the true damage zone. Image processing techniques are then required to separate out the damage zone from the resin rich regions.

Since the resin rich regions are small in comparison to the damage zone, a filtering technique which smoothes out small pockets of low density while preserving large low density regions would work best. Figure 27 shows an original CT image, a filtered CT image, and the corresponding threshold image from the filtered image. The filtered image was created by applying a 7 pixel median filter to the original image. This filter takes a 7 x 7 square pixel area and sets the center pixel to the median value of all the pixels in the square area. This serves to smooth out all low density regions smaller than 7 pixels square while preserving low density regions greater than 7 pixels square. The filter worked well as shown in the threshold image which accurately depicts the damage zone shape and size while not including any of the resin rich pockets created from the laminate cross-weave.

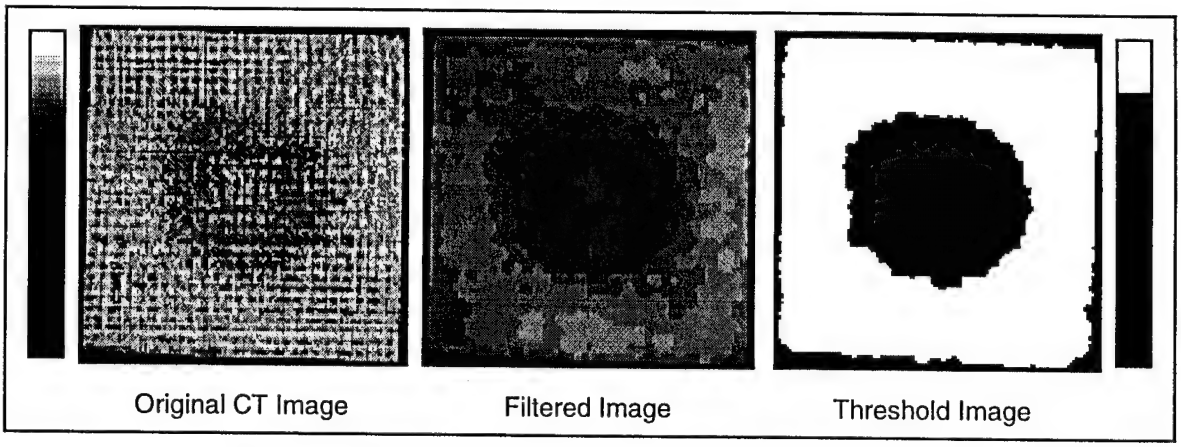

Figure 27. Damage evaluation process on impact panels

Figure 28 shows a graph representing the damage zone calculations for a number of contiguous CT slices through an impacted panel. As shown, the damage zone is greatest at the back face of the panel and is smallest about 1/4 the way in from the impact side. The data have been very useful in verifying the accuracy of models used to predict the damage state resulting from a particular impact event.

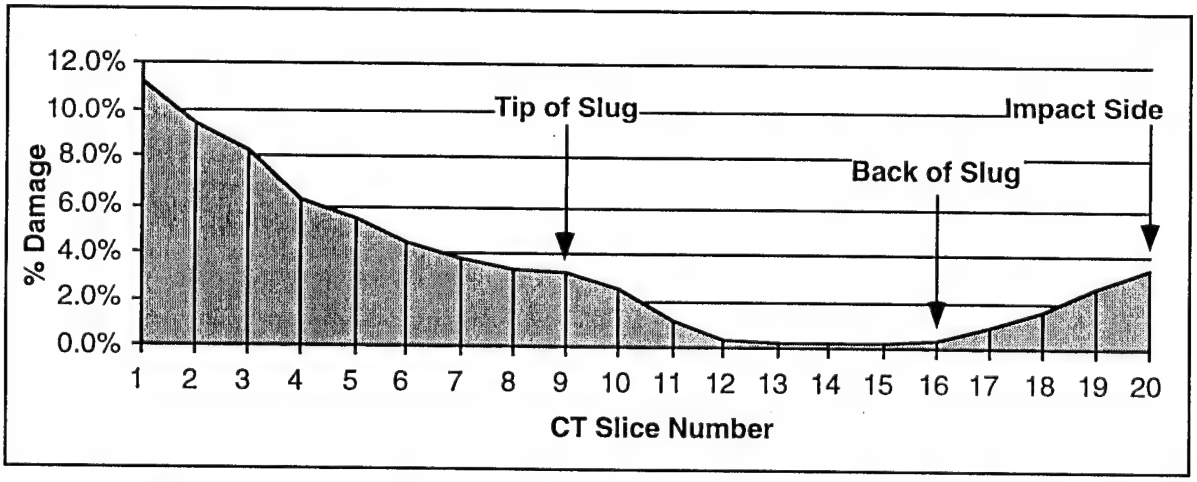

Figure 28. Graph of damage zone variation through thickness of panel

Hinge Casting

- Process Development
- Failure Analysis
- Quality Assurance

CT was used to assist the manufacturer of hinge castings in identifying the cause of premature failures. The hinges had suffered from a high infant mortality failure rate. Several castings were inspected with the LAM/DE CT system. Figure 29 shows an image from the inspections. The central low density pocket corresponds to the failure region noted in failed components. Figure 30 shows the detected CT values along the arrow in Figure 29. The CT analysis indicated to the manufacturer that excessive porosity in this region was causing the failure. These data were used to then investigate tool design or casting process changes that would significantly reduce or eliminate the porosity from occurring in this high stress area.

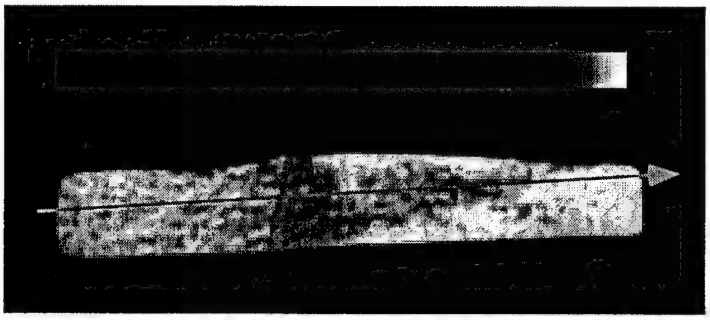

Figure 29. LAM/DE CT image of a hinge casting

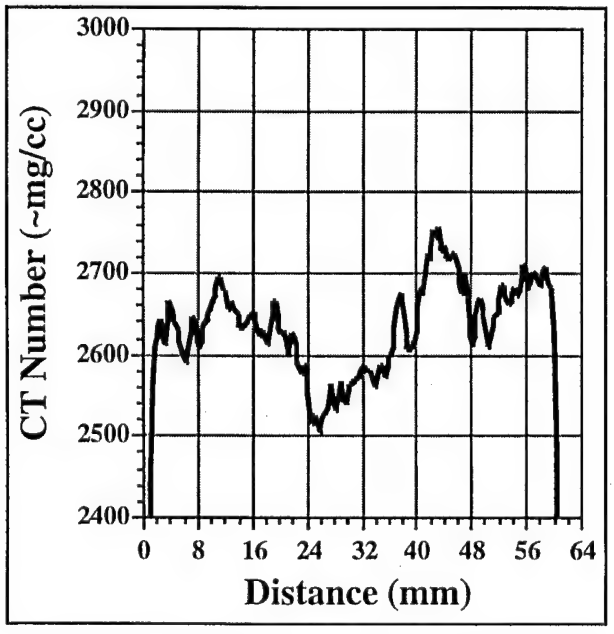

Figure 30. Density line-out from hinge casting

Fuel Pump

- **Failure Analysis**

The failure investigation of a fuel pump was assisted by the CT inspection of the cast housing. The failure event resulted in the erosion of the housing near a vent hole. Body material from the housing ejected through the vent hole. The failure analysis team sought a nondestructive means of measuring the erosion zone and characterizing the shape of the erosion. CT inspections were conducted on both the LAM/DE and Tomoscope systems. Figure 31 shows a CT image produced by the LAM/DE system along the longitudinal centerline of the erosion zone. Three transverse Tomoscope images that illustrate the primary characteristics of the erosion zone are featured in Figure 32. The locations of the Tomoscope images relative to the longitudinal CT image are annotated in Figure 31. CT inspection provided nondestructive geometrical characterization of the erosion zone for the failure analysis team.

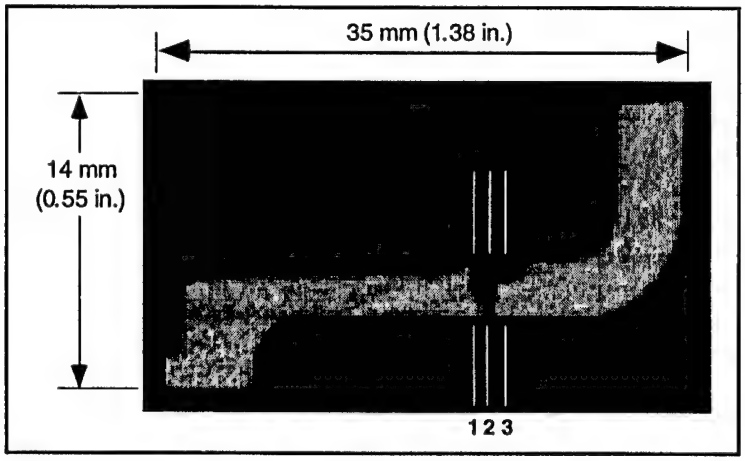

Figure 31. LAM/DE longitudinal CT image of fuel pump

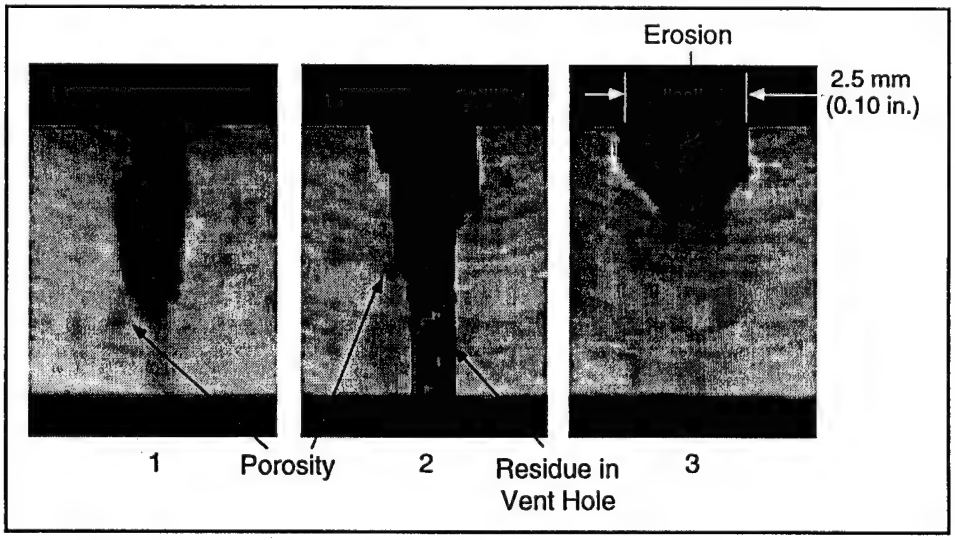

Figure 32. Tomoscope transverse CT images of fuel pump

Tenth Century Statue

- **Art Authentication**

A LAM/DE CT study of a tenth century Tibetan statue was conducted with the primary goal of authenticating the work of art. The statue is cast in bronze and stands about 6 inches tall. Figure 33 shows a digital radiograph of the statue along with a CT image through the centerline. A key point of information in authenticating the statue is protrusion of tin sheets into the base of the statue. These tin sheets are referred to as dedications or prayer scrolls and contain text inscribed on the surface of the thin sheets. The CT imagery showed the anticipated extent of protrusion for an authentic statue. This example serves to illustrate the wide variety of applications for this technology.

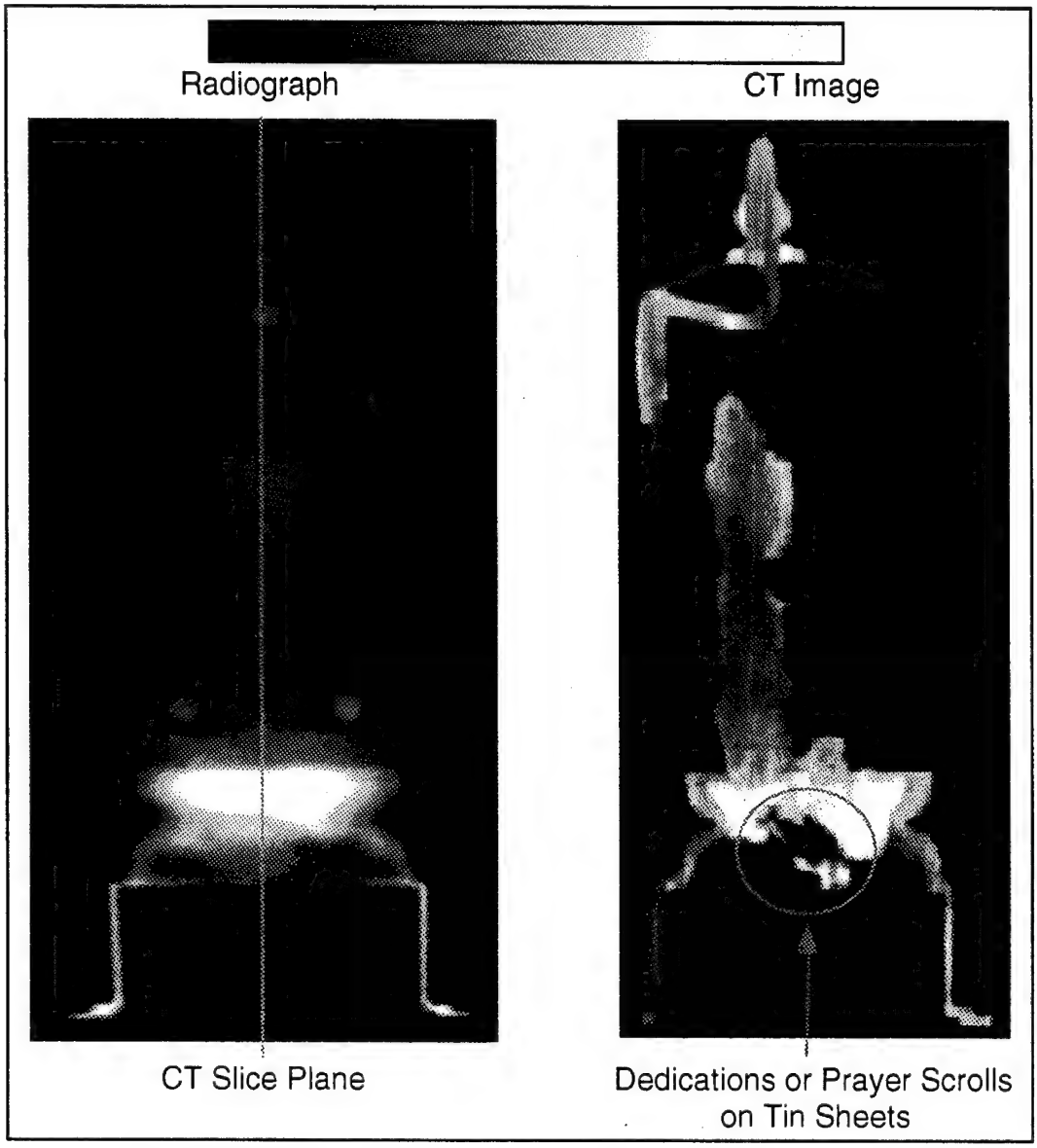

Figure 33. DR and CT images of a 10th century Tibetan statue

Carbon Samples

- Quality Assurance

Five carbon samples were scanned on LAM/DE to determine the sensitivity of LAM/DE to small density variations in carbon. The samples were approximately 25 mm (1 in.) in diameter and about 50 mm (2 in.) high. Each sample was weighed and measured using standard methods to determine the density of the samples accurate to 3 decimal places. A representative CT image is shown in Figure 34 and the measured density value is written below each sample. As shown, some of the density differences were as small as 0.004 g/cc. Ten CT slices were taken through the samples at different locations and a statistical mean was calculated from the pixels for each sample. For each of the 10 scans, the order and magnitude of the density differences were in accordance with the measured density values. It was determined for this study that density differences over an area of 300 mm^2 could be determined to within 0.004 g/cc. Clearly, a noncontact, nondestructive tool capable of very sensitive density measurements can provide many benefits to manufacturing processes and quality assurance.

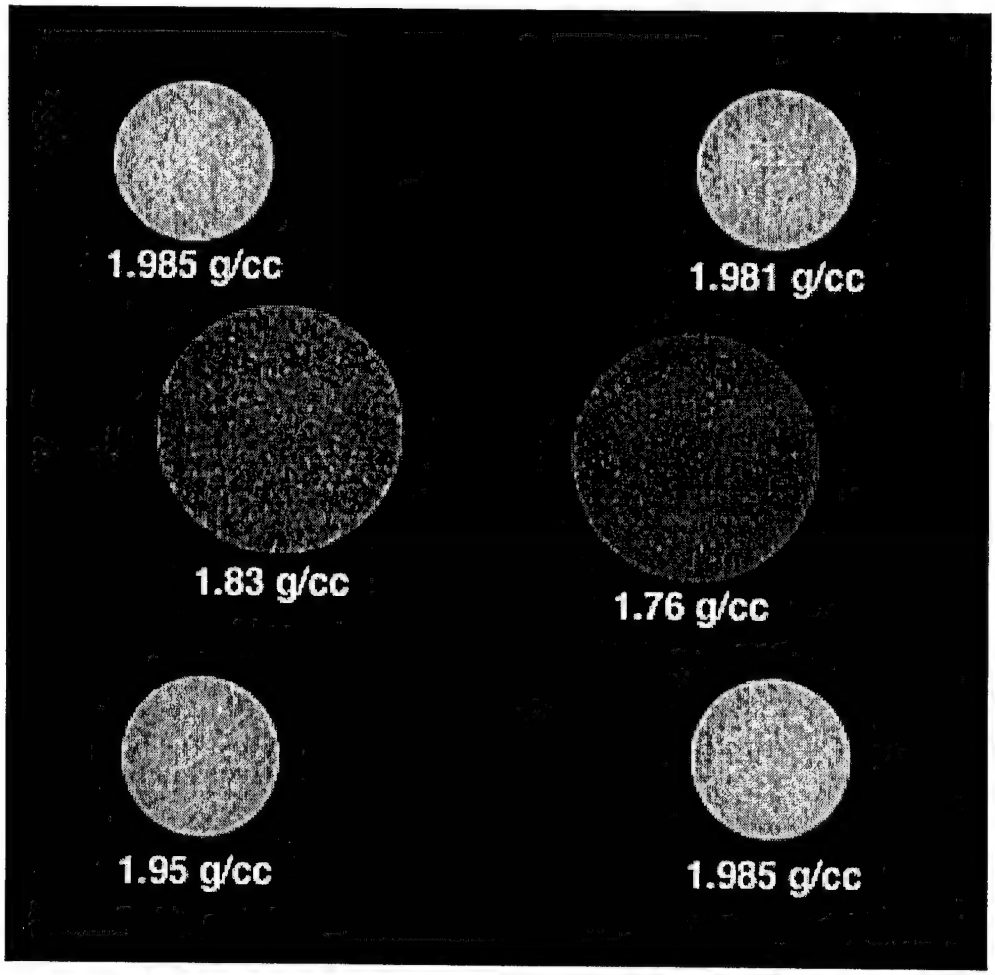

Figure 34. CT images of carbon samples

Carbon Foams

• **Process Development**

Low-density carbon foams (<60 mg/cc) were scanned using the LAM/DE system's unique flexibility.[21-23] A benefit of the LAM/DE system's dual energy capability (see Appendix A, Section A1.4) is that the system possesses two sets of X-ray detectors. The front and rear detectors are used simultaneously in dual energy imaging; for standard X-ray imaging situations either set of detectors can be used. This results in great dynamic range because the detector sets were optimized for different energy interactions.

Utilizing the front detectors only, high-quality CT images were obtained from these very low-density objects, even while running at 420-keV. Each sample measured approximately 100 mm x 18 mm and 12 mm high. The CT image in Figure 35 shows density variations between the five samples as well as density variations within some of the samples. The left two samples show a slightly higher density at the outside edges. The right most sample shows some regions of higher density through the cross-section. The CT images were valuable in determining the effect of different processing methods. Due to their fragile nature, destructive analysis of these samples was impractical. CT provided an excellent tool to quickly determine the density variations between and within samples and this information was directly used by researchers developing processes for the production of a uniform carbon foam.

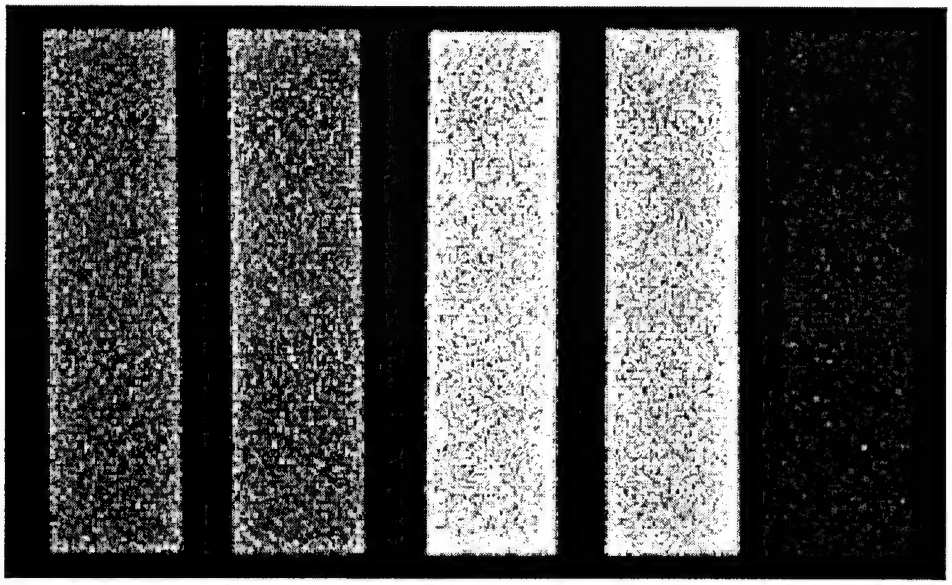

Figure 35. CT images of low density carbon foams

Fatigue Test Specimen

- **Model Verification**

Extensive testing was conducted on an aluminum compact tension specimen using a load frame *in situ* during CT inspection. The specimen was fatigue tested in a large load frame until the crack had progressed several millimeters. A special load frame designed and built by researchers at Georgia Tech was used to apply force to the specimen in order to open up the crack. The load frame with the specimen was placed on Tomoscope and several contiguous CT slices were taken through the crack zone. (See Figure 36.) Figure 37 shows three contiguous CT slices through the part under a load of 80 pounds. The study showed that the crack was not planar and as shown in the CT images, the crack runs in and out of the CT slice plane several times. The slice thickness here is 125 microns. Future work is planned in this area which should continue to provide information on crack morphology.

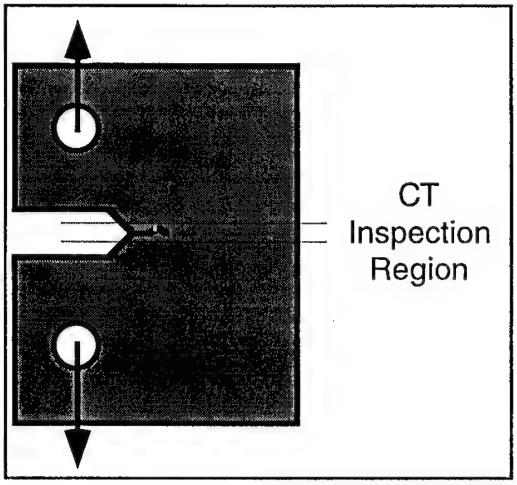

Figure 36. Load frame configuration

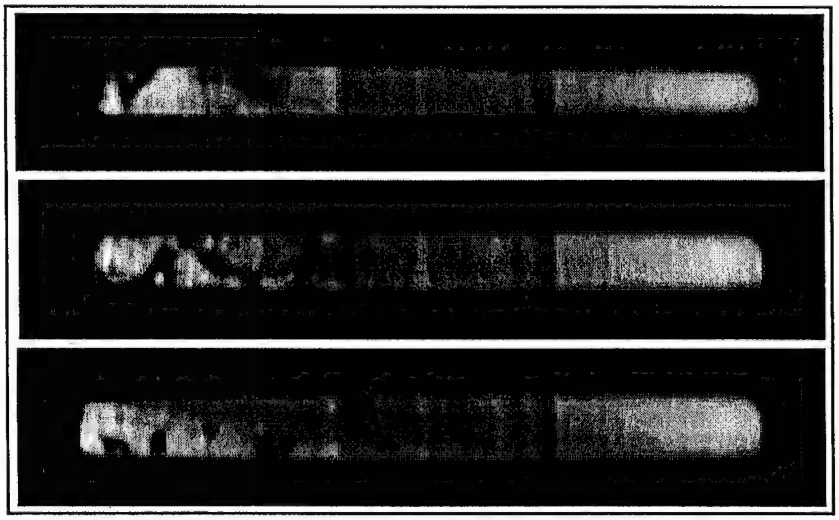

Figure 37. Fracture specimen under load

Solid Rocket Propellant

- Model Verification
- Quality Assurance
- Chemical Migration

Figure 38 shows a Tomoscope CT image of a solid rocket propellant sample. The goal of CT inspection was identification of nitroglycerine migration. The chemical migration can be seen as the red region in the upper right of the image. The data were used to compare with model predictions of nitroglycerine migration. Future studies could be used on a set of samples to determine the migration over time and under differing conditions. An unanticipated result of the inspection was identification of high density inclusions in the sample. These are seen as white flecks throughout the image. Finding the inclusions initiated additional research to better understand the propellant.

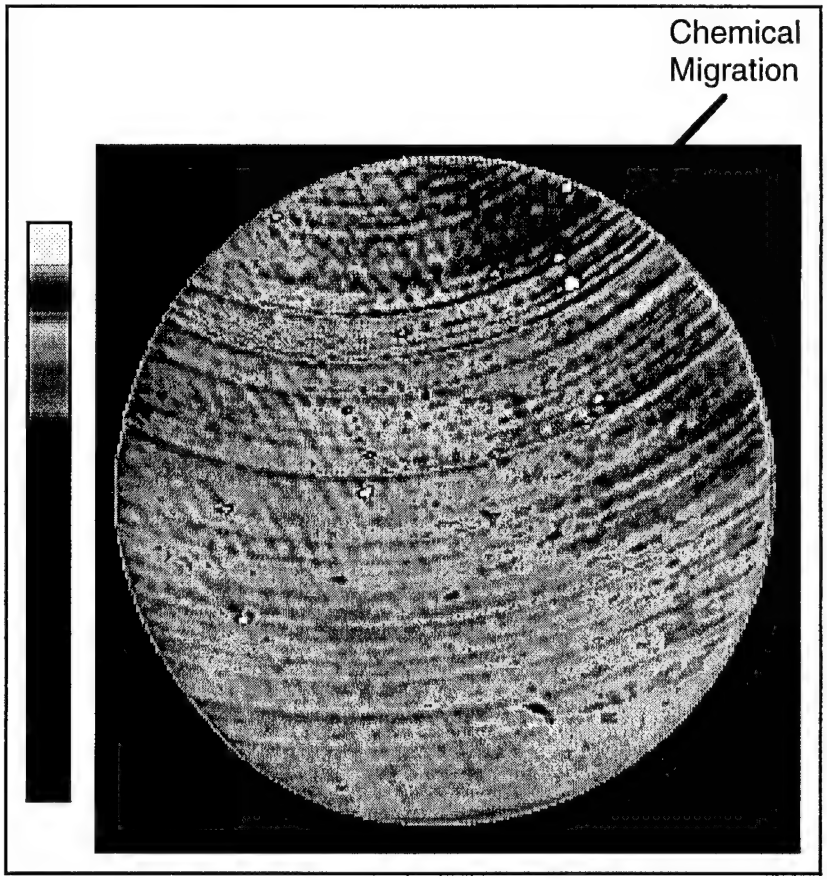

Figure 38. Tomoscope CT image of a solid rocket propellant sample

Thermal Storage Units

- Process Development
- Pedigree Evaluation
- Model Verification

NASA is developing a thermal storage system for zero-gravity space applications to capture and employ solar energy. The system is based on repeated melting and solidification of lithium fluoride salts. The salts melt as they absorb solar energy. This energy can then be extracted when needed by drawing heat away from the salts and allowing them to cool and solidify. The solidification pattern in relation to salt-surface contact is critical to the proper operation of the thermal storage units. To accommodate for expansion and contraction of the lithium fluoride, the canister is not completely filled. It is desirable to know how well the material fully envelops the central core upon solidification for maximum heat transfer efficiency. CT is a natural choice to nondestructively provide the densification characterization of the salts.

Figure 39 shows CT imagery acquired from a preliminary design of the thermal storage units following testing on the space shuttle. The dark regions near the open central core indicate lower density and thus an inability to fully extract thermal energy. The data obtained from this preliminary design assisted researchers in developing the current design.

Figure 40 shows imagery acquired from the current design of the thermal storage units following flight on the space shuttle. The new unit design consists of a small canister about 3 inches in length and less than 3 inches in diameter. It contains a concentric metallic core which provides the thermal extraction conduit. CT again provided clear information on the solidification patterns of the salts. These data are used to verify and improve modeling predictions and to further assist in the development of the thermal storage system.

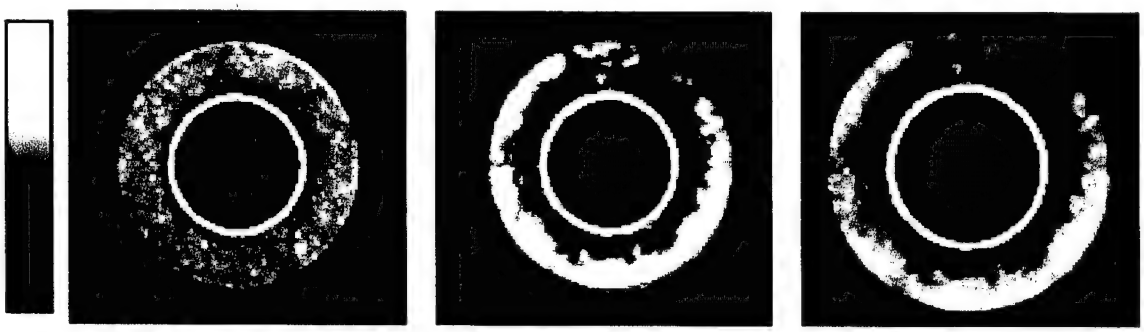

Figure 39. Original thermal storage unit design

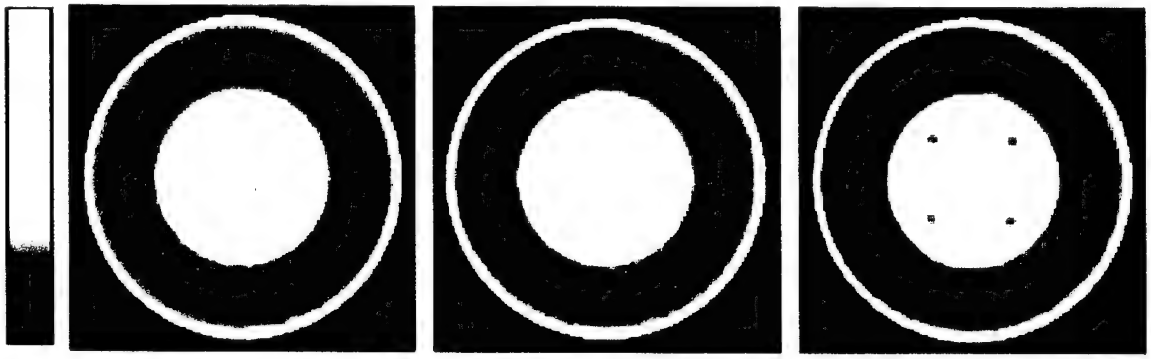

Figure 40. Second generation thermal storage unit design

Air Conditioner Unit

- Process Development
- Design Verification
- Model Verification

Figure 41 shows a LAM/DE CT image of an automotive air conditioner compressor. The outside ring is the unit housing, the reddish areas are steel components, and the blue region is an aluminum casting. Significant porosity is seen in the aluminum casting on the left side of the inner casting.

These data are useful in a variety of ways. First, the image illustrates the ability of CT to inspect fully assembled components to look for defects or problems in the assemblage. Second, it illustrates the ability to identify the size, location, and extent of porosity in cast metal components. This capability can help refine the casting tool configuration and casting procedure to either eliminate the porosity from the structure or control it to within design criteria. The porosity data could be used directly in a finite element model of the structure to determine the effect of this porosity on the performance of the casting. Overall, using CT during casting process development can greatly assist in developing efficient casting processes that meet the needs of the application.

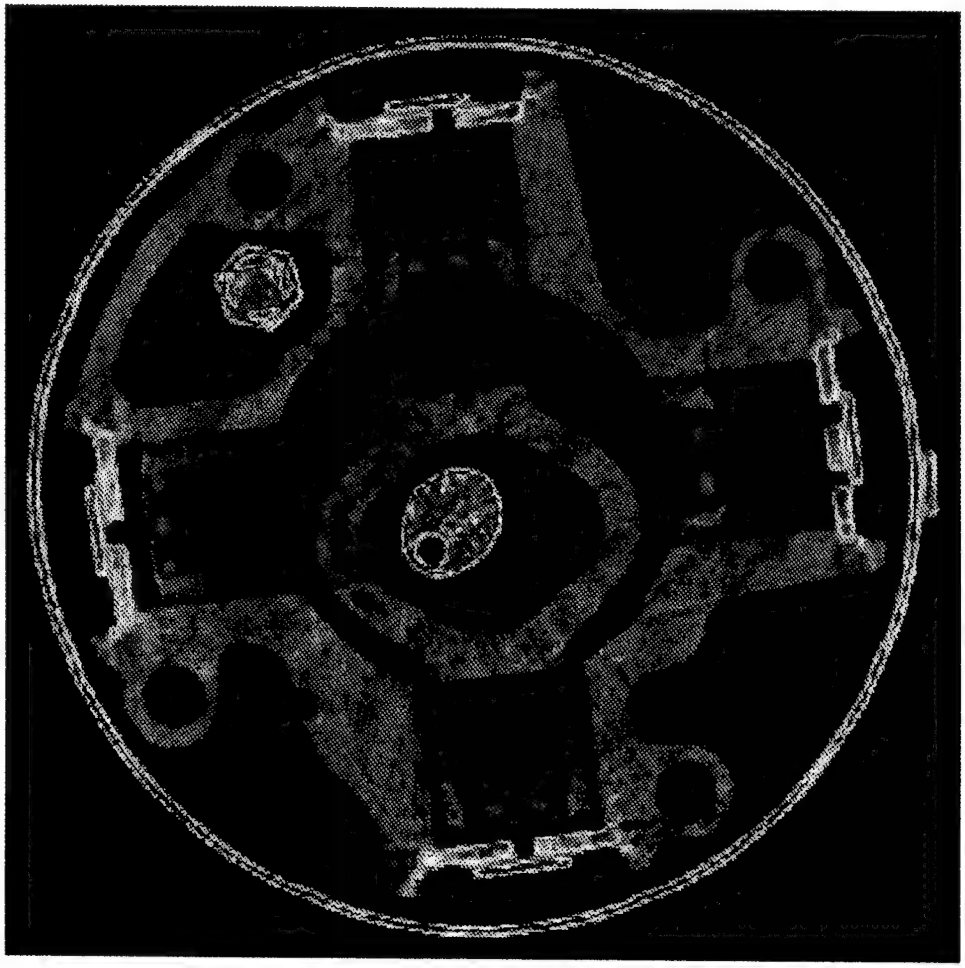

Figure 41. CT image of air conditioner pump

Airbag Initiators

• **Process Development**

A study of initiators for automotive airbag inflators was conducted on the LAM/DE and Tomoscope CT systems. Three initiators manufactured with minor process variations were studied to identify the effects of the process variations on the final product. Figure 42 shows a LAM/DE CT image of the three initiators along with a detail section from a Tomoscope CT image. The Tomoscope image corresponds to the initiator at the left in the LAM/DE image. CT analysis revealed significant variations among the three initiators in density and porosity. The results of the study were beneficial in establishing an improved understanding of the manufacturing process and effects of process variations.

It is interesting to note that for this case the higher resolution Tomoscope image provided relatively little information beyond that provided by the LAM/DE images other than identifying shape and size of lower density regions. The study showed that the information provided by LAM/DE was sufficient to determine differences in the initiators due to processing variations. Higher resolution does not necessarily mean better information. This is important to keep in mind when specifying a CT system. Higher resolution provides a great deal more information in most cases, but it raises the price of a new system. Spatial resolution requirements can affect an entire range of components, subsystems, and procedures.[24] If the detail provided by a high resolution system is not required, it should not be specified in the procurement of a system.

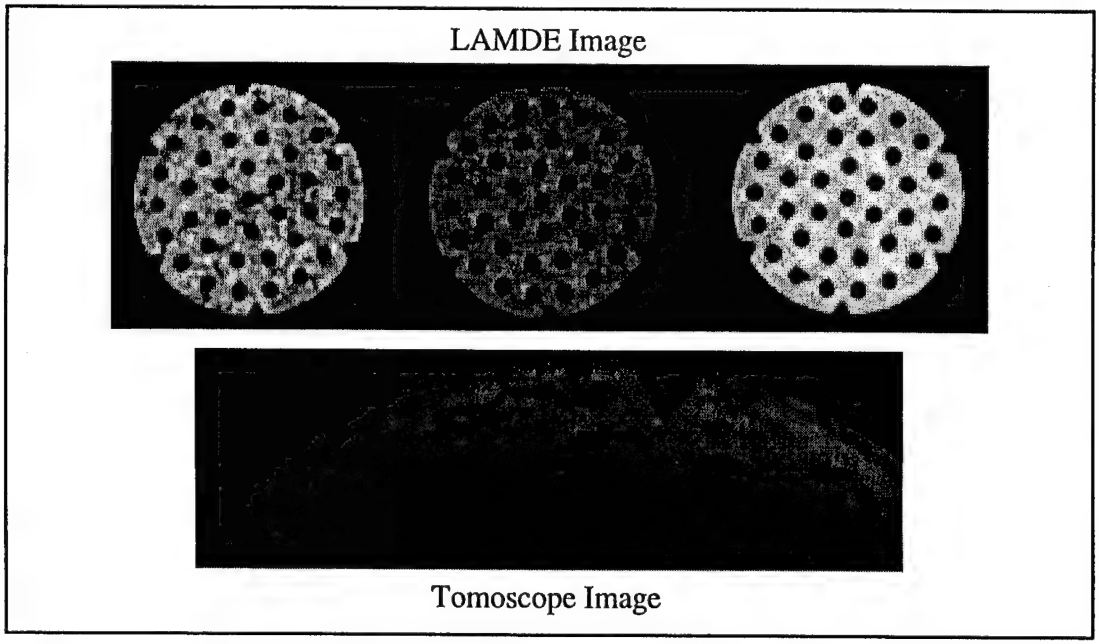

Figure 42. Initiators from automotive airbag inflators

Crystal Oscillator

- **Failure Analysis**
- **Quality Assurance**

The crystal oscillator unit shown in Figure 43 contains a quartz crystal in a miniature glass envelope. Post-mortem analysis testing of similar units has shown failures in the lead support area of the crystal in the form of loss of contact between lead wires and support posts. The purpose of CT inspection of the oscillator was demonstration of the ability to analyze the failure region. The unit tested had no failure. Following CT inspection, the unit will be vibrated to failure after which additional CT inspection is anticipated. To assess the lead wire to support post bonds, four adjoining Tomoscope CT scans were acquired (bottom figures). Each CT image represents a 250 micron slice plane through the region. Bonding of each wire can be seen in one or a combination of two images. No anomalies were detected in the bonds.

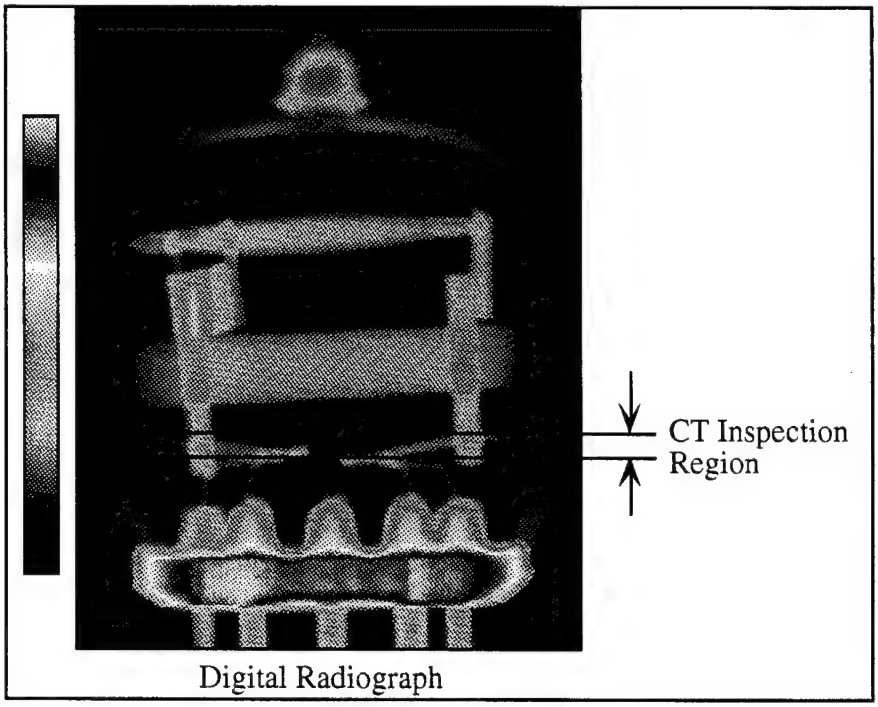

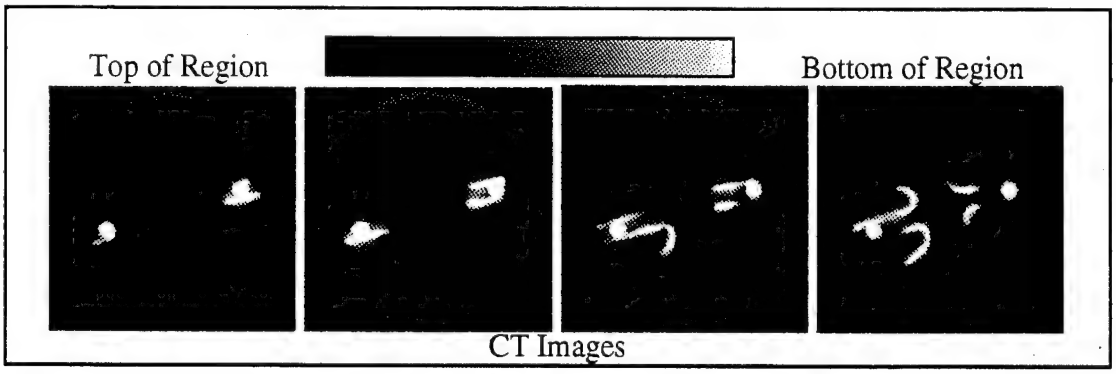

Figure 43. DR and CT images of a crystal oscillator

Electric Insulator

- **Failure Analysis**
- **Quality Assurance**

CT inspection of an electrical insulator revealed low density regions in several locations at the interface of the iron cast housing and the fiberglass core. Figure 44 shows a digital radiograph of the insulator with the CT inspection region identified. Figure 45 includes four contiguous LAM/DE CT slices through an area where the iron casting narrows. Low density regions were identified throughout the area. It appears that the casting first narrows at one side and then the other (see slice 3). This causes a contortion of the fiberglass core and a disbond first on one side (slices 1 and 2) and then the other (slice 3). It was shown that the distortion of the fiberglass core had caused failure of the insulator.

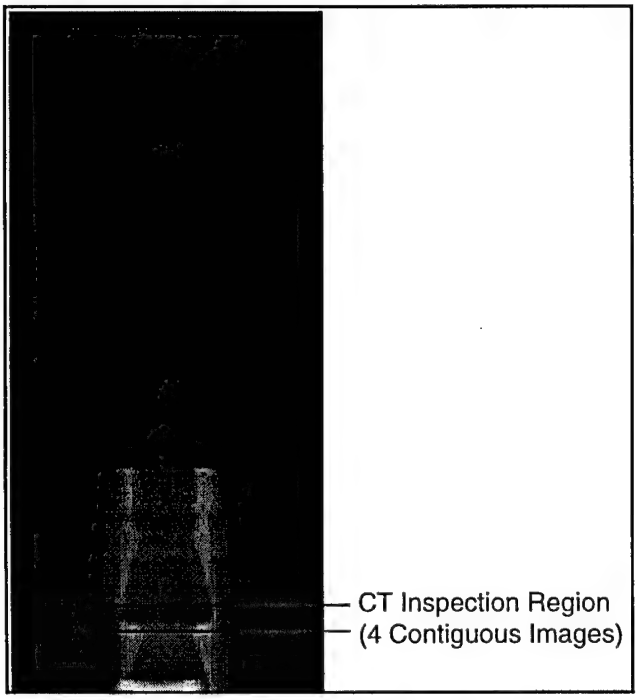

Figure 44. Digital radiograph of electrical insulator

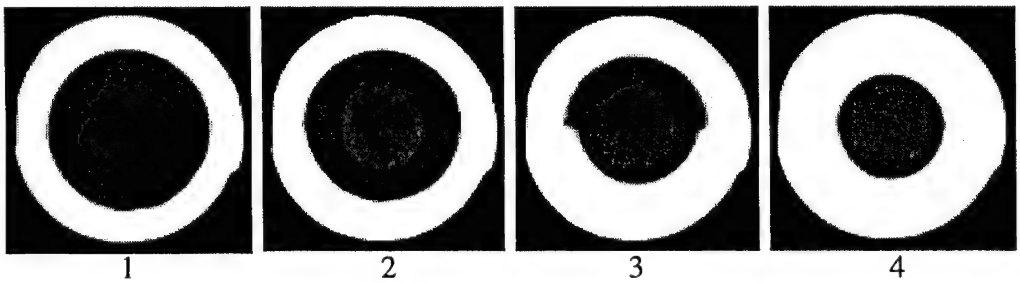

Figure 45. LAM/DE CT images of electrical insulator

4.0 Future Enhancements

The Wright Laboratory CT Research Facility has long been a leader in the development and application of CT technology. The LAM/DE CT system was one of the first systems with laminography and dual energy imaging. Tomoscope is the first CT system capable of an optimal resolution of 25 μm. The Wright Laboratory/Materials Directorate has sponsored numerous programs for fundamental CT research resulting in many innovative hardware and software designs. Other government agencies including NASA, ARPA, DLA and EMTEC have also sponsored projects to expand the application of CT. This section will summarize anticipated system hardware and software enhancements arising from upcoming and ongoing research projects.

4.1 Tomoscope CT System Upgrade

Through funding from a Phase II, Air Force Small Business Innovative Research (SBIR) program, ARACOR recently completed the design and implementation of a new high-resolution detector package to replace the original Tomoscope detector system. The new "TOMO II" detector takes advantage of the latest advances in scientific-grade charge-coupled device (CCD) technology to achieve substantial improvements in readout noise and detector quantum efficiency. The CCDs are coupled to a scintillator-loaded fiber optic which converts X-rays to light. The system is controlled by a high-speed UNIX workstation. Under software control, the detector package can be configured to a new source-to-object distance, optimized for the absorption properties of a given object or source energy, or configured to provide tailored dual-energy images. The workstation also provides a number of sophisticated image reconstruction and analysis tools.

Through funding from a separate Phase II SBIR program with L&W Research of Wallingford, Connecticut, a 360 keV micro-focus X-ray source has been developed for use with the Tomoscope CT system.[25] This program has been successful in designing and fabricating an X-ray source with improved beam flux, beam energy, reliability, maintainability, and ease of use. The new X-ray source is expected to decrease scan times, improve signal-to-noise characteristics and allow for scanning of larger objects than currently possible with the 195 keV source.

4.2 Improved Reverse Engineering Capabilities

Many improvements to the reverse engineering capabilities of the CT facility will be implemented in the next few years. Reverse engineering refers to the ability to acquire CT data on a part and transform that data to a full computer-aided design (CAD) description of the part. This can be useful for a number of reasons. First of all, the reverse engineered CAD description can be compared with the original CAD description to check for out-of-tolerance conditions in the part. This is best utilized during manufacturing process development to verify that the manufacturing process is producing parts of acceptable quality before proceeding to full manufacturing production. This can also be used for spot checks during full production to ensure that part quality is maintained. For example, in a casting operation, the first article castings can be inspected with CT, and these data can be used to create a CAD description of the casting. This CAD representation can be compared to the original, as-designed CAD description to check for the conformance of the part geometry with the intended part geometry. The tool maker can then use this information to modify the tool to conform with the as-designed geometry. This process can be much more efficient than current methods of first article cut ups and manual dimensional measurements of critical areas. An example of how the

data can be displayed is shown in Figure 46. A visual representation of the differences between the CT-derived CAD outline (white) with the original CAD outline (black) is shown. This can point to manufacturing processes that may need to be altered to make the part better conform to the design.

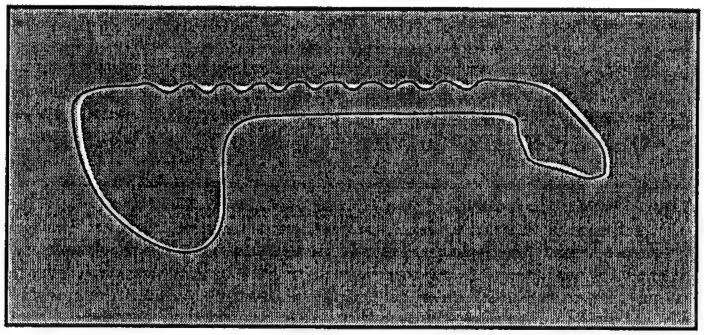

Figure 46. Illustration of CT used for dimensional verification

Another area where reverse engineering can be useful is the area of replacement parts. There are many situations in and out of the military where replacement parts are needed and original CAD descriptions or drawings do not exist or the original drawings are unreadable. Other situations arise when manufacturing changes were made on the shop floor, and the drawing was never updated. In these situations, reverse engineering an existing, operational component using CT can be much more efficient than trying to recreate or correct a drawing or convert a hard copy drawing to CAD format. It is desirable in many situations to convert a hard copy drawing to CAD so that manufacturing processes that utilize CAD descriptions (i.e., CNC machining or rapid prototyping) can be made available.

A third area where reverse engineering can be useful is in the area of structural analysis. A design engineer often models a structural component using finite elements or another structural analysis technique to determine the stress and strain distribution, dynamic response, or thermal properties of the part. This modeling is usually done on the as-designed part which contains no flaws or imperfections. Reverse engineering on an as-manufactured part can provide information to model the actual part configuration and determine if this configuration is acceptable given the expected loading conditions. Here, CT data need to be evaluated for part boundaries as well as the internal properties of the part itself. This information needs to then be output in such a way that it is compatible with structural analysis software such as finite element analysis.[26] Figure 47 shows an example of this. The left shows the original CT image of a metal-matrix composite ring. The image is first segmented in regions corresponding to different ranges of CT density values. Four ranges were chosen in this example: titanium cladding, reinforced core, low fiber volume fraction, and high fiber volume fraction. A finite element mesh is then applied to the image using the segmentation as the basis for the mesh. Then the image segmentation pertaining to the high and low fiber volume fractions of the core is used to classify the stiffness and strength properties of the individual elements. An illustration of what the final mesh might look like is shown on the right. By automating this process, the structural analysis engineer can quickly model the geometry and stiffness variations of the ring. In this example, the stiffness variations of the core are classified into three zones (i.e., high, low, and average fiber volume fractions). Further refinement of these tools could result in more than three classifications and more control over the mesh geometry in order to make the finite element representation as accurate as possible.

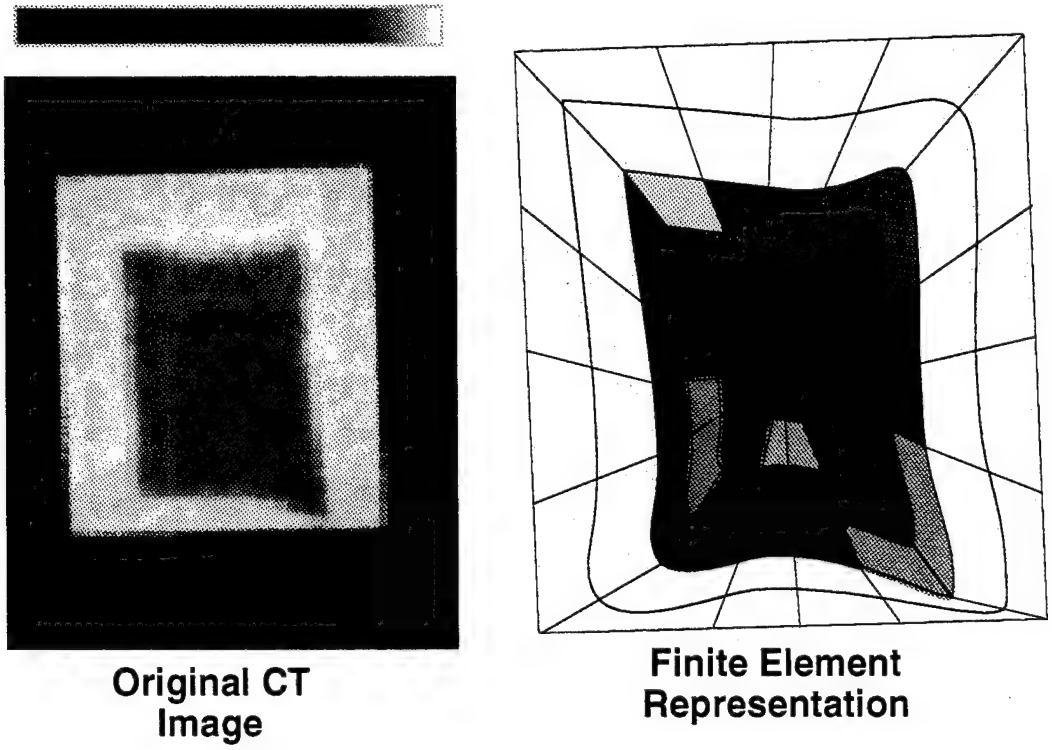

Figure 47. Illustration of conversion of CT image to finite element representation

In most cases, the reverse engineering enhancements to the Wright Laboratory CT Research Facility will come through software tools being developed by ARACOR with funding from other sources. As this software is developed, it will be made available to the Wright Laboratory for testing and eventual use for applications studies coming through the facility. Figure 48 gives a summary of the different programs in progress that will result in reverse engineering software to be provided to the CT facility. The first column gives a brief description of the software capability, the second column lists the funding source, and the third column lists the expected completion date of the project.

It is anticipated that the Wright Laboratory CT Research Facility will be at the forefront in applying these new technologies. This will provide greatly expanded capabilities in this area and open the door to many new types of potential applications. It is also expected that the results of application studies using these tools will provide key information for further development and implementation of these tools within the Air Force and in commercial industry.

Capability	Funding Source	Completion Date
Conversion of CT data to 3-D CAD surface models	NASA-Marshall	Spring 1995
Linkage of CT data to finite element modeling software	NASA-Marshall	Spring 1995
Linkage of CT data with rapid prototyping equipment	DLA	Fall 1995
Linkage with solidification modeling software	DLA	Fall 1995
Automated dimensional variance reporting	ARPA	Fall 1996

Figure 48. Table summary of reverse engineering future capabilities

4.3 Improved Image Analysis Capabilities

CT data are inherently digital so that digital image processing routines can be developed to better analyze the image data. A typical CT image comprises over 2 megabytes of information. To make quantitative use of the data, the user often wants to reduce the size of the data set to a form that only contains the essential information desired. Other cases exist where image processing may enhance particular features which may not be readily apparent. Image processing tools exist in many forms and many have been used within the program. Others have yet to be developed or need to be refined in order to function efficiently. Three key areas for image processing of CT data are data segmentation, data classification, and data visualization. A brief description of these concepts is presented below.

Image segmentation refers the segmentation of particular features from a composite image to create isolated regions or segments containing certain properties. An example is shown in Figure 49. A high-resolution CT image is shown on top with a segmented version below. The segmentation routine separates the fibers from the matrix and creates a binary image where the fibers are black and the matrix is white. In fact, the data set can be reduced even further by defining the sample cross-section boundary and the fiber centers since the fiber diameter is the same for all fibers in this composite. If fiber placement is the only essential information required from the CT image, then this image segmentation routine can be an effective way to quickly extract this information. There are many different forms of image segmentation algorithms and each has its strengths and weaknesses. New segmentation routines are being developed continuously and their development will simply expand the options available. Segmentation algorithms are often most efficient when some prior knowledge of the part configuration is available beforehand. In these cases, customized algorithms can be developed to operate on a very specific type of image data. For example, a customized routine to extract fiber centers from a CT image of a composite material could be developed to run very efficiently for that particular application. More generalized segmentation algorithms may be required for more general applications.

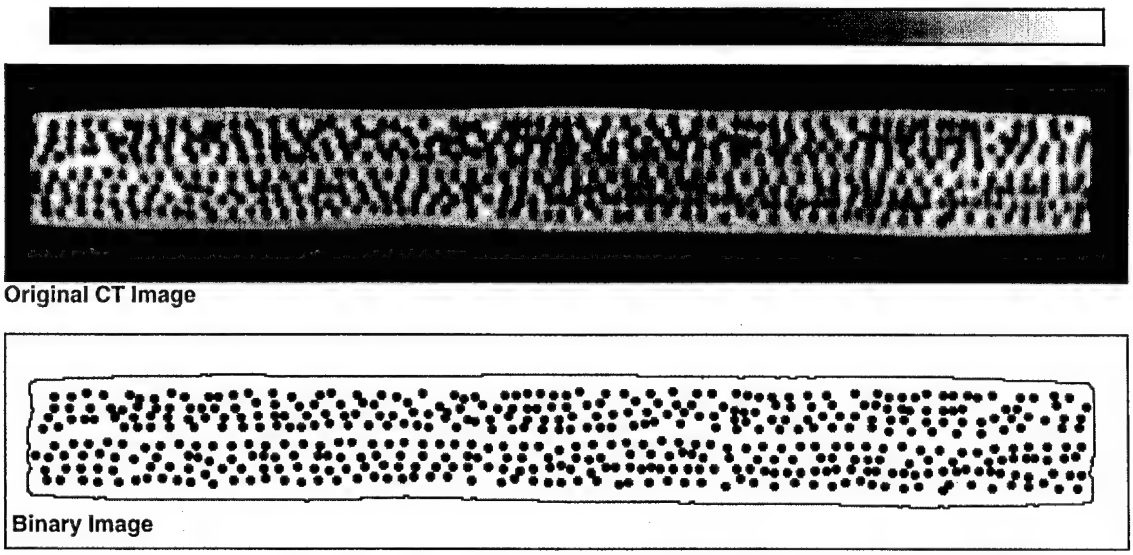

Figure 49. Illustration of image segmentation

Image classification is a specific subset of image segmentation. Image classification refers to the ability to classify, or assign specific properties, to segmented regions of an image. In the example above of the metal-matrix composite, image classification would be the process of assigning a specific identifying number to the fiber locations versus the matrix locations. In the example shown in Figure 47 with the MMC ring, image classification results in four regions (titanium cladding, reinforced core, low fiber volume fraction, and high fiber volume fraction) which can each be assigned a unique number. Classification is useful for input to other software such as modeling packages. The classification can then be used to set the appropriate properties for each segmented region. For example, the finite element mesh shown in Figure 47 has elements with four different physical properties based on the image classification. Classification not only refers to different material properties, but geometry properties as well. Image classification can be used to identify separate objects in three dimensions. For example, objects that may appear separate in a particular CT slice may be connected in three dimensions and classification algorithms determine this connectivity.

Image visualization refers to the ability to visualize data in efficient ways. The actual display of a CT image is an image visualization technique. The CT data consist of numbers that represent the X-ray attenuation of specific volumes (voxels) within the imaging volume. A CT image is a representation of those numbers where the image colors represent different ranges of CT image values. CT data are often acquired in three-dimensions as a series of 2-D CT slices. 3-D visualization techniques refer to visualization methods to represent 3-D data sets. Figure 50 shows a 3-D rendering of a data set of MMC ring data. Data were acquired on the ring at 10° angular increments to produce 36 image cross sections around the ring. These 36 images were stacked into a rectangular volume and then viewed as a 3-D data set. In this case, the outside of the ring is made transparent gray and the boundary of the reinforced region is made transparent blue. The areas of low fiber volume fraction are highlighted as yellow. Simulated lighting is applied to the image so that the 2-D image on the page appears as a 3-D object in space. 3-D data visualization techniques can be useful in analyzing large sets of data or for viewing features or patterns in 3-D which may not be apparent in separate 2-D representations. For example, the 3-D visualization in Figure 50 shows the low fiber volume fraction areas as forming a consistent pattern of going from one side to the other in the reinforced core. This particular data visualization helped to isolate a manufacturing problem that was easily identified when viewing the data in this manner.

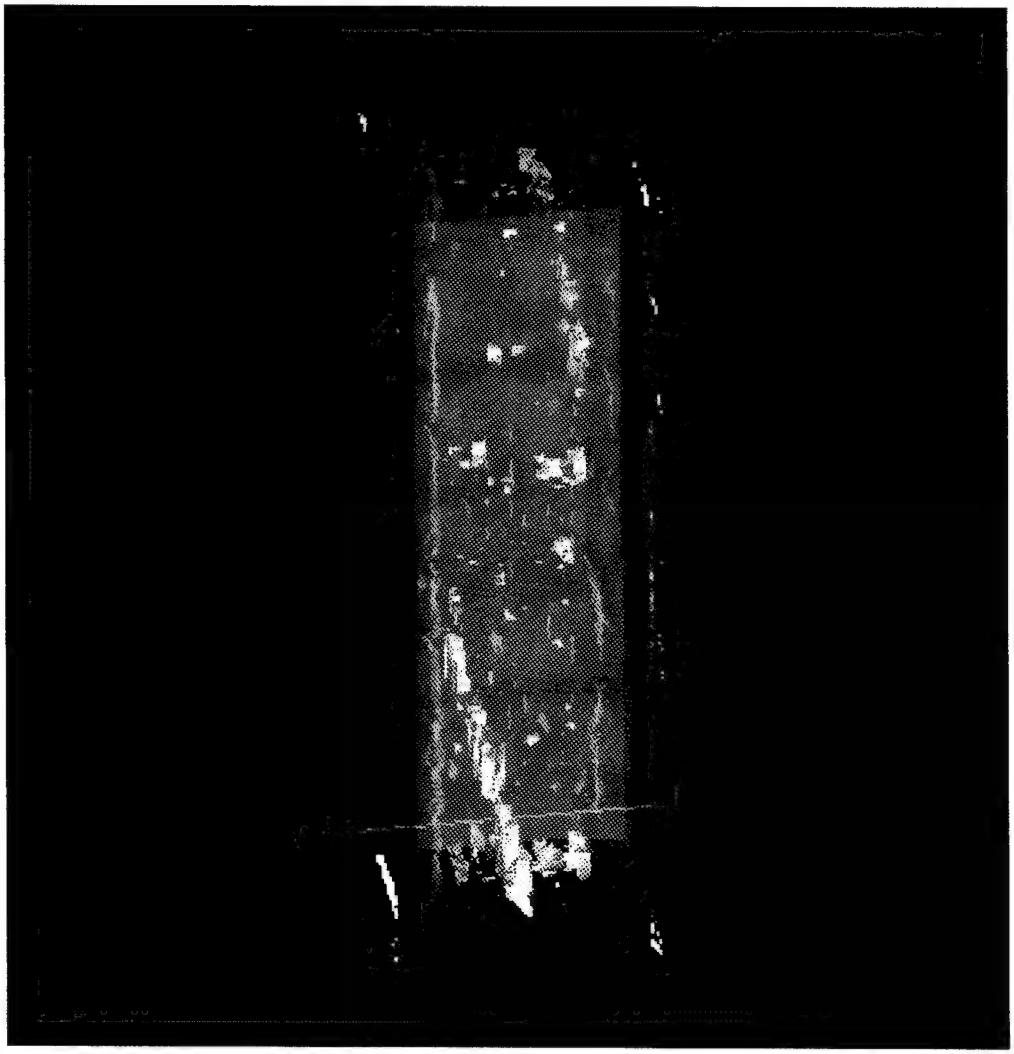

Figure 50. Assemblage of MMC ring images into rectangular 3-D representation

The goal of image analysis is to simplify image interpretation and to provide the user with tools to quickly highlight and extract the information of interest. The upgrades to the Wright Laboratory CT Research Facility in this area will come from the availability of new computer systems to better handle the image analysis routines, the purchase of commercially available image analysis software, the development of new image processing algorithms, and the utilization of new image processing software currently being developed by ARACOR. The ARACOR developed software, when completed, will be made available to the CT facility for testing and eventual use for applications studies coming through the facility. Figure 51 gives a summary of the different programs in progress that will result in image analysis software to be provided to the CT facility. The first column gives a brief description of the software capability, the second column lists the funding source, and the third column lists the expected completion date of the project.

Capability	Funding Source	Completion Date
3-D registration and visualization methods	NASA-Lewis	Spring 1995
Segmentation of fibers, cracks, and porosity in 2-D and 3-D CT data of metal-matrix composites.	NASA-Lewis and NSF	Spring 1996
Classification of fibers, matrix, and damage in 2-D and 3-D CT data of metal-matrix composites	NASA-Lewis and NSF	Spring 1996
Extraction of fiber distribution, alignment, and volume fractions from 2-D and 3-D CT data of composite materials	ARPA, NASA-Lewis, and NSF	Spring 1996

Figure 51. Table summary of image analysis future capabilities

Again, it is anticipated that the Wright Laboratory CT Research Facility will be at the forefront in applying these new image analysis technologies. This will provide greatly expanded capabilities in this area and open the door to many new types of potential applications. It is also expected that the results of application studies using these tools will provide key information for further development and implementation of these tools within the Air Force and in commercial industry.

5.0 References

1. Hounsfield, G.N., "A method of and apparatus for examination of a body by radiation such as x-ray or gamma radiation," *Patent Office, London, Pat. Spec.1283915*, 1972.

2. Yancey, R.N. and Stanley, J.H., "A New Radiographic Corrosion Inspection Capability," AFWAL-TR-88-4234, Air Force Wright Aeronautical Laboratories, Materials Laboratory, Wright-Patterson AFB, OH, December 1988.

3. Yancey, R.N. and Stanley, J.H., "A New NDE Capability for Thin-Shelled Structures," AFWAL-TR-88-4225, Air Force Wright Aeronautical Laboratories, Materials Laboratory, Wright-Patterson AFB, OH, December 1988.

4. Smith, J.A., "Improved High Resolution X-ray NDE," FR835-94, Advanced Research and Applications Corporation, Sunnyvale, CA, March 1994.

5. Yancey, R.N., "Applications of High Resolution CT," Proceedings of the ASNT Industrial Computed Tomography - II Conference, San Diego, CA, 20-24 May 1991.

6. Yancey, R.N., and Mitchell, C.R., "Nondestructive Evaluation of Composites Using Digial Radiography and Computed Tomography," Proceedings of NDE Applied to Process Control of Composite Fabrication Conference, St. Louis, MO, 1994.

7. Armistead, R.A. and Yancey, R.N., "Computed Tomography for the NDT of Advanced Engineering Materials," *Materials Evaluation*, May 1989.

8. Yancey, R.N., "The Use of Computed Tomography in Material Process Evaluation," *Review of Progress in Quantitative Nondestructive Evaluation,* 12, 1992.

9. Halada, J., Klacka, R.W., and Yancey, R.N., "CT Inspection of Thick Carbon/Silicon Carbide Composites Made Via Chemical Vapor Infiltration," Proceedings of the 16th Annual Conference on Composites, Materials, and Structures, NASA, Cocoa Beach, FL 12-15 January 1992.

10. Neel, S.T., Eliasen, D.S., and Yancey, R.N., "Dimensional Measurement of Internal Features in Complex Castings," *Review of Progress in Quantitative Nondestructive Evaluation,* 14, 1994.

11. Eliasen, D.S., Neel, S.T., and Yancey, R.N., "Dimensional Measurement of Internal Features in Aerospace Castings," Proceedings of the 1994 ASNT Fall Conference, Atlanta, GA, 1994.

12. Yancey, R.N., Eliasen, D.S., Neel, S.T., Stanley, J.H., and Dzugan, R., "Reverse Engineering Using Computed Tomography," *Proceedings of the Fifth International Conference on Rapid Prototyping,* pp. 141-149, 1994.

13. Yancey, R.N., "Using Computed Tomography (CT) Data for the Micromechanical and Structural Modeling of Advanced Composites," *Proceedings of the First International Conference on Composites Engineering,* 1, pp. 577-578, 1994.

14. Yancey, R.N. and Baaklini, G.Y., "Computed Tomography Evaluation of Metal-Matrix Composites for Aeropropulsion Engine Applications," ASME Paper 93-GT-4, American Society of Mechanical Engineers, N.Y., N.Y., 1993.

15. Baaklini, G.Y., Yancey, R.N., and Doehnert, W.J., "NDE of High-Temperature Materials and Related Subscale Engine Components," Third Conference on NDE for Aerospace Requirements, Huntsville, AL, 4-6 June 1991.

16. Baaklini, G., Bhatt, R., and Yancey, R.N., "Preliminary X-Ray Monitoring of Damage Accumulation in SiC/RBSN," Proceedings of the 1990 HITEMP Review, NASA-Lewis Research Center, Cleveland, OH, 30-31 October 1990.

17. Yancey, R.N., Baaklini, G.Y., and Klima, S.J., "NDE of Advanced Turbine Engine Components and Materials by Computed Tomography," Proceedings of the ASME International Gas Turbine and Aeroengines Congress, Orlando, FL, 3-6 June 1991.

18. Baaklini, G.Y. and Yancey, R.N., "Ceramic Matrix Composites Characterization by Using X-ray Microtomography and Ultrasonics," 17th Annual Conference on Composites and Advanced Ceramics, Cocoa Beach, FL, January 1993.

19. "Carbon-carbon brake disks produced 100 times faster," *Advanced Materials & Processes*, Oct. 94, p. 14

20. Yancey. R.N., Neel, S.T., and Eliasen, D.S., "High-Energy Computed Tomography Evaluation of Ballistically Impacted Fiberglass," Proceedings of the 1994 ASNT Fall Conference, Atlanta, GA, 1994.

21. Moddeman, W.E., Yancey, R.N., Kramer, D.P., Firsch, D.W., Trainer, P.D., Weirup, D.L., Logan, C.M., Pontau, A.E., Antolak, A.J., and Morse, D.H., "Characterization of Low-Density Carbon Foams by X-ray Computed Tomography (CT) and Ion Microtomography (IMT)," Proceedings of Symposium "U" - Advanced Tomographic Imaging Methods for the Analysis of Materials, Materials Research Society Fall Meeting, Boston, MA, 26 Nov - 1 Dec 1990.

22. Moddeman, W.E., Kramer, D.P., Sheppard, D.L., Birkbeck, J.C., Fagin, P.N., Schleitweiler, P.M., Merten, C.W., Yancey, R.N., Hughes, M.E., "Interfacial Pores Observed by X-ray Computed Tomograph (CT) in Inconel-718 Metal Reinforced Glass-Ceramic Composites," Proceedings of the 1992 ASNT Spring Conference, Orlando, FL, 30 March - 3 April 1992.

23. Moddeman, W.E., Kramer, D.P., Firsich, D.W., Trainer, P.D., Hughes, M.E., and Yancey, R.N., "Quantitative Nondestructive Density Determinations of Very Light-Weight Carbon Foams," Proceedings of the 1991 Review of Progress in Quantitative NDE, Brunswick, ME, 28 Jul - 2 Aug, 1991.

24. "Standard Guide for CT System Selection," American Soceity for Testing and Materials (ASTM), Designation: E 1672.

25. Renwick, S.P. and Hansen, H.J., "High Energy Microfocus X-Ray Source," Paper Summaries of the 1994 ASNT Fall Conference Professional Program, September 19-23, 1994, pp. 47-48.

26. Yancey, R.N., "Structural Characterization of Metal-Matrix Composites Using Computed Tomography Data," Phase I Final Report, NASA-Lewis Research Center, 1994

Appendix: Technical Background

A1.0 Introduction

This appendix presents a discussion of the X-ray imaging modalities available at the Wright Laboratory/Materials Directorate X-ray Computed Tomography Research Facility. Factors affecting image quality and measurements of those factors are also presented.

A1.1 X-ray Attenuation

The fundamental building block of X-ray imaging is the X-ray attenuation measurement. A ray path through an object can be considered to be comprised of a number, n, of volume elements. A large number of X-ray photons, N_o, impinge upon the object. As the beam penetrates the line of volume elements, a certain number of photons interact with the material. This interaction is described by the linear attenuation coefficient of the material, μ.[A1] The remaining intensity of the X-ray beam exiting the material, N, is then measured. The transmitted radiation is related to a sum (or line integral) of X-ray attenuation measurements. This is illustrated in Figure A1.

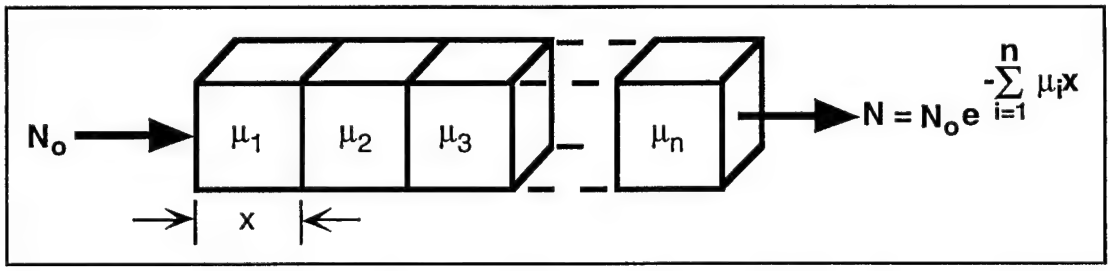

Figure A1. X-ray attenuation

In radiography, the transmitted X-rays are projected onto a sensitized film creating an X-ray opacity map of the object. Each pixel of the radiograph corresponds to a line integral measurement; object features in the same ray path are superposed. Computed tomography differs from radiography in that attenuation information of individual volume elements are extracted from a set of attenuation measurements gathered from many angles around the object. Pixels in a CT image represent individual volume elements rather than lines of volume elements (see Figure A2). In practice, volume elements (or voxels) in the ray path are composed of inhomogeneous material representing multiple attenuation values. CT is unable to differentiate materials within each voxel. The CT measure of a voxel composed of multiple elements represents a composite attenuation value for the volume.

A1.2 Computed Tomography

X-ray computed tomography is a nondestructive, noncontact inspection technique. CT employs a finely collimated X-ray beam to inspect planes (of finite width) within the object. X-ray attenuation measurements are gathered from multiple angles around the object. Sophisticated computer algorithms are applied to these measurements to reconstruct a faithful representation of the cross-sectional profile. Thus, the measurement assigned to a pixel of a CT image approximates the average density of a corresponding volume element in the object.

Because CT images are densiometrically correct, part characterizations are obtained without physical sectioning.

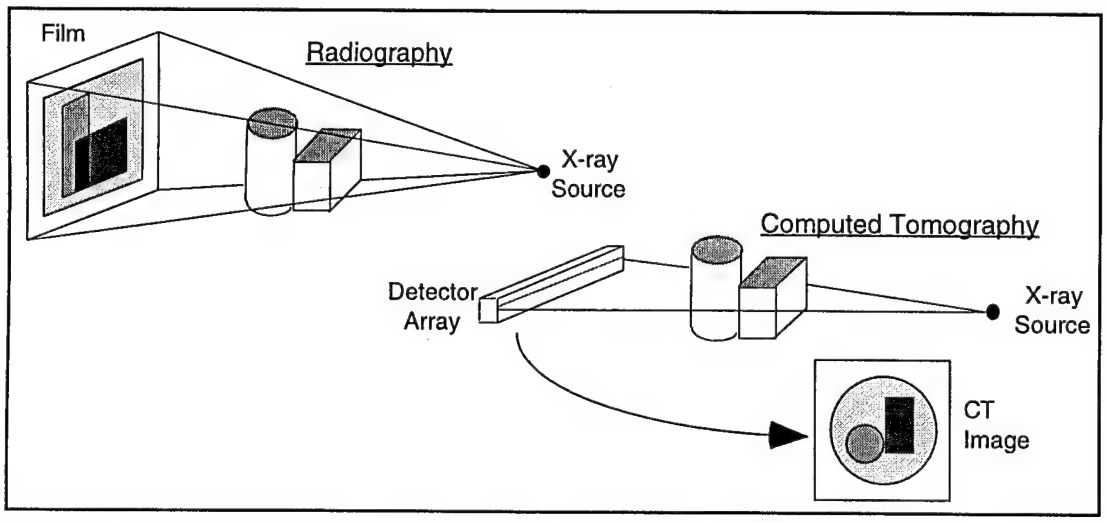

Figure A2. Comparison of CT and conventional film radiography

A1.3 Digital Radiography

Like film radiography, digital radiography (DR) produces a two-dimensional projection image. Figure A3 illustrates the acquisition of a DR image using a CT platform. The object is positioned facing the X-ray source and is moved perpendicular to the plane of the fan beam. X-ray transmission data are collected at small vertical increments and are stacked to form the radiograph. Digital radiographs are commonly used before collecting CT data as a defect screening tool and to determine CT scan plane references.

While film radiography provides images with excellent spatial resolution, DR has a clear advantage over film radiography in terms of dynamic range. While film typically can record a dynamic range of -2 orders of magnitude in exposure, DR systems can provide 4-5 orders of magnitude, making it possible to faithfully record a much greater range of X-ray intensities in a single exposure. By manipulation of the digital display, one can effectively present the information in a single digital radiograph that would require several separate exposures in film radiography. The wide dynamic range of DR also makes it relatively immune to errors in exposure, which often require re-takes in film radiography.

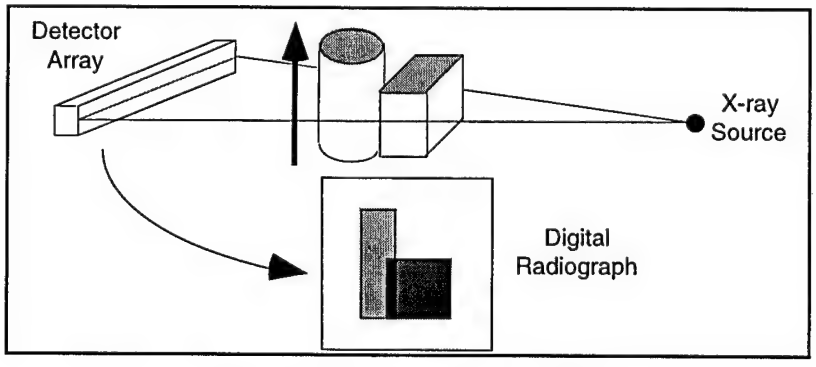

Figure A3. Digital radiography

There are, at least, five other notable advantages of DR over film radiography. 1) The DR image can be displayed almost immediately after acquisition. This makes DR much more amenable to use as an in-process inspection tool. 2) The need for development and the accompanying equipment and chemicals is obviated, thus eliminating some of the costs. 3) Because they are already in digital format image processing algorithms can be applied to DR images without first digitizing the image. 4) Digital image data may be transmitted to remote locations for viewing, processing, or storage. And 5) digital images may be stored compactly and, as the cost of storage media comes down, more and more economically. Also, depending on the storage medium, digital data can remain intact virtually indefinitely. Film, on the other hand, is bulky to store and, if handled too frequently or improperly, can be damaged, resulting in degradation in image quality.

A1.4 Dual Energy Techniques

Dual energy techniques can extract material constituent information.[A2-A5] In conventional radiography, a measurement is made of all the photons that reach the detector regardless of their energy signature. For dual energy imaging, the X-ray attenuation measurements are made at two depths within the linear detector array or by two in-line detectors separated by a filter. This has the effect of separating the energy levels into two distinct bands. The front region of the detector array preferentially absorbs lower energy photons and is most sensitive to photoelectric attenuation which depends on atomic number. Higher energy photons have greater penetrating power and tend to interact with the rear of the detector array which is more sensitive to Compton attenuation which depends on electron density. In some situations, the difference in the interaction physics at the two energy bands produces images based on material composition, not just approximate density. For example, Figure A4 shows examples of dual energy radiography. The standard radiograph at the left shows a beaker of aluminum bolts with four steel bolts randomly placed in the mixture. This image was acquired with the rear detector array which is more sensitive to density. The radiograph on the right highlights the steel bolts. It was generated through a linear combination of attenuation data from the front detector array (which is more sensitive to the photoelectric effect and hence atomic number) and attenuation data from the rear detector array. Dual energy imaging worked well in this situation because the atomic number difference between steel and aluminum is much greater than the density difference between the two materials. Additional image processing can be conducted to better separate the Compton and photoelectric effects and is required when the difference between the two effects is not as pronounced.

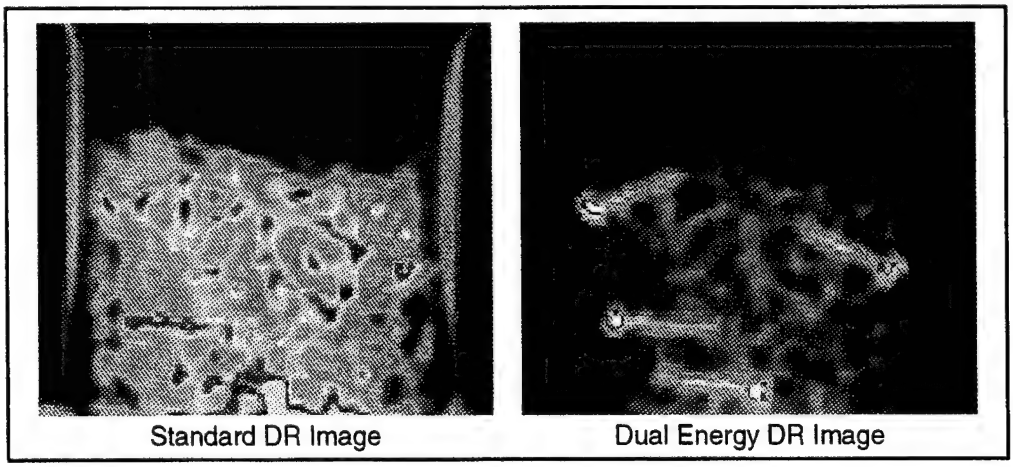

Figure A4. Dual energy radiography

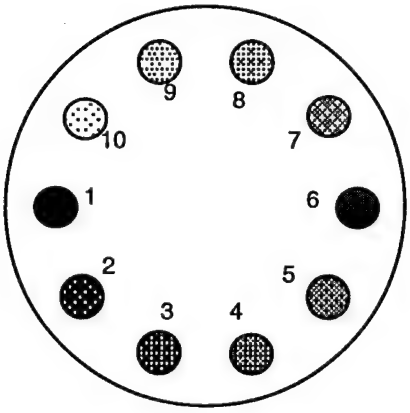

Material	Density (g/cc)
1 - Air Gap	0.000
2 - High Molecular Weight Polyethelene	0.945
3 - Nylon	1.156
4 - Nylatron®	1.165
5 - Acrylic Pexiglass (core material)	1.193
6 - Delrin®	1.507
7 - Magnesium	1.784
8 - Teflon®	2.179
9 - Aluminum	2.704
10 - Titanium	4.423

Figure A5. Illustration of density phantom

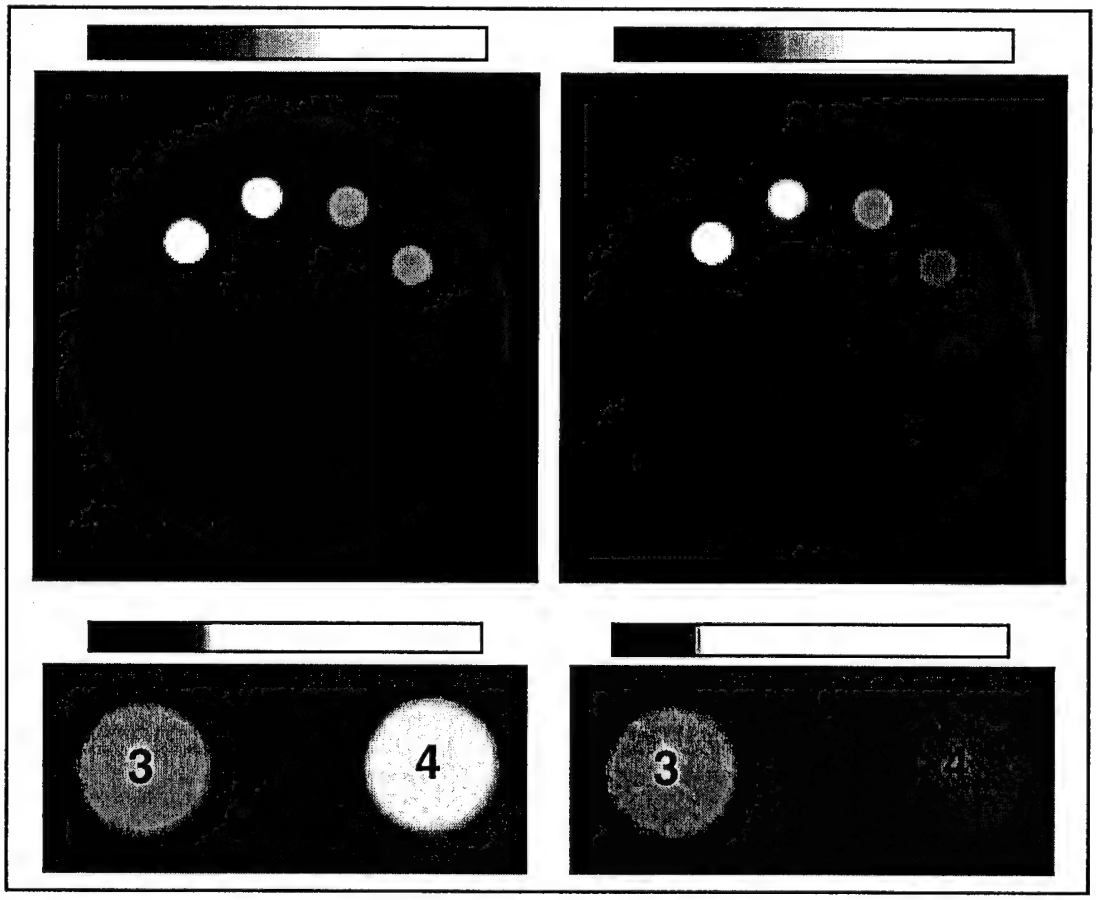

Figure A6. Front and rear detector images of density phantom

Dual-energy CT is also sensitive to variations in material composition. Figure A5. shows an illustration of a density phantom used to evaluate density and material composition sensitivity of CT systems. The phantom is a 150 mm (6.0 in.) diameter acrylic disk with plugs of different densities. Some of the plugs are very close in density, especially plugs 3, 4 and 5. Figure A6 shows LAM/DE CT images of the density phantom. The top left image is the front detector image which is most sensitive to material composition variations. The top right image is the rear detector image which is most sensitive to density variations. The bottom two images

are magnified views of plugs 2, 3, and 4 from the corresponding images on top. The front detector image shows plug #4 with a higher CT number than the acrylic host material and the rear detector image shows plug #4 indistinguishable from the acrylic host. As shown in Figure A5, the density of plug #4 is slightly lower than the acrylic host material and explains why it is indistinguishable from the host material in the rear detector image. Plug #4 is composed of Nylatron which is Nylon mixed with small amounts of MoS_2. Since Mo is a high atomic number material, it raises the effective atomic number of the nylon material which accounts for the higher CT number for the front detector image.

A1.5 Laminography

Laminography is a radiographic technique that generates a focused plane of interest within an object, while defocusing the surrounding regions.[A6-A9] A laminograph differs from a CT image in that features not in the plane of the laminograph appear as blurred features superposed on the focused plane. An image is produced in laminography by collecting digital radiographic data from a series of angles. The image plane of interest is defined and extracted from the radiographic data set. Many laminographic images can be extracted from the same radiographic data set. Laminography has been successful in specialized applications, such as the inspection of solder bonds in printed circuit board assemblies.[A10]

Figure A7 shows the configuration of a laminography phantom designed and fabricated to characterize the laminographic performance of the LAM/DE system. The phantom consists of an aluminum fixture which holds any given number of laminographic phantom plates. A set of 16 plates, 4 each of carbon, acrylic, aluminum, and steel were fabricated with holes and notches of various sizes. These holes and notches went down halfway through the thickness of the plate. The hole and notch pattern were rotated 90° for each of the 4 plates of each material. This gave 4 plates of each material that could be placed in the fixture where the hole and notch pattern would be oriented at a different angle. Each plate is 6.35 mm thick with each hole and notch penetrating 3.175 mm into the plate. In addition to the aluminum fixture that was designed to hold the plates vertical, acrylic spacers were used to space the plates a given distance apart.

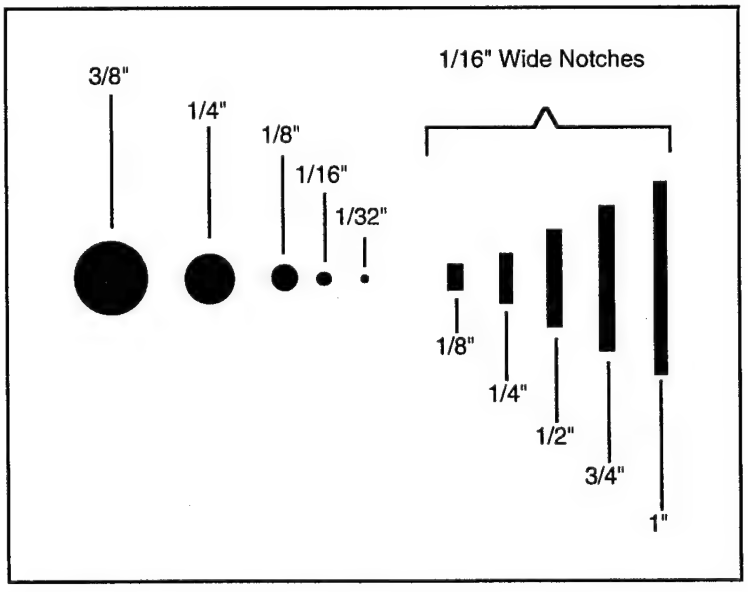

Figure A7. Sketch of hole and notch pattern in laminography phantom plates

Figure A8 shows the laminographic images for a certain configuration of the laminography phantom. The plates were placed in the fixture so that the aluminum plate was in front, the acrylic plate next, the steel plate next, and the carbon plate in the back. The plates were spaced 6.35 mm apart and each plate had the hole and notch pattern oriented differently. The laminography data set consisted of 18 256x256 radiographs at 10° angle spacing and taken with a 2.0 mm square detector aperature. The image on the bottom left corner corresponds to the laminogram of the steel plate in the plane of the notches. The details of all the holes and notches are seen very clearly. Unfortunately, the pattern of the steel plate holes and notches show up in all of the images and not just the image focused on the plane of the steel plate. The aluminum plate is oriented so that the notches are on top and the holes on the bottom. The details can be seen clearly except near the center of the plate where the steel shadow gets in the way. In the image of the acrylic plate, the notches are on the left and the holes on the right. The holes and notches can be faintly seen and again the steel shadow gets in the way. Finally, the carbon plate has the holes oriented at the top and the notches at the bottom. Some of the holes can barely be seen and most of the notches are undetectable. The steel shadow shows up more clearly than the features in the carbon plate. This data set shows the strengths and weaknesses of laminography. For high contrast features (such as air in steel), laminography works well. For lower contrast features (such as air in carbon), laminography is not very sensitive.

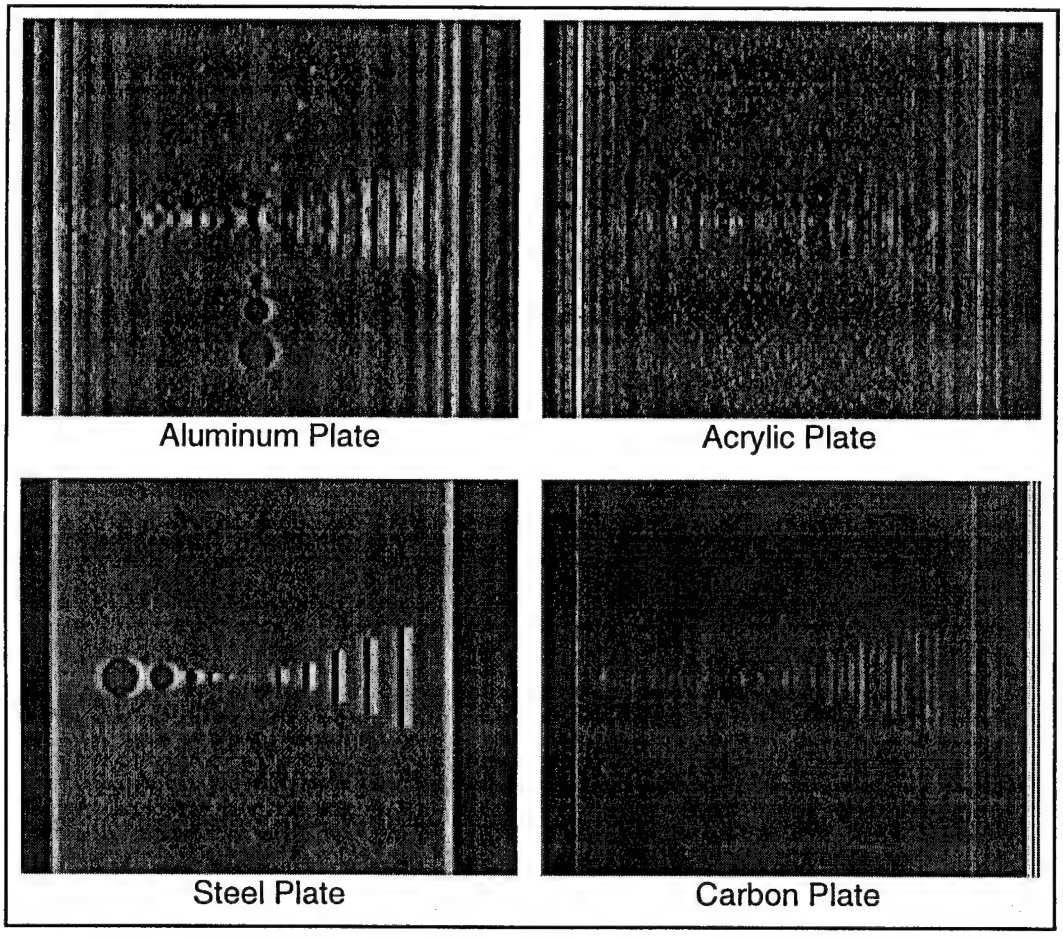

Figure A8. Laminographic images of laminography phantom plates

The laminographic inspection of a drill bit case further illustrates the capabilities of laminography. Figure A9 shows a set of four laminograms of the case. The drill bit case consists of 4 rows of drill bits where each row is missing 2 drill bits. The laminography data

set consists of 32 256 x 256 radiographs spaced at a 5.625 ° angle spacing and taken with a 2.0 mm square detector aperture. Each image shown in Figure A9 corresponds to a given row in the drill bit case. The locations of the missing drill bits can be seen in each image. The image in the lower right corner is of the row with the smallest drill bits. The drill bits are smaller in diameter than the deterctor aperture setting and thus, it is more difficult to detect the missing drill bits here. There are 17 drill bit locations in this row and numbers 6 and 11 from left to right are missing. This particular object has high contrast (steel and air) and demonstrates the sensitivity of laminography for high contrast objects.

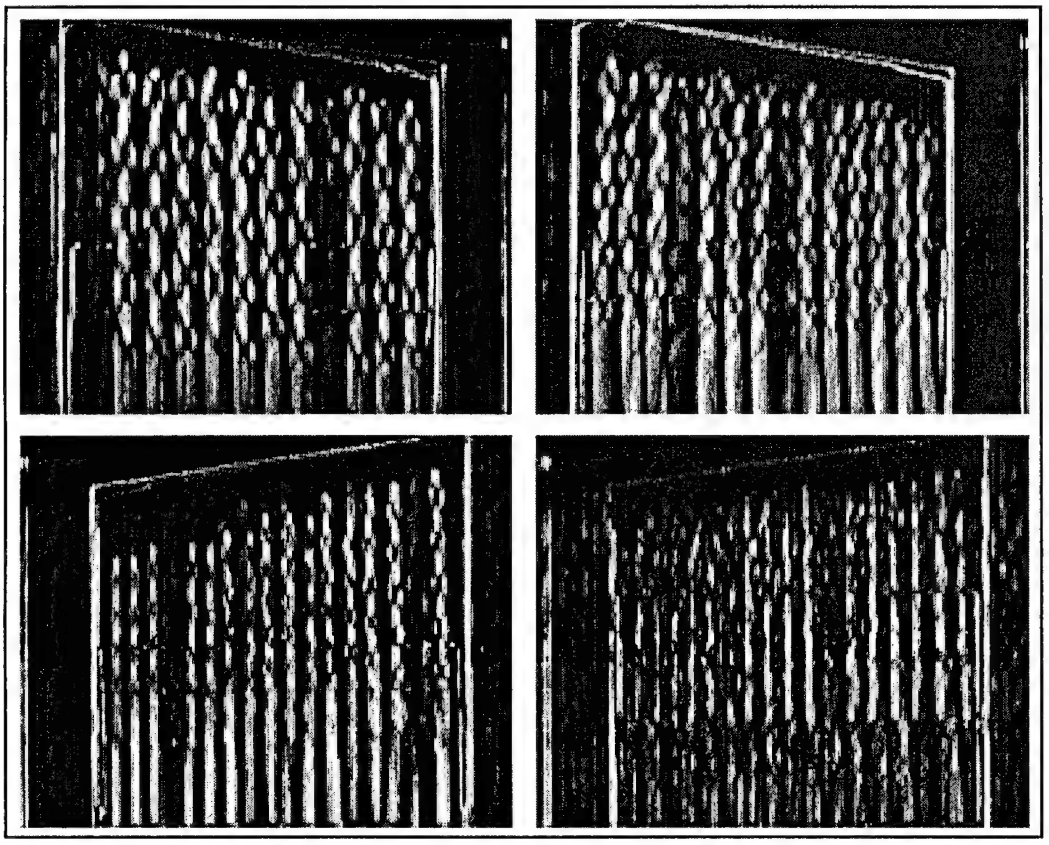

Figure A9. Laminographic images of a drill bit case with missing drill bits

A1.6 Image Quality

This section presents an introduction to the three major factors that affect the diagnostic utility of digital X-ray imagery: noise, spatial resolution and contrast resolution.

A1.6.1 Noise

Statistical variations in the number of photons striking the detector per unit time are the primary source of noise in a properly operating CT scanner. These variations have been termed statistical or quantum noise. Statistical noise when reconstructed in a CT image of a uniform material (e.g., an aluminum cylinder) appears as patternless variations.[A11-A13] Figure A10 shows the CT image of a uniform aluminum cylinder. A unique color scale has been assigned to the image to enhance the quantum noise.

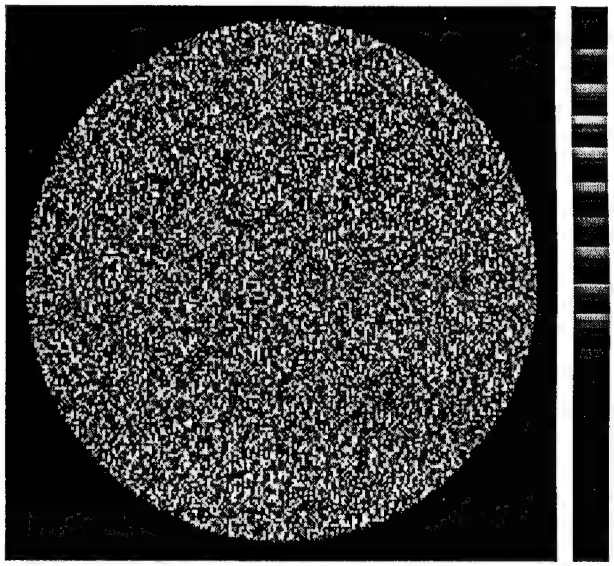

Figure A10. Quantum noise

Structured noise and artifacts can also be present in reconstructed images in the form of streaks, arcs and rings. A common cause of semicircular and circular artifacts is imbalance between detector elements. The major contributors to streak artifacts are object motion during data acquisition, defects in the scanner (such as an alignment error or electrical noise),[A14] and aliasing.[A15-A16] The first two sources of streak artifacts can be virtually eliminated, aliasing artifacts cannot.

Aliasing results from undersampling a structure with high frequency spatial components. For example, the interface between air and the aluminum edge of a cylinder can be described by a set of functions of given frequencies in the spatial domain. To capture the entire set of functions with X-ray attenuation measurements, the object must be sampled at a spatial frequency greater than two times the highest spatial frequency of the interface. This sampling rate is termed the Nyquist frequency. Frequencies beyond the Nyquist sampling limit reappear (not necessarily visibly) as low frequency oscillations (or streaks) in the reconstructed CT image. Aliasing can be eliminated only by sampling at infinitely small intervals. Of course, this is prohibited by the cost and physical size limitations of detectors. Thus, all CT scanners cope with aliasing artifacts.

Beam hardening is another major source of image artifacts.[A17-A18] Beam hardening occurs in polychromatic X-ray beams due to photons of lower energy being preferentially attenuated. As the beam passes through the object it becomes harder or proportionately richer in high-energy photons. The effective energy of the beam varies at each point in the object. Because X-ray attenuation is a function of beam energy, the attenuation measurement of a uniform sample varies along with the effective beam energy as a function of the beam penetration depth. Beam hardening manifests in a CT image as an apparent drop in density towards the center of the object. This effect has been termed a "cupping artifact." The degree of cupping increases with increased density. Post-processing of CT images can reduce or eliminate the effects of beam hardening. Figure A11 shows the CT image of an aluminum disk with the color scale set to accentuate the cupping artifact. The graph of Figure A11 illustrates the drop in reported density near the center of the disk.

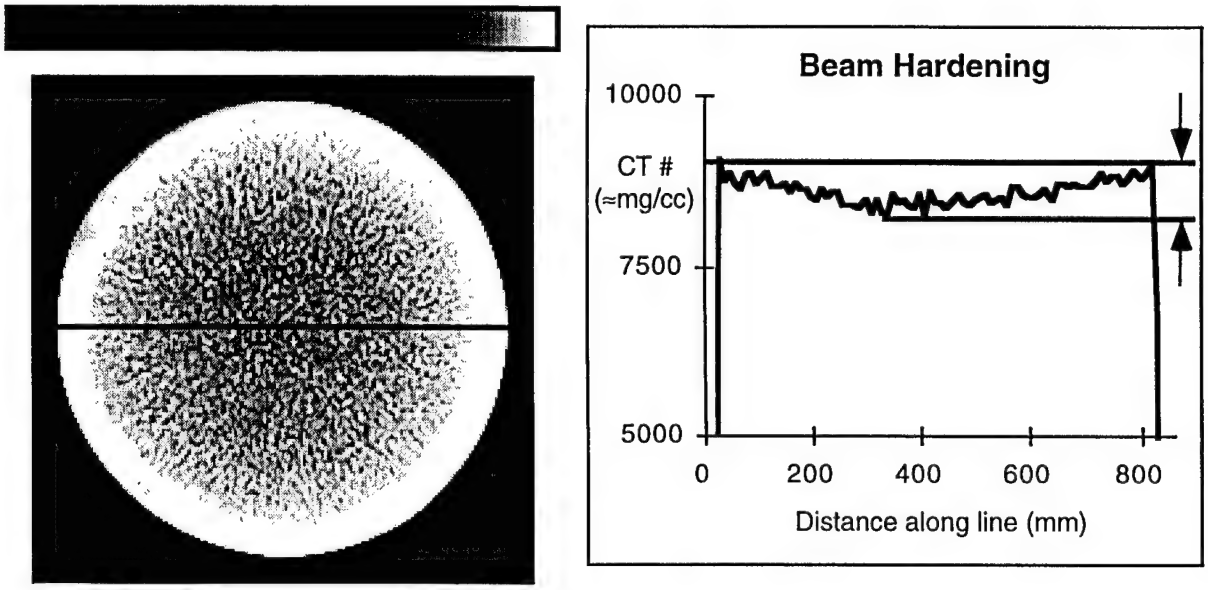

Figure A11. Beam hardening

A1.6.2 Spatial Resolution

Spatial resolution is the ability to distinguish small objects separated by a small distance. It is quantitatively related to the inverse of the minimum separation of two resolvable objects. Spatial resolution has historically been measured by imaging a high contrast edge or point. CT values plotted across the edge or point reveal a graph of the edge response function and the point spread function (PSF), respectively. Ideally, this response should be a delta function (or spike) with an amplitude equal to that of the linear attenuation of the material. However, due to the finite sizes of source spots and detectors, the PSF is blurred.[A19] Less blur or spread is seen in the PSF with better spatial resolution.

A1.6.3 Contrast Resolution

Contrast resolution (or contrast sensitivity) is the ability to discern contrast differences between two adjacent regions. Inherent contrast of an object is determined by the size and attenuation coefficient of the structure relative to the background. Factors affecting contrast resolution include quantum noise (which is related to the dose), electrical and mechanical noise, detector efficiency, artifacts, and the reconstruction algorithm. Under ideal imaging conditions, quantum noise is the most important factor affecting contrast resolution.

It is important to discuss the relationship between spatial resolution and contrast resolution. The relationships among factors relating to image quality have been well documented.[A20-A21] The variance in detected values σ^2 is related to spatial resolution width r, slice thickness h, and dose D, as:

$$\sigma^2 \propto \frac{1}{r^3 h D}$$

Thus, the contrast resolution could be improved (variance reduced) by sacrificing spatial resolution, or by increasing either the slice thickness or dose. In addressing the quality of an image or the capabilities of an imaging system it is important to review both the contrast resolution and the spatial resolution.

A1.7 Performance Measurement

The primary indicators of CT equipment performance are spatial resolution and contrast sensitivity. The measurement of these indicators can be accomplished in various ways. However, the most dependable measure of spatial resolution is the modulation transfer function (MTF) and the best measure of contrast sensitivity is the contrast discrimination function (CDF).[A22] The MTF is closely related to the point spread function (PSF); the MTF is the normalized amplitude of the Fourier transform of the PSF. ASTM has chosen the MTF for specifying spatial resolution.[A23] However, a numerical representation of spatial resolution (rather than a function) is traditional. The cutoff frequency of the MTF (the spatial frequency at which the modulation equals 10%) or the full-width at half-max (FWHM) of the PSF adequately represent the spatial resolution in numerical form.

Contrast sensitivity provides a measure of the lower limit of detectability. The measure of contrast sensitivity is dependent upon feature size and by the noise in an image. Thus, contrast sensitivity is expressed as a function of feature size. Figure A12 and Figure A13 show the MTF and CDF for the LAM/DE and Tomoscope CT systems, respectively. The CDF is drawn for given confidence intervals. The contrast discrimination functions in Figure A12 and Figure A13 are drawn for a false-negative rate of 50% and false-positive rates of 0.1%, 1.0% and 10%. The false-positive rate refers to incorrectly identifying noise as a defect. The false-negative rate refers to losing a defect in the background noise.

It should be noted that the MTF and CDF are dependent on the size and material of the calibration phantom. Typically, these functions are generated for specific imaging situations; the size and material of the calibration phantom are selected to simulate a test object. The graphs for LAM/DE were generated with a 6-inch-diameter aluminum disk. Thus, these graphs would be accurate for an imaging situation such as a large aluminum casting with typically 6-inch material chord lengths. The Tomoscope graphs were generated with a one-quarter-inch-diameter tungsten pin.

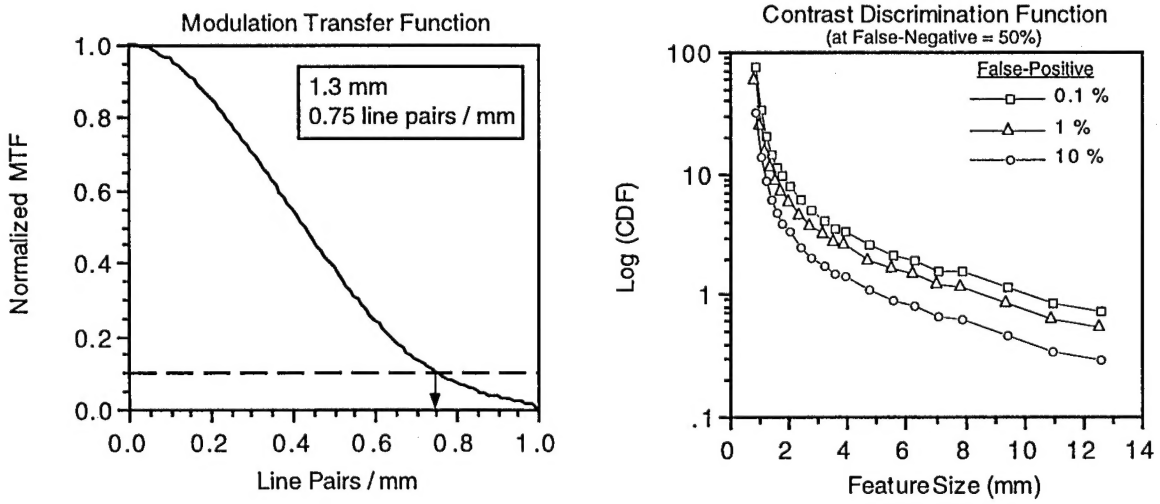

Figure A12. MTF and CDF for the LAM/DE CT system

For purposes of illustration, Figure A14 compares the PSF of the LAM/DE and Tomoscope CT systems. The Tomoscope system was designed as a high-resolution scanner for small objects. LAM/DE is a medium resolution scanner capable of inspecting a broad range

of object sizes and materials. Figure A15 shows LAM/DE and Tomoscope CT images of an MMC rod. Although the scans are of different sections of the rod, the same basic structure appears in each. The images clearly show the difference in resolution of the two systems. In the Tomoscope image, individual fibers can be detected. However, in the LAM/DE image, only the core as a whole is detectable.

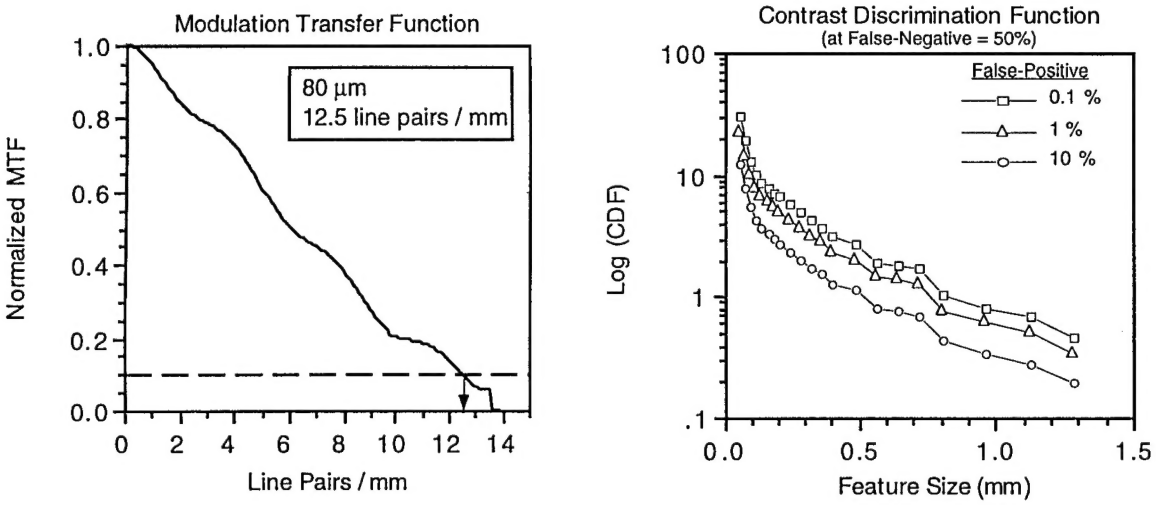

Figure A13. MTF and CDF for the Tomoscope CT system

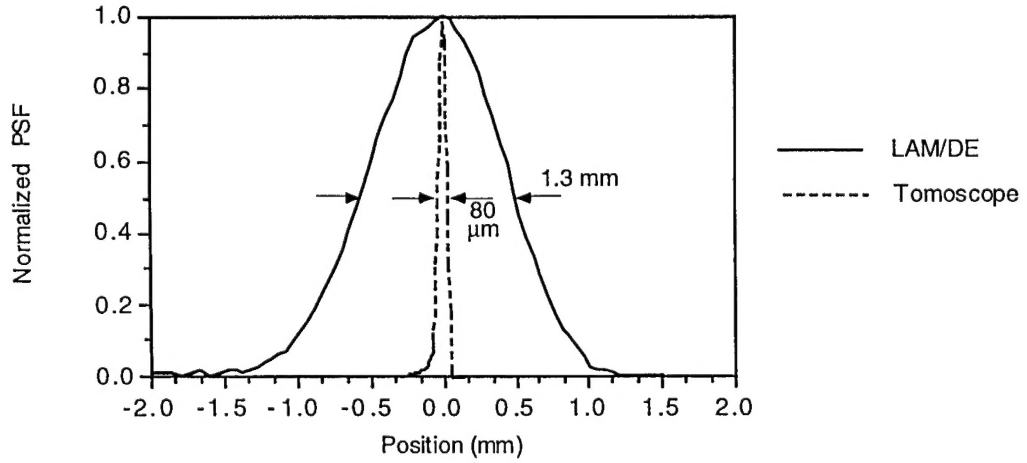

Figure A14. LAM/DE and Tomoscope point spread functions

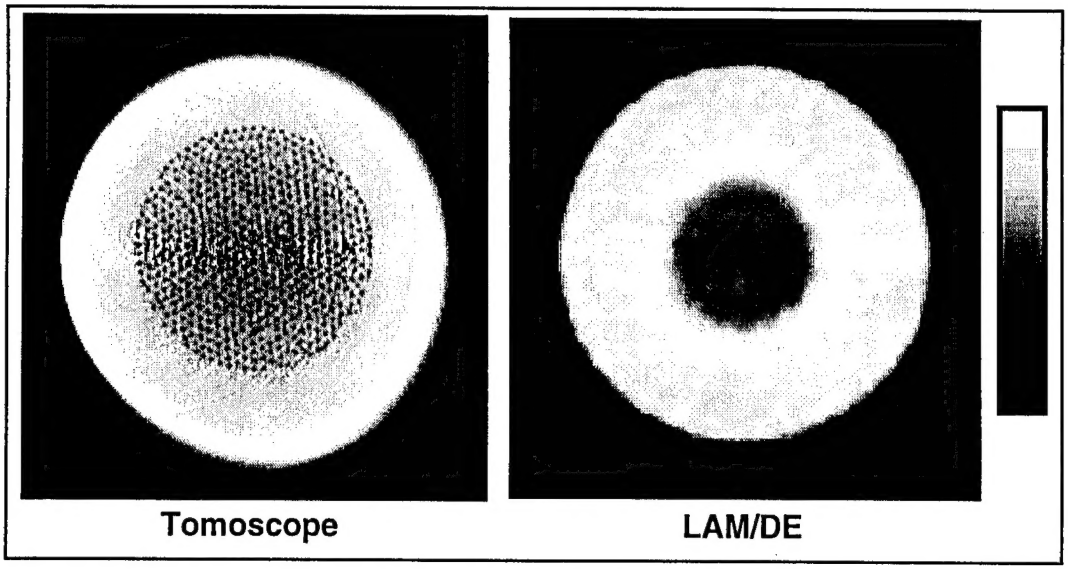

Figure A15. Comparison of image resolution for LAM/DE and Tomoscope

A1.8 Appendix References

A1. D.E. Cullen, M.H. Chen, J.H. Hubbell, and S.T. Perkins, "Tables and graphs of photon-interaction cross sections from 10 eV to 100 GeV derived from the LLNL evaluated photon data library," *Report UCRL-50400-Vol.6-Rev.4,* (Department of Energy, Washington, DC, 1989).

A2. R.E. Alvarez, and A. Macovski, "Energy Selective Reconstructions in X-ray Computerized Tomography," *Phys Med Biol,* Vol. 21, 1976, pp. 733-744.

A3. P. Engler, and W.D. Friedman, "Review of Dual-Energy Computed Tomography Techniques," *Materials Evaluation,* May 1990.

A4. R.N. Yancey and J.H. Stanley, "A New Radiographic Corrosion Inspection Capability," AFWAL-TR-88-4234, Air Force Wright Aeronautical Laboratories, Materials Laboratory, Wright-Patterson AFB, OH, December 1988.

A5. C.V. Kropas, T.J. Moran, and R.N. Yancey, "Effect of Composition on Density Measurement by X-ray Computed Tomography," *Materials Evaluation,* April 1991.

A6. G.W. Files (Ed.), "Planigraphy," Medical Radiographic Technic, pp. 152-159, Charles C. Thomas (publ.), 1949.

A7. D.G. Grant, "Tomosynthesis: A Three-Dimensional Radiographic Imaging Technique," *IEE Trans. on BME,* Vol. 19, No. 1, pp. 20-28, Jan 1972.

A8. Nishimura, et al., "Digital Tomosynthesis Using a Scanned Projection Radiographic System," SPIE Conference on Digital Radiography, 1981.

A9. R.N. Yancey and J.H. Stanley, "A New NDE Capability for Thin-Shelled Structures," AFWAL-TR-88-4225, Air Force Wright Aeronautical Laboratories, Materials Laboratory, Wright-Patterson AFB, OH, December 1988.

A10. R.H. Bossi and R.J. Kruse, "X-ray tomographic inspection of printed wiring assemblies and electrical components," *WRDC-TR-90-4091,* Boeing Aerospace Company, 1990.

A11. H.H. Barrett, S.K. Gordon and R.S. Hershel, "Statistical limitations in transaxial tomography," *Computers in Biology and Medicine,* vol. 6, pp. 307-323, 1976.

A12. D.A. Chesler, S.J. Riederer, and N.J. Pelc, "Noise due to photon counting statistics in computed X-ray tomography," *J. Comput. Assist. Tomogr.,* vol. 1, pp. 64-74, 1977.

A13. S.J. Riederer, N.J. Pelc and D.A. Chesler, "The noise power spectrum in computed X-ray tomography," *Phys. Med. Biol.,* vol. 23(3), pp. 446-454, 1978.

A14. G. Kowalski, "Suppression of ring artifacts in CT fan-beam scanners," *IEEE Trans. Nucl. Sci.,* vol. NS-25(5), pp. 1111-1116, 1978.

A15. R.A. Brooks, G.H. Glover, A.J. Talbert, R.L. Eisner and R.A. DiBianca, "Aliasing: a source of streaks in computed tomography," *J. Comput. Assisted Tomog.,* vol. 3(4), pp. 511-518, 1979.

A16. C.R. Crawford and A.C. Kak, "Aliasing artifacts in computerized tomography," *Applied Optics,* vol. 18(21), pp. 3704-3711, 1979.

A17. A.J. Duerinckx and A.Macovski, "Nonlinear polychromatic and noise artifacts in X-ray computed tomography images," *J. Comput. Assisted Tomog.,* vol. 3(4), pp. 519-526, 1979.

A18. R.A. Brooks and G. Di Chiro, "Beam hardening in X-ray reconstructive tomography," *Phys. Med. Biol.,* vol. 21(3), pp. 390-398, 1976.

A19. G.H. Glover and R.L. Eisner, "Theoretical resolution of computed tomography systems," *J. Comput. Assisted Tomog.,* vol. 3(1), pp. 85-91, 1979..

A20. R.A. Brooks and G. Di Chiro, "Statistical limitations in X-ray reconstructive tomography," *Medical Physics,* vol. 3, pp. 237-240, 1976.

A21. J.C. Gore and P.S. Tofts, "Statistical limitations in computed tomography," *Phys. Med. Biol.,* vol 23(6), pp. 1176-1182, 1978.

A22. "Standard Test Method for CT System Performance," American Soceity for Testing and Materials (ASTM), Designation: E 1690.

A23. "Standard Practice for Computed Tomographic (CT) Examination," American Soceity for Testing and Materials (ASTM), Designation: E 1570 - 93.